INTERNATIONAL MATERIALS REVIEWS
https://doi.org/10.1080/09506608.2022.2153217

Developing alkaline titanate surfaces for medical applications

Matthew D. Wadge [a], Jamie McGuire [a], Kathryn G. Thomas[a], Bryan W. Stuart[a], Reda M. Felfel [a,b,c], Ifty Ahmed [a] and David M. Grant [a]

[a]Advanced Materials Research Group, Faculty of Engineering, University of Nottingham, Nottingham, UK; [b]Physics Department, Faculty of Science, Mansoura University, Mansoura, Egypt; [c]Advanced Composites Group, University of Strathclyde, Glasgow, UK

ABSTRACT

Improving the surface of medical implants by plasma spraying of a hydroxyapatite coating can be of critical importance to their longevity and the patient's convalescence. However, residual stresses, cracking, undesired crystallisation and delamination of the coating compromise the implants lifetime. A promising alternative surface application is an alkali-chemical treatment to generate bioactive surfaces, such as sodium and calcium titanate and their derivatives. Such surfaces obviate the need for high temperatures and resulting micro-crack formation and potentially improve the bioactive and bone integration properties through their nanoporous structures. Also, metallic ions such as silver, gallium and copper can be substituted into the titanate structure with the potential to reduce or eliminate the infections. This review examines the formation and mechanisms of bioactive/antibacterial alkaline titanate surfaces, their successes and limitations, and explores the future development of implant interfaces via multifunctional titanate surfaces on Ti-based alloys and on alternative substrate materials.

ARTICLE HISTORY
Received 18 June 2021
Accepted 22 November 2022

KEYWORDS
Titanate; biomaterial; implant; surface; modification; substitution; antibacterial; bioactive; multifunctional

Introduction

The number of people in the world aged 65 years or over is projected to more than double in 2050 from its 2015 value. The global population of this age range currently is approaching 1.5 billion [1]. According to the National Joint Registry (NJR), the prevalence of hip replacements in the United Kingdom has continually increased, with 101,384 primary hip replacements out of over 109,000 total hip replacement procedures (including revisions) being conducted in 2019 [2]. Currently, failure of hip implants occurs predominantly through aseptic loosening, accounting for 40% of single-stage revisions in 2018, with infection affecting 6% [2]. Despite current outlooks showing greater hip survivorship than previously thought; 57.9% of hip replacements last 25 years according to Evans et al. [3], further advances are still required to ensure improved quality of life for an ever-aging population while mitigating the need for subsequent revision surgeries.

Implant surfaces are critical to *in vivo* devices. Controlling the properties of these surfaces to achieve appropriate extracellular environments, therefore enhancing the implant-tissue bond, especially in the case of total joint replacements to create strong and long-lasting natural fixation, is a demanding and necessary paradigm within orthopaedic research. This extends further when considering additional bone-related research, such as with dental implants. Due to the complexity of the implanted environment, each implant must be specifically designed for the intended implant site. Regarding dental implants [4,5], a trans-mucosal component is required to penetrate the soft tissue, such as abutment devices, which lies between the anchoring implant in the bone (usually a screw), and the functional component of the dental prosthesis (i.e. the crown) [4]. Therefore, carefully designing how these different materials and structures interact physically and chemically is essential. Ultimately, the critical factors in the success of these components are the chemical, structural and morphological properties of the implanted surface.

A key research area, therefore, for such implants is the modification of surfaces to enable greater adhesion to surrounding bone tissue [6,7]. Durability and *in vivo* success of an implant are dependent upon osteoconductive growth around an implant through osteoblastic recruitment. Presently, the only FDA-approved method for providing hydroxyapatite (HA) structure on the surface of implants is via high-temperature (>10,000°C for the flame centre; > 1500°C for particle temperature [8]) plasma spraying delivering a thick coating of hundreds of microns. HA is a form of calcium phosphate, which mimics the main mineral

CONTACT Matthew D. Wadge matthew.wadge3@nottingham.ac.uk Advanced Materials Research Group, Faculty of Engineering, University of Nottingham, Nottingham, UK; David M. Grant david.grant@nottingham.ac.uk Advanced Materials Research Group, Faculty of Engineering, University of Nottingham, NG7 2RD Nottingham, UK

component, crystal and chemical structure of cortical bone: $Ca_{10}(PO_4)_6(OH)_2$ [8]. However, despite these coatings being ideal for improving implant biocompatibility, they suffer from inherent issues such as residual stresses, for example, 20–40 MPa tensile, and cracking resulting from the manufacturing temperatures used [9,10]. This ultimately results in coating spallation, and in turn, generation of aseptic loosening (sustained osteolysis and failure between the implant and bone in the absence of infection [11]) *in vivo* through macrophage activation and subsequent inflammatory responses [9–13].

To negate the limitations of implant coatings, surface modifications have been considered, such as the production of sodium titanate layers. By directly modifying the surface, the issue of coating spallation can be minimised. Kokubo et al. demonstrated that sodium titanate, generated apatite *in vitro* and could be synthesised at 60°C; much lower than conventional plasma spraying methods. The sodium modifier in the Ti–O framework, allowed for ion-exchange reactions to take place with Ca^{2+} ions in the extracellular environment/simulated body fluid (SBF), which over time could produce the necessary apatite that can lead to bone maturation [14]. Generation of such surface layers is achieved by the immersion of titanium, typically (Cp-Ti) in 5 M NaOH solution at 60°C for 24 h. This process is then followed by heat treatments at 600°C for 1 h (ramp rate of 5°C min^{-1}), in order to densify and further crystallise the resulting titanate structure [15–17]. Successful studies both *in vitro* and *in vivo* resulted in the implantation of NaOH-treated Ti–6Al–2Nb-Ta alloy femoral stems and acetabular cups into 10,000 patients in Japan [18]. Further work by Kizuki et al., Yamaguchi et al. and many others has demonstrated the ability for incorporating various ions into the titanate structure through solution-based ion-exchange reactions [19–21]. Other elements such as calcium (Ca), magnesium (Mg), silver (Ag) and strontium (Sr) have been successfully incorporated into the titanate structure, searching for improved bioactivity and antibacterial properties, as well as improved tailoring for specific applications [20–22].

This review will explore the impact of medical titanate structures, since the initial work by Kim et al. [23] and Kokubo et al. [24] in 1996. Older reviews on the subject [25–28], have only detailed the alkaline titanate film formation through wet-chemical conversion. Here we explore the impact of alternative titanate morphologies (such as nanorods [29], nanotubes [30] and nanobelt sheets [31]), material structures (titanate glasses [32]) and material properties (piezoelectric biomedical titanates [33]) and provide a prospective on their biomedical potential. Furthermore, the antibacterial potential of these surfaces has only partially been described within a broader review of antibacterial surfaces by Spriano et al. [34]. In this review, all literature on doped titanate structures with antibacterial properties have been collated and their impact critically discussed. Therefore, an additional perspective on the efficacy of the titanate surfaces as antibacterial materials will also be presented, regarding the trade-off between bacterial death and the recovery of cellular response in the same environment. This is increasingly important as the focus on antibacterial surfaces is an ever-prevalent issue, considering the current rise in antibiotic resistance, widely considered to be the next pandemic [35], and therefore the need for alternative solutions to antibiotics [36]. In the final section, we present future directions and the latest research which explores the need to provide titanate structures in alternative forms and to expand the applicability of alkaline titanate surfaces. The latter is key to maximising the impact by delivery on alternative substrate materials (i.e. ceramics, polymers, composites), thus imparting the biomedical properties of alkaline titanates onto candidate bioinert materials [37].

Ti and its alloys

Advantages of Ti as a biomedical material

Titanium (Ti) is a lustrous transition metal found in group 4, period 4 of the periodic table [38]. Despite finding applications in many fields, including aerospace and automotive industries, its prevalence in biomaterials has increased significantly over the past few decades [39–41]. A key feature of Ti, due to the amorphous passivated surface layer, is its bio-inertness; bioinert materials are defined as a material, by which, 'no chemical reactions occur between the implant and the tissue … [and] no direct contact with the adjacent bone tissue [is observed]' [42]. The proposal of Ti and its alloys as an alternative to the widely used 316L stainless steel (SS) and Cobalt-Chromium (Co–Cr) alloys, was due to its excellent corrosion resistance, and minimal allergenic and immunogenic potential when implanted; Ni, Co and Cr have all been quantified as being harmful to the human body [43]. Furthermore, its Young's modulus (105–117 GPa, however, still higher than cortical bone: 3–20 GPa [44]) results in lower amounts of stress shielding compared to 316L SS and Co–Cr–Mo alloys (Table 1) [43].

Within the Ti alloy family, Ti–6Al–4V has been particularly used in medical applications, most notably hard tissue replacements, such as orthopaedic joint arthroplasties. Despite the preferable mechanical properties compared to 316L SS and Co–Cr alloys, α (Cp-Ti) and α+β (Ti–6Al–4V) alloys still have elastic moduli greater than human bone, which can result in stress shielding effects. Interestingly, Ti-β alloys, such as Ti–Nb–Ta–Zr alloys,

Table 1. Mechanical properties of common metals used in replacement hip implants for the femoral stem and acetabular cup casing compared to natural cortical and cancellous bone.

Material	Young's Modulus (E)/GPa	U.T.S/MPa	Density (ρ)/g cm^{-3}	Poisson's ratio (ν)	Max. elongation/%	Reference
316L Stainless Steel	189–210	465–950 (207–1160)	7.9–8.1	0.30	40–55	[41,45–51]
α+β Ti Alloys (e.g. Ti6Al4V (F136))	105–117	960–970 (780–1050)	4.4–4.7	0.32–0.33	10–17	[41,45–52]
β-Ti Alloys (e.g. Ti–Nb–Ta–Zr)	45–100	600–1110	8.3–8.4	0.3	10–40	[53–57]
Co–Cr Alloys (e.g. CoNiCrMo (F562))	200–240	600–1795 (430–1795)	7.2–9.2	0.30	8–50	[41,45–48,50–52]
Nitinol (NiTi) Alloy	50–110 (Austenitic) 25–50 (Martensitic)	780–1196	6.45	0.33	5–20	[58,59]
Cortical (Lamellar) Bone	3–20 (1–40[a])	90–140 (50–150[a])	1.8–2.1	0.30	1.3–1.7	[41,45–49,51,60,61]
Cancellous (Trabecular) Bone	0.01–3 (0.01–13[a])	1–20	0.05–0.1	0.3–0.4	N/A	[41,48,49,62–65]

[a]Indicates orientation dependence due to anisotropy. Values outside brackets are the most common, with values inside giving full literature ranges.

which have a body-centred cubic (BCC) structure, do present Young's modulii that are more favourable for orthopaedic applications [66] (Ti–Nb–Ta–Zr alloys exhibited values ca. 48–55 GPa, with 40 GPa being seen in the Ti–35Nb–4Sn system; roughly half the value of Ti–6Al–4V), due to its BCC structure [67]. However, a number of issues do persist with β alloys, particularly difficulty in homogenously melting Ti, as well as the inclusions of Nb, Ta (β-stabilisers) and Zr (Neutral elements), which can cause biocompatibility issues due to chemical macro-segregation (difficulty in forming a single equiaxed β phase), limiting their commercial usage in medical settings [66].

NiTi shape memory alloys (SMA) have also been of interest to many surgeons as a useful material for medical devices requiring *in vivo* movement. Not only does it possess low elastic modulus (ca. 30 and 80 GPa for its martensitic and austenitic forms, respectively), but it also exhibits superelasticity and shape memory effect (SME). Despite extensive use in various medical applications, such as orthodontic wires and stents, there are concerns of the dissolution of Ni ions, which have the potential to induce allergic, toxic or carcinogenic effects, as described by Shabalovskaya [68]. Due to failures of devices *in vivo*, *in vitro* performances being inconsistent, as well as a report of 33 failed stents/grafts which had been retrieved from patients (5–43 months post-implantation), exemplify the lack of understanding of the surface chemistry of this material, in particular, its susceptibility to intergranular corrosion. Critically, alloys containing Ni should be avoided in the first instance; however, if their properties cannot be replicated, such as SME, surface modification is a logical step to improve the corrosion resistance and minimise any adverse biological effects.

Inherent limitations

Despite titanium's excellent properties, fundamental issues remain regarding its deployment as a biomaterial. First, its lower hardness (ca. 200 H_v [69,70]) and wear resistance result in an inability to be used for articulating surfaces, such as the femoral head [71]. Second, prior to any surface modification, pure Ti cannot confer a bond to living bone (passivated TiO_2 layers are known to be bioactive; however, the thin (ca. 5 nm) nature of such a coating is insufficient protection to corrosion [72]) and therefore, over time, its fixation *in vivo* is not stable. Cementation of the implant using poly (methyl methacrylate), or PMMA, to the surrounding tissue has been employed since 1953; however, this process also possesses limitations, since the exothermic curing reaction can initiate tissue necrosis [73].

In addition, chemical issues persist, especially when considering the complexity of the live environment in which these materials will be implanted. No matter the metal/alloy being used, corrosion will occur due to the extremely harsh body environment, in which body fluid contains chloride ions (Cl^-), proteins, as well as the variation in pH levels depending upon the area of implantation (3.5–9) [74]. Depending on the alloy being implanted, and its particular alloying elements, the corrosion resistance will vary considerably due to the passivating film formed from the alloy inclusions. For example, Nakagawa et al. [75] showed a Ti–0.2Pd alloy exhibited greater corrosion resistance (the amount of Ti dissolved (0.1% NaF/24 h) at pH 4 was 800 and 22 μgcm^{-2} for pure Ti and Ti–0.2Pd, respectively) over a wide pH range (3–7 at 37 ± 0.1°C, through dilution of 0.05–2% NaF with H_3PO_4) due to the surface concentration of Pd. In addition, the ability of alloys to re-passivate their surfaces following corrosion, the chemical makeup of this re-passivated film compared to the native oxide, plus the ease of dissolution and reprecipitation, are significant factors in the corrosion resistance of the alloy [76]. In addition, the presence of proteins can either have a positive or detrimental effect on the corrosion resistance of the alloy being implanted.

Additionally, osseointegration, and more simply biocompatibility, of an implant material heavily relies on its topography and chemical nature [74]. Release of metallic ions, whether through leaching, wear or otherwise, can cause inflammation, irritation, and/or sensitisation of the surrounding tissue. If not

carefully balanced, inflammatory responses through pro-inflammatory cytokines, chemokines and matrix metalloproteases, may result in osteoclast activation, ultimately causing bone deterioration, osteolysis and implant loosening [77]. Ti–6Al–4V suffers from the addition of Al and V, both considered cytotoxic elements, which have been known to be associated with longer-term health conditions, such as Alzheimer's, neuropathy and ostemomalacia [78–81]. The topic of corrosion and limitations of Ti alloys in medical settings has been extensively reviewed by Geetha et al. [74].

Current processes employed for surface modification of Ti

To address the issue of bone bonding, many researchers have investigated the ability to confer bone bonding to previously bioinert implant materials, specifically metals and alloys. This has been succinctly reviewed by Jäger et al., taking into account mechanical, chemical and physical surface modifications of titanium materials [82]. However, despite all these different modification processes, one method, in particular, has received a great deal of attention and has been commercially exploited: plasma spraying of hydroxyapatite (HA).

Plasma spraying of HA: the current 'gold standard'

Since the work performed by Getter et al. in 1972, HA has been investigated and used widely as a coating material for biomedical implants [83–85]. Its mimicry of the mineral component of bone, making up 70–90% of its dry mass, makes it an ideal surface modification, since it is inherently bioactive [86–88]. Furthermore, the primary method, which remains the only FDA-approved method for conveying a HA coating to implants, is through plasma spraying; their mechanical adhesion of 55–62 MPa is above the minimum requirement of 50.8 MPa [88,89]. Plasma spraying (Figure 1) utilises a carrier gas (usually argon, or a mixture with other gasses) to carry HA particles through a low voltage and high current electrically discharged plasma, as described by Herman [90]. This melts the particles sufficiently, that upon impingement on the substrate surface, they solidify into a coating.

Plasma spraying offers rapid deposition rates (1×10^6 particles $m^{-2}s^{-1}$) and sufficiently low costs. However, despite these advantages, plasma spraying, as well as other thermal spraying techniques, such as vacuum arc coating, has inherent disadvantages including poor adhesion [91]; non-uniform coating density [92]; and excessive temperatures (ca. 1500 K [8]) leading to deleterious phase transformations and residual surface stresses (20–40 MPa tensile) [93–95], which can result in the formation of micro-cracks [96]. Their brittle nature can result in spalled particles *in vivo*. The production of these spalled particles may induce phagocytic pathways through macrophage activation and may eventually lead to aseptic loosening of the implant, although direct determination of the cause of this multifactorial aetiology is still fiercely debated within the literature [97–99].

Alternative methodologies for HA generation

In recent years, different approaches have been considered as alternative methodologies for the current FDA standard. Alternative coating methods for generating HA on implants have been reviewed by Yang et al. and demonstrate the advantages and disadvantages of each coating method [100]. However, substantial issues remain within all techniques mentioned, especially regarding biomedical coatings, resulting in alternative lines of enquiry. For example, ion-implantation, which is the process of bombarding the sample surface with an ion beam of sufficient energy to implant the bombarding ion into the surface (Figure 2), as well as electrochemical methods, have shown promise in bioactive scenarios, through the production of apatite in SBF. Studies by Armitage et al. [101], Nayab et al. [102] and Rautray et al. [103], demonstrated successful implantation of calcium in titanium (Ti) and titanium alloys, with further work on the implantation of oxygen (O) [104], sodium (Na) [105], magnesium (Mg) [106] and

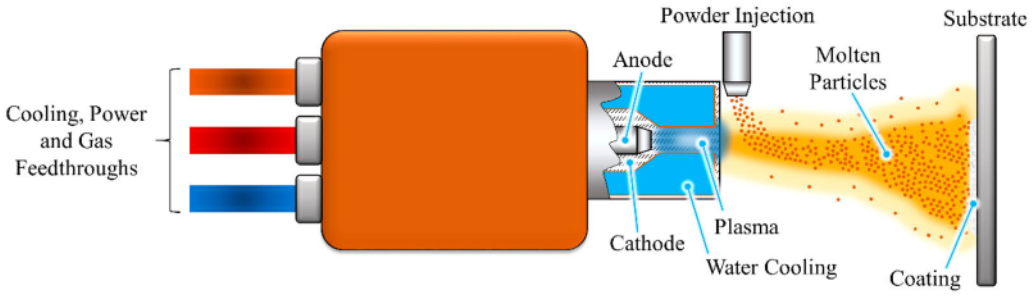

Figure 1. Plasma spraying schematic demonstrating the deposition of molten HA particles onto the required substrate.

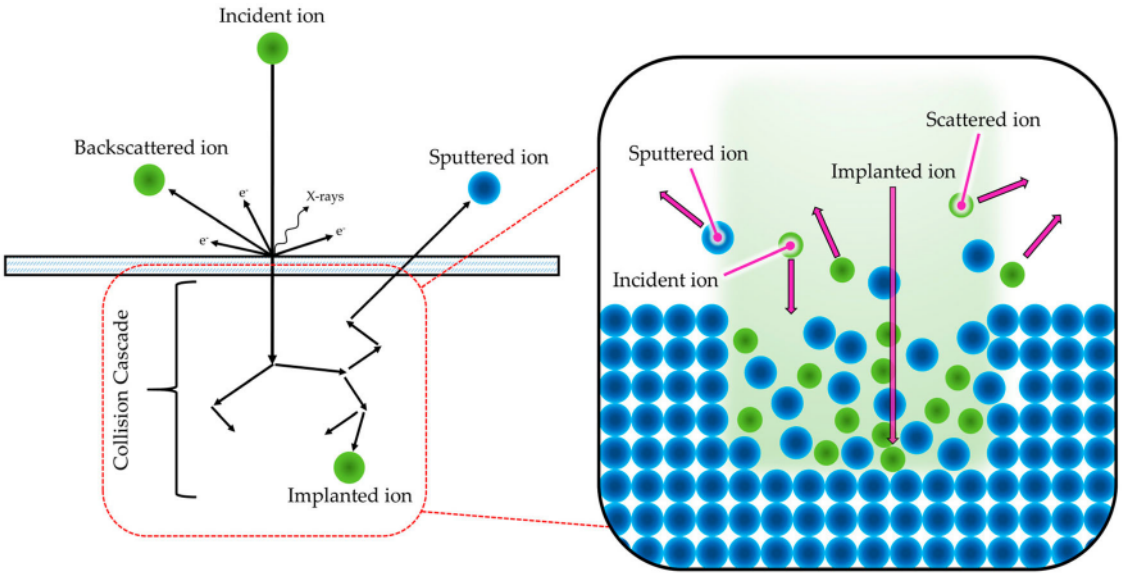

Figure 2. Schematic representation of ion–solid interactions, which is the principle mechanism employed for ion implantation.

even silver (Ag) [107] into Ti structures being detailed within the literature. Despite their advantages, the above techniques require complex, and costly, equipment in order to generate such surfaces/coatings. Furthermore, these processes cannot successfully coat complex geometries, such as surface plasma-sprayed, porous implants (e.g. 300+ μm thick, 30% non-interconnected porosity, mean pore size 250 μm, $R_a = 21–28$ μm [108,109]), resulting in further alternative methods being sought [103].

In addition, a number of other technologies, although not FDA approved, are utilised to deposit CaP coatings onto implants (Table 2). Plasma electrolytic oxidation for example, is used by Nobel Biocare to produce calcium phosphate coatings on their dental implants [110]. The complexity of the regulatory process to successfully demonstrate long-term efficacy, coupled with the multiple requirements of the produced CaP coating (appropriate chemical phases, optimal surface roughness/porosity, long-term stability, some degree of sub-stoichiometry to induce bioactivity, etc. [111]) has resulted in limited FDA approval, and hence clinical usage. Other techniques are reviewed by Rahman [112]. It is, therefore, advantageous to develop coatings and surface modifications, which can generate apatite *in vivo*, since this *in situ* formation is more likely to form apatite with appropriate properties for subsequent bone formation; hence the investigation into alkali-titanate structures.

Medical alkaline titanates

Ever since the work of Li et al. in 1994, on the induction of bone-like HA on titanium substrates through the generation of gel-like titania on its surface, surface modification through chemical routes has been considered of great practical importance, with ever-increasing numbers of papers (Figure 3) [113]. Their study demonstrated that the hydroxyl groups formed on the surface were bioactive in nature, in addition to the negative surface potential. Therefore, appropriate generation of such groups on titanium, while ensuring a negative surface charge, would hypothetically induce apatite formation *in vitro* in SBF, and in extension *in vivo* [113].

The formation of osteoconductive HA, through submersion in SBF, is a well-known technique utilised in *in vitro* assessment of a substrate's bioactivity (ISO 23317:2014) [114]. In comparison to HA found within the physiological environment, the SBF solution is regarded as supersaturated, as demonstrated by Lu et al. [115]. The higher the supersaturation of a solution, the greater the probability of molecular collision, which ultimately leads to the formation of stable nuclei and, therefore, HA crystal growth [116]. As SBF is supersaturated with respect to Ca^{2+} and HPO_4^{2-} ($S°_{(HA)} = 1.42$; S° is defined as the thermodynamic saturation level, where $S° > 0$ indicates the compound will precipitate [117]), and metastable thus spontaneous apatite growth has been reported to occur from nucleation points within a vessel, such as cracks/scratches. However, a significant number of studies have contraindicated the use of SBF as an *in vitro* predictor of *in vivo* bioactivity, for example, *β*-TCP has extensively been shown to bond to bone *in vivo*, yet will not demonstrate a bioactive response in SBF [118]. This test, therefore, should be corroborated with additional *in vitro* assessments such as cytocompatibility assays (Neutral Red, AlamarBlue), osteogenic potential assays (Osteocalcin, Alkaline phosphatase), prior to *in vivo* testing. For example, a recent review by Kokubo et al. [25] and additional studies by Bohner et al. [117] and Kokubo et al. [119,120], described the efficacy of SBF as a technique

Table 2. Comparison of HA coatings techniques explored within the literature.

Technique	Thickness/ μm	Advantages	Disadvantages
Thermal spraying	30–200	• High rate of deposition • Low cost	• Line of sight • Decomposition induced through high temp. • Amorphous coating (rapid cooling)
Sputter coating	0.5–5	• Uniform coating thickness • Dense coating	• Line of sight • Expensive & time consuming • Amorphous coatings
Pulsed laser deposition	0.05–5	• Crystalline & amorphous coatings • Dense and porous coatings	• Line of sight
Dynamic mixing method	0.05–1.3	• High adhesive strength	• Line of sight • Expensive • Amorphous coatings
Dip coating	50–500	• Inexpensive • Quick deposition • Complex substrates possible	• High sintering temp. • Thermal expansion mismatch
Sol–gel	<1	• Complex shapes possible • Low processing temp. • Cheap coatings (very thin)	• May require controlled atmosphere • Expensive raw materials
Electrophoretic deposition	100–2000	• Uniform coating thickness • Rapid deposition • Complex substrates possible	• Difficult to prevent cracking • High sintering temp.
Biomimetic coating	<30	• Low processing temp. • Can form bone-like apatite • Complex shapes possible • Can incorporate bone growth stimulating factors	• Time consuming • Requires replenishment • Constant pH necessary (SBF)
Hot isostatic pressing	200–2000	• Dense coatings	• Cannot coat complex structures • High temp. • Thermal expansion mismatch • Elastic property differences • Expensive • Removal/interaction of encapsulated material
Plasma electrolytic oxidation	5–100	• Can produce uniform, porous ceramic coatings • High adhesion • Can aid corrosion resistance of underlying substrate. • Various microstructures and thicknesses can be created	• Complex deposition mechanism, since the coating is persistently remade during deposition. • Difficult to generate high Ca content coatings due to limited solubility of Ca salts.

Table adapted and extended from Yang et al. [100].

for assessing bone-bonding capabilities through apatite formation. The review draws upon an additional review by Zadpoor [121], in which of 33 studies investigated, only 76% (25/33) predicted *in vivo* bioactivity through the *in vitro* SBF method, with 5 of the 8 that did not predict bioactivity, demonstrating no apatite formation on any of the biomaterials tested. Other predictive *in vitro* environments exist to understand specific medical material/implant applications. For example, artificial saliva since its local environment is significantly different to most orthopaedic scenarios.

Both classical (direct nucleation) and non-classical (amorphous calcium phosphate as the precursor) pathways have been studied extensively in the literature, with the study by He et al. [122] demonstrating via *in situ* liquid cell transmission electron microscopy a more in-depth perspective. It was found that mineralisation initiates due to ion-rich and ion-poor (Ca^{2+} and PO_4^{3-}) solutions, with both classical and non-classical nucleation pathways observed. The ion-rich and ion-poor solutions phase separate, with the driving force for HA crystal growth being the reduction in surface energy, followed by agglomeration and coalescence. A schematic, taken from the study by He et al. is provided below (Figure 4).

The inception of bioactive titanates and their apatite-forming potential

The first studies that introduced alkali and heat treatment processes in order to improve Ti biocompatibility were by Kokubo et al. and Kim et al. in 1996 [23,24]. Their work was followed on from corrosion studies by Revie et al. [123], Hurlen et al. [124], Arsov et al. [125], and Prusi et al. [126], who suggested that hydrated TiO_2 would be produced in alkaline solutions such as KOH. This work was then carried further by Li et al., who demonstrated TiO_2 gels (produced via sol–gel method) successfully induced bone-like apatite in

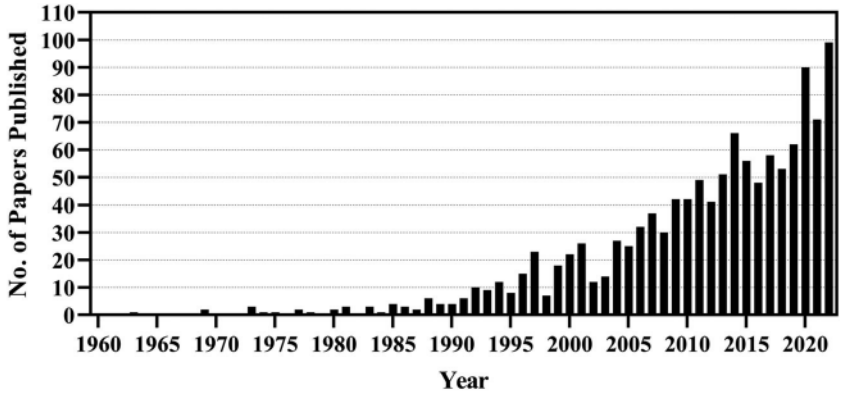

Figure 3. Number of papers published in Scopus using the Boolean search: "titanate" AND ("*medical" OR "bioactive" OR "wet chemical") up to, and including, November 2022.

SBF [113]. Kim et al. hypothesised that if such layers could be subsequently generated *in vivo*, bone-like apatite may be generated, enhancing the bioactivity of such a surface [23]. The initial alkali-treatment outlined by Kim et al. consisted of a 5–10 M NaOH or KOH (5 mL at 60°C) treatment of Ti or Ti alloy substrates for 24 h, followed by rinsing in distilled water, ultrasonic cleaning for 5 min and air drying at 40°C. Subsequently, heat treatments were also incorporated to increase the stability of the produced titanate structure (the methodology of which is outlined in Figure 5) [127].

The mechanism of sodium titanate formation

Initially, the passivated surface layer, TiO_2, is partially dissolved by the alkali solution:

$$TiO_2 + OH^- \rightarrow HTiO_3^- \quad (1)$$

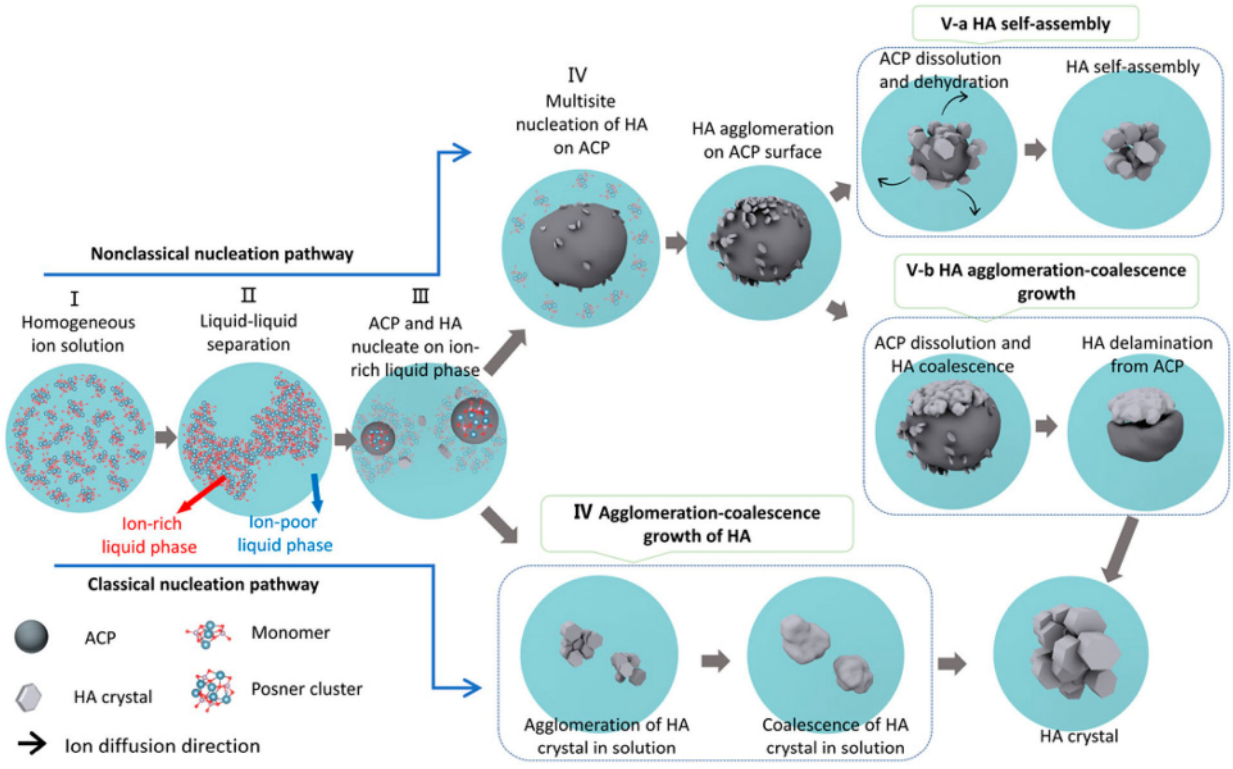

Figure 4. Schematic representation of the HA crystallization pathways. HA crystal formation can be divided into classical and non-classical nucleation pathways. For the non-classical nucleation pathway, there are five stages: homogeneous ions in solution (stage I), liquid–liquid separation forming ion-poor and ion-rich liquid phases (stage II), the formation of ACP and HA in ion-rich liquid phase (stage III), multisite heterogeneous nucleation of HA on the surface of ACP (stage IV) and ACP-HA phase transformation (stage V). Stage V can proceed by two different scenarios: One is HA growth only by ACP dissolution–HA reprecipitation followed by HA self-assembly (stage V-a), and the other one is the ACP dissolution–HA reprecipitation followed by HA growth via agglomeration and coalescence and then delamination from ACP (stage V-b). For the classical nucleation pathway, in stage III, the HA crystals directly nucleate from the ion-rich liquid phase. The HA crystals grow by agglomeration and coalescence (stage IV, bottom). Reproduced from He et al. [122], with permission from Science.

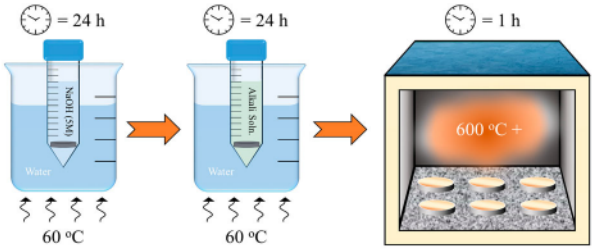

Figure 5. Full methodology of titanate conversion, including intermediate ion-exchange steps in order to convert the produced sodium titanate structures into alternative alkali titanates described in this review. Furthermore, the final furnace heat treatment stage is also outlined in order to increase the stability of the produced titanate structures through crystallisation.

As demonstrated by numerous studies [124,125,128–131], the above reaction occurs concurrently with the hydration of the Ti metal; Equations (2–4), causing oxygen penetration into the top 1 μm of the surface.

$$Ti + 3OH^- \rightarrow Ti(OH)_3^+ + 4e^- \quad (2)$$

$$Ti(OH)_3^+ + e^- \rightarrow TiO_2 \cdot H_2O + \left(\frac{1}{2}H_2\right) \uparrow \quad (3)$$

$$Ti(OH)_3^+ + OH^- \rightarrow Ti(OH)_4 \quad (4)$$

The negatively charged $HTiO_3^-$ generated through the alkali attack combine with the alkali ions present within solution, most notably Na^+, which results in an alkali-titanate layer, with the chemical formula: $M_xH_{2-x}Ti_yO_{2y+1}$; $0 < x < 2$ and $y = 2,\ 3,$ or 4. The depth of penetration for both sodium and oxygen is ca. 1 μm with ca. 8 at.% Na at the surface [132]. Heat treatment of the samples was then conducted between 400 and 800°C for 1 h to assess the effects on the formed layer [23]. The original amorphous sodium titanate that was formed during the NaOH treatment, partially converted into crystalline sodium titanate at temperatures above 600°C, with small quantities of rutile (TiO_2) also being formed (XRD; Figure 6). By 800°C, fully crystalline rutile and sodium titanate had formed, with no amorphous layers present. The sodium titanate formed following heat treatment is isomorphic to the layer formed initially [132]. Not only can this process occur on pure Ti, but its applicability to medically relevant Ti alloys, including Ti–6Al–4V, Ti–6AL–2Nb–Ta, and Ti–15Mo–5Zr–3Al [23,24,133,134], is also seen.

Successful formation of sodium titanate structures has also been seen on equiatomic NiTi SMA [135–140]. As described previously (Section Advantages of Ti as a biomedical material), NiTi has a varied history, due in part to its corrosion resistance, and leaching of the potentially immunogenic, toxic and carcinogenic Ni ions [68]. It was, therefore, a natural step to attempt

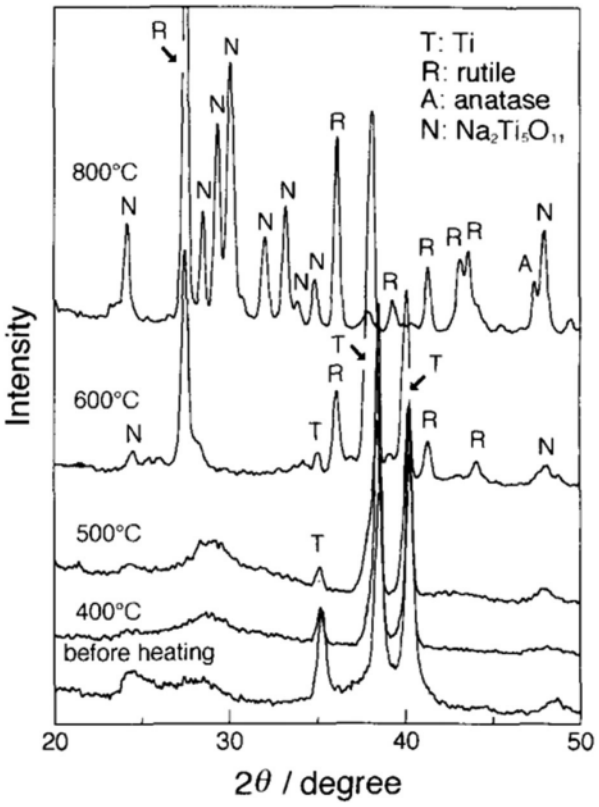

Figure 6. XRD patterns of the surface of Ti substrate treated with 10M NaOH at 60°C for 24 h and heated at various temperatures for 1 h. Reproduced from Kim et al. [23], with permission from Wiley.

to modify the surface of NiTi devices, to not only improve corrosion resistance, but to also enhance the biological properties. However, when attempting to utilise the same sodium titanate modification process, it was found that this alone is detrimental to its corrosion resistance. This is likely due to alkali attack of the surface enhancing Ni leaching, as well as the formed sodium titanate layer exhibiting less corrosion resistance than inherent passivated titanium oxide layers (i_{corr} = ca. 1×10^{-4} *v.* 3.9×10^{-5} A cm^{-2}, respectively) [135,138]. Therefore, most studies on NiTi require additional coating (e.g. hexadecyltrimethoxysilane [135,138]) of the sodium titanate-modified surface to allow its utilisation, for example in cardiovascular applications.

A more recent study by Conforto et al. [141] illustrates that these early interpretations may not be fully correct. Here, diffraction rings were clearly present in TEM diffraction patterns, thus it is likely to be nanocrystalline in nature rather than amorphous, with a monoclinic structure of $Na_2Ti_6O_{13}$. Indeed in the original XRD (Figure 6) in the pre-heat-treated sample, broad peaks are present, which is indicative of nanocrystallinity [142]. Kim et al. [23] interpreted the crystalline titanate structure as $Na_2Ti_5O_{11}$; however, a study by Bamberger and Begun [143] highlighted that this structure is unlikely to exist, with the monoclinic $Na_2Ti_6O_{13}$ structure being more likely, in the

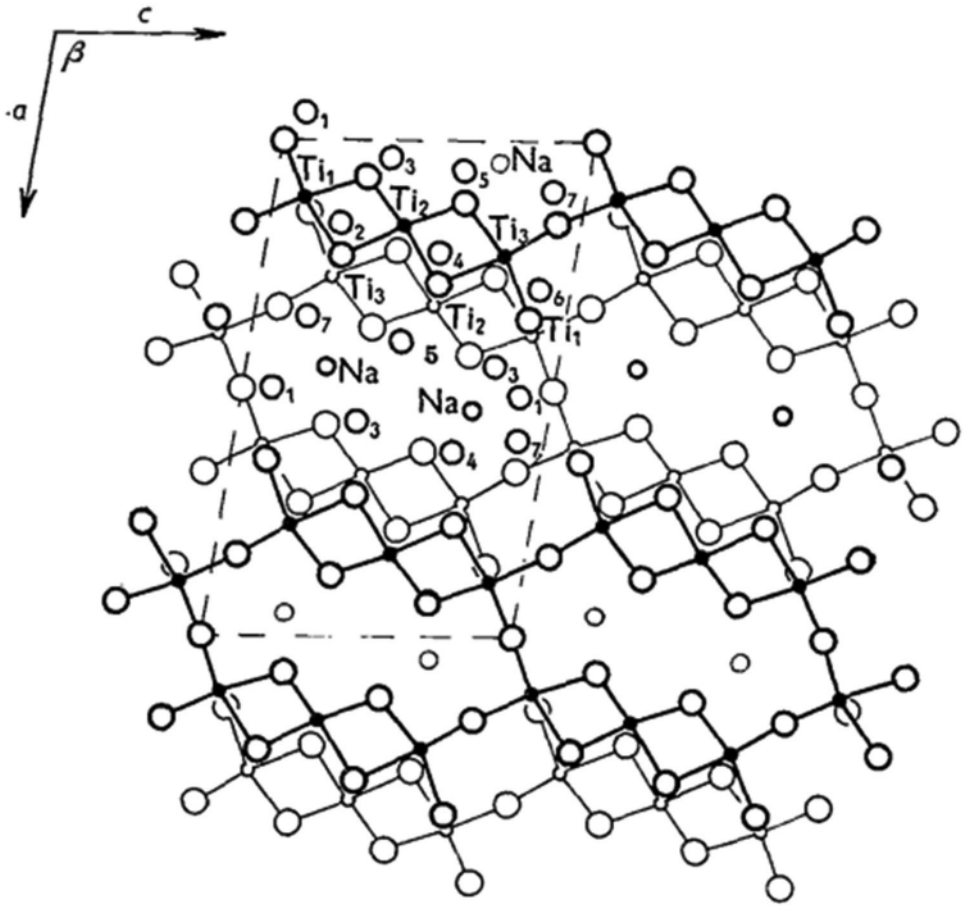

Figure 7. Structure of $Na_2Ti_6O_{13}$, as illustrated by Andersson and Wadsley [144], projected on to (010). Small circles are titanium, medium are sodium and the largest, oxygen. The atoms in heavier outline are at $y = 0$ and the lighter at $y = ½$. Reproduced with permission of the International Union of Crystallography.

general form $A_2Ti_nO_{2n+1}$. The structure, illustrated in Figure 7, has unit cell dimensions of $a = 15.131 \pm 0.002$ Å, $b = 3.745 \pm 0.002$ Å, $c = 9.159 \pm 0.002$ Å, $\beta = 99.30 \pm 0.05°$, with a crystal space group of C2/*m*, C_{2h}^3 ($Z = 2$) [143,144].

Apatite formation mechanism of alkali-titanate surfaces

Apatite formation (pictorially described in Figure 8) occurs on alkaline titanate surfaces through complex ion-exchange reactions either *in vitro* in SBF or *in vivo*. The level of electrostatic attraction of Na^+ within the sodium titanate layer is not enough to hold it in place when H_3O^+ ions are in solution. Therefore, the exchange of H_3O^+ with Na^+ results in Ti–OH bonds forming on the surface. Furthermore, this reaction causes an increase in the pH of the environment surrounding the surface, which in turn causes the surface to become negatively charged, as detailed by Gold et al. [145]. The mechanism of apatite formation is a result of research data conducted by various research groups [14,146,147].

Takadama et al. used X-ray Photoelectron Spectroscopy (XPS) and X-ray Diffraction (XRD) to quantify the composition of the top surface layers of the substrate [146]. It was found (Figure 9) that HA formation began at around day 2, with complete conversion occurring within 3 days. Furthermore, high-resolution scans of Ca 2p, O 1s, Na 1s and P 2p all corroborated the initial findings. From the Na 1s spectra, Na^+ began eluting within 30 min, while Ca 2p peaks were found as early as 30 min (deconvoluted as calcium titanate: $Ca_3Ti_2O_7$). The Ca 2p peaks exhibited a slight shift in binding energy at 2 days, which was deconvoluted as hydroxyapatite. P 2p did not exhibit a peak until 48 h submersion in SBF, indicating Ca had ion exchanged into the surface prior to the attraction of phosphate ions onto the surface. However, the most significant piece of data was the formation of Ti–OH bonds within 30 min of SBF immersion. This partially confirmed the hypothesis that these bonds were essential for indirect apatite formation through calcium titanate formation [146].

XPS results were corroborated by Takadama et al. whereby transition electron microscopy (TEM) combined with energy-dispersive X-ray (EDX) analysis was employed to understand the structural alteration during apatite formation [14]. Initially, a fine network structure of ca. 500 nm was observed on the alkali- and heat-treated samples. Upon immersion in SBF, Ca inclusion was noted within 0.5 h, with an

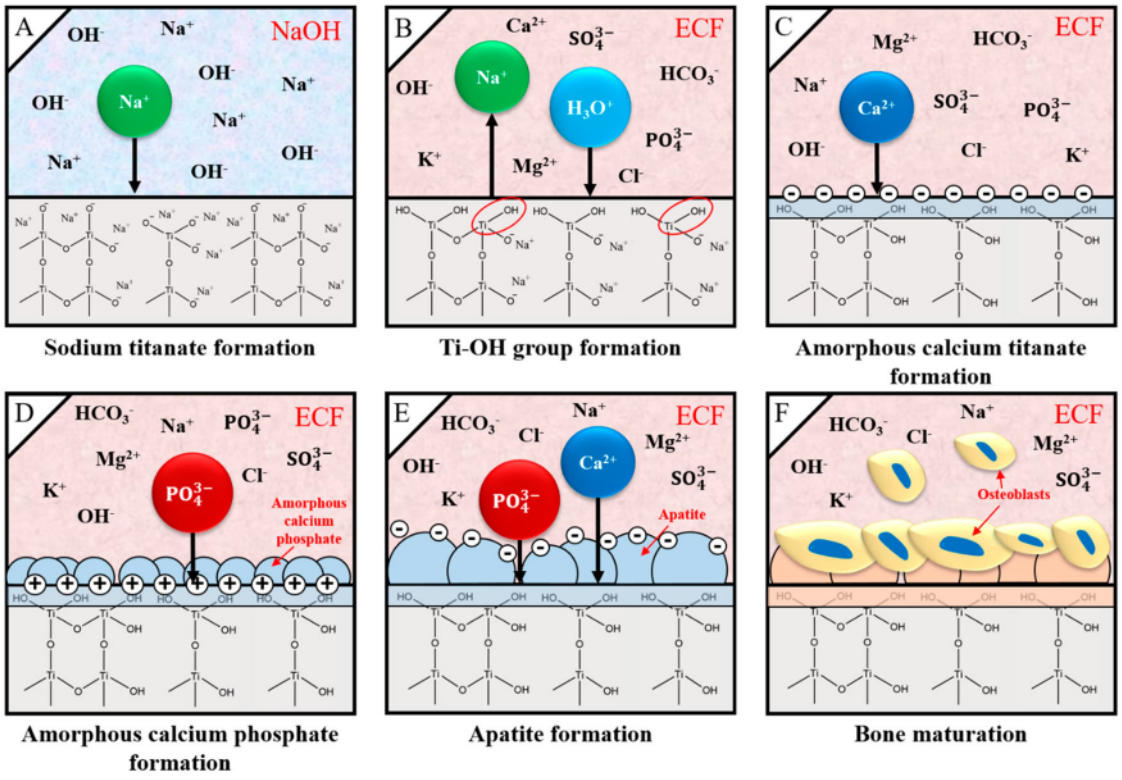

Figure 8. Schematic diagram demonstrating a simplistic mechanism of apatite formation through conversion of sodium titanate structures. (A) Details of the formation of sodium titanate through the diffusion of Na and O into the thin (ca. 5 nm) passivated TiO_2 layer. (B) shows the ion-exchange of Na^+ for H_3O^+ (hydronium) ions in solution, to form Ti–OH groups on the surface. (C) Due to the negative Zeta potential of this surface, positively charged Ca^{2+} ions are electrostatically attracted to the surface, forming an amorphous calcium titanate. (D) The relative abundance of Ca^{2+} ions on the surface forms a positively charged surface, which electrostatically attracts phosphate (PO_4^{3-}) ions to produce an amorphous calcium phosphate layer. (E) Over time, this layer can convert through further ion-exchange reactions, into apatite. (F) Osteoblast action eventually will convert this layer into bone, enabling 'natural' adhesion and integration between the implant and the surrounding environment.

amorphous calcium titanate and calcium phosphate (Ca:P = 1.4) forming within 24 and 36 h, respectively. By 72 h, the Ca:P ratio was approximately 1.65, close to stoichiometric HA (1.67) [14]. Yamaguchi et al. further demonstrated the morphological changes that occurred during the submersion of sodium titanate layers within SBF, producing apatite as seen in Figure 10 [148].

Li et al. explored vacuum pressures during the heat treatment process (ca. 10^5–10^{-3} Pa) [149]. Their results showed that at higher vacuum pressures, the structure exhibited larger pores sizes, while improving the HA formability in SBF [149]. Takedama et al. postulated that the formation of apatite on alkali-treated titanium occurred through electrostatic interactions between the surface, and specific ions within the aqueous solution [14]. Kim et al. investigated Zeta (ζ) potential, in regard to soaking time in SBF [147]. The ζ potential (V) was quantified using the Smoluchowski equation [150], seen below:

$$\zeta = \frac{\eta u_e}{\varepsilon_r \varepsilon_0}$$

where u_e is the electrophoretic particle mobility ($m^2V^{-1}s^{-1}$), η is the solution viscosity (Pa s (or N s m^{-2})), ε_r is the relative permittivity/dielectric constant and ε_0 is the permittivity of a vacuum (8.8×10^{-12} Fm^{-1} (or NV^{-2})). The work corroborated that ion-exchange reactions between Na^+ and H_3O^+ occurred first, generating negative Ti–OH bonds (negative ζ potential), which then attracted positive Ca^{2+} (increasing the ζ potential due to localised Ca^{2+} concentrations), followed by negative phosphate ions, forming calcium titanate (within 0.5 h) and calcium phosphate (within 42 h), respectively (Figure 11) [147]. Within 72 h, apatite had been formed on the surface, due to the much lower solubility of HA with respect to calcium phosphate in the body environment. Furthermore, it is well known that HA has a negative charge in the body environment due to the presence of hydroxyl and phosphate groups on its surface, as demonstrated by the potential at 72 h (Figure 11) [151]. Interestingly, a trend that has been seen in a few studies [147,152], is the incorporation of carbonate, sodium and magnesium into the apatite layer formed in SBF, which is more akin to that of bone-like apatite. This is due to the SBF being supersaturated with respect to apatite even under normal conditions [153].

In order to completely assess the dependence of pH of the treatment medium on apatite formation,

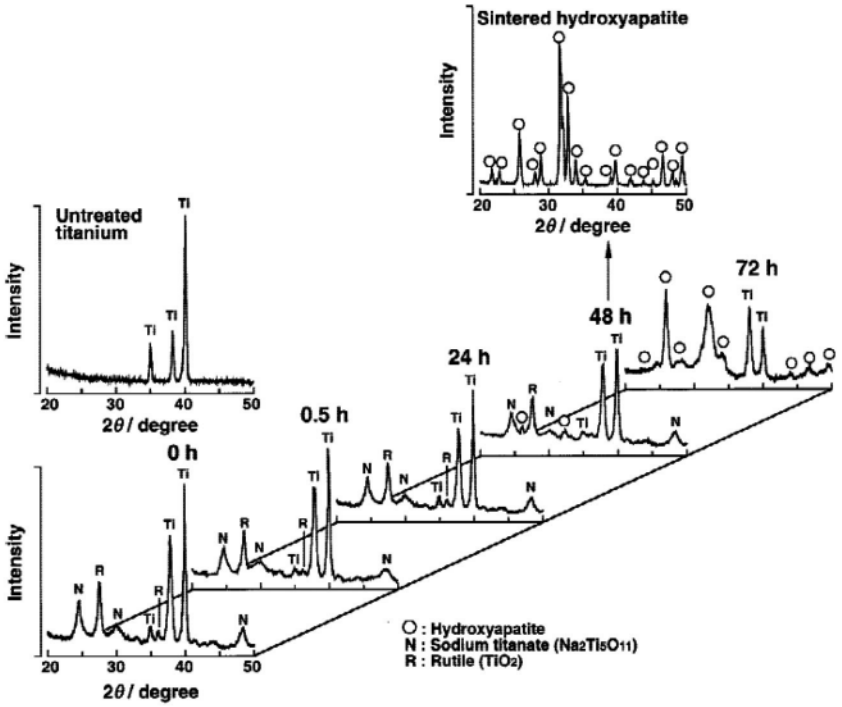

Figure 9. XRD spectra of sodium titanate surfaces and their transformation into apatite following submersion in SBF over 72 h. Figure reproduced from Takadama et al. [146], with permission from John Wiley and Sons.

systematic alteration of NaOH and HCl solution pH from 0 to 14 was conducted at 60°C for 24 h, followed by heat treatment at 600°C. The study by Pattanayak et al. indicated a pH of $1.1 \leq x \leq 13.6$ inhibited the occurrence of apatite formation, while pH values below 1.1 and above 13.6 generated apatite within 3 days (Figure 12(A)) [154]. It was also demonstrated that apatite formation depends on the surface charge, rather than surface roughness and specific crystalline phases. When Ti metal is subjected to acid treatment, as outlined previously, followed by subsequent heat treatment, the surface ζ potential is positive (Figure 12 (B)). Conversely, for alkali-treated substrates, the ζ potential is negative. The theory that ζ potential affects apatite formation is further substantiated through the fact that natural Ti, despite the same heat treatment process, does not generate apatite on its surface, since the surface ζ potential is neutral (Figure 12(C)) [154].

Further reactions occur within the aqueous SBF solution, whereby, the negative surface attracts Ca^{2+}, forming an amorphous calcium titanate surface. The accumulation of Ca^{2+} ions result in an overall positive surface charge, which subsequently attracts PO_4^{3-} (phosphate) ions, forming an amorphous calcium phosphate. This surface is metastable and subsequently matures into apatite, which was found to occur within 3 days in SBF [148].

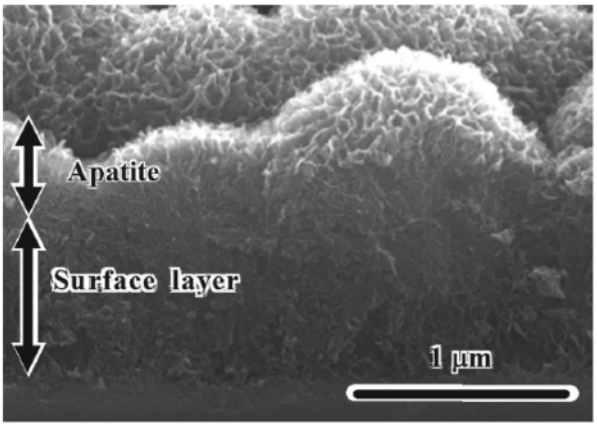

Figure 10. SEM image of the formation of apatite on the surface of alkali- and heat-treated titanium surfaces after 1-day immersion in SBF. Figure reproduced from Yamaguchi et al. [148], with permission from The Ceramic Society of Japan.

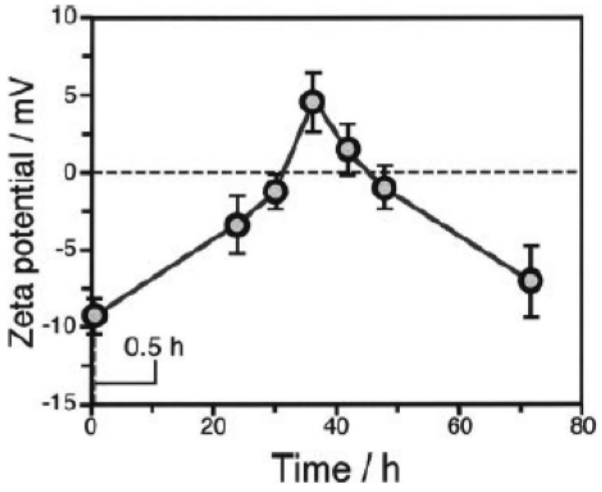

Figure 11. Zeta (ζ) surface potential as a function of soaking time in SBF. Figure reproduced from Kim et al. [147], with permission from John Wiley and Sons.

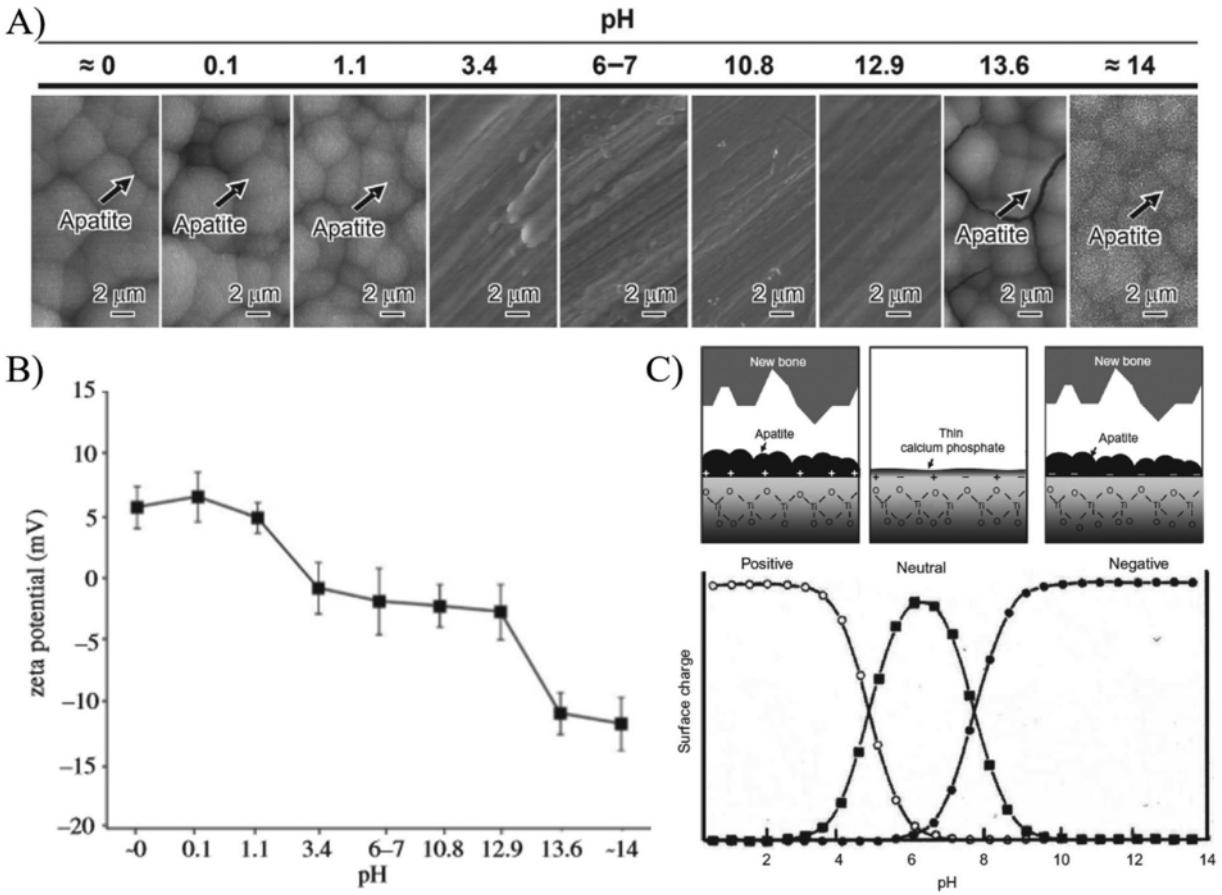

Figure 12. (A) Morphological changes as a function of solution pH during alkali-/acid treatment of Ti substrates. (B) Zeta (ζ) potential measurements as a function of solution pH. (C) Representation of surface charge with respect to solution pH, and its effect on apatite formation on the surface. Figures adapted from Pattanayak et al. [154], with permission from the Royal Society.

Development of novel titanate structures for biomedical applications

Novel titanate structures have been explored, typically as composite coatings, porous scaffolds, orthopaedic microspheres, and protein/drug delivery carriers. These have been derived to achieve more cost-effective manufacturing routes, with targeted, location-specific biological effects. For example, Mozafari et al. formulated 50–125 nm $ZrTiO_4$/Bioactive glass thin films via sol–gel followed by spin coating to form consecutive multi layers [155]. In a methods article by Triviño-Bolaños et al. [156], sodium titanate was moulded, pressed and sintered to form porous rutile $TiO_2/Na_{0.8}Ti_4O_8/Na_2Ti_6O_{13}$ scaffolds to eliminate the use of toxic solvents often used in nanoparticle synthesis and/or to reduce costs associated with methods such as hydrothermal synthesis. Further examples of porous scaffolds (ca. 75% porosity via MicroCT, ca. 100–500 μm pore sizes, with ca. 100 μm wide struts) were developed by a slurry coating of polymer foams using TiNbZr powders, which were sintered and followed by hydrothermal titanate formation to mimic geometries of cancellous bone (Figure 13(A)) [157]. In addition, electrochemical routes by anodic oxidation have been used within the literature to form 'nanoflower-like' titanate coatings, driven by applied voltages/currents or 350 V and 70 mA cm^{-2} in a custom electrolyte of β-glycerophosphate, calcium acetate and NaOH. The high surface area nanoflower-like constructs were found to be bioactive in SBF, in good agreement with previous alkaline titanate studies (Figure 13(B)) [158].

Bio-silks, which are readily developed for medical composite matrices and are generated out of silk fibroin, have been altered to increase mechanical performance by integration of 2D titanate nanosheets followed by ion-exchange reactions with silver solutions for antibacterial dental applications [159]. By incorporating nanoparticles within the silk matrix, a change in the mechanical properties can be achieved through interaction between the particles and the fibroin chains. An alternative application by Colusso et al. showed silk titanate multilayers fabricated by consecutive spin coating with an ability to change colour based on atmospheric humidity changes applicable in sensing applications, which may be utilisable in a biomedical setting to provide minimally invasive detection and/or diagnosis. Modifying the relative humidity range from 10 to 80% induced repeatable modification in the transmittance wavelength, attributed to the change in refractive index of the multilayer due to swelling via water

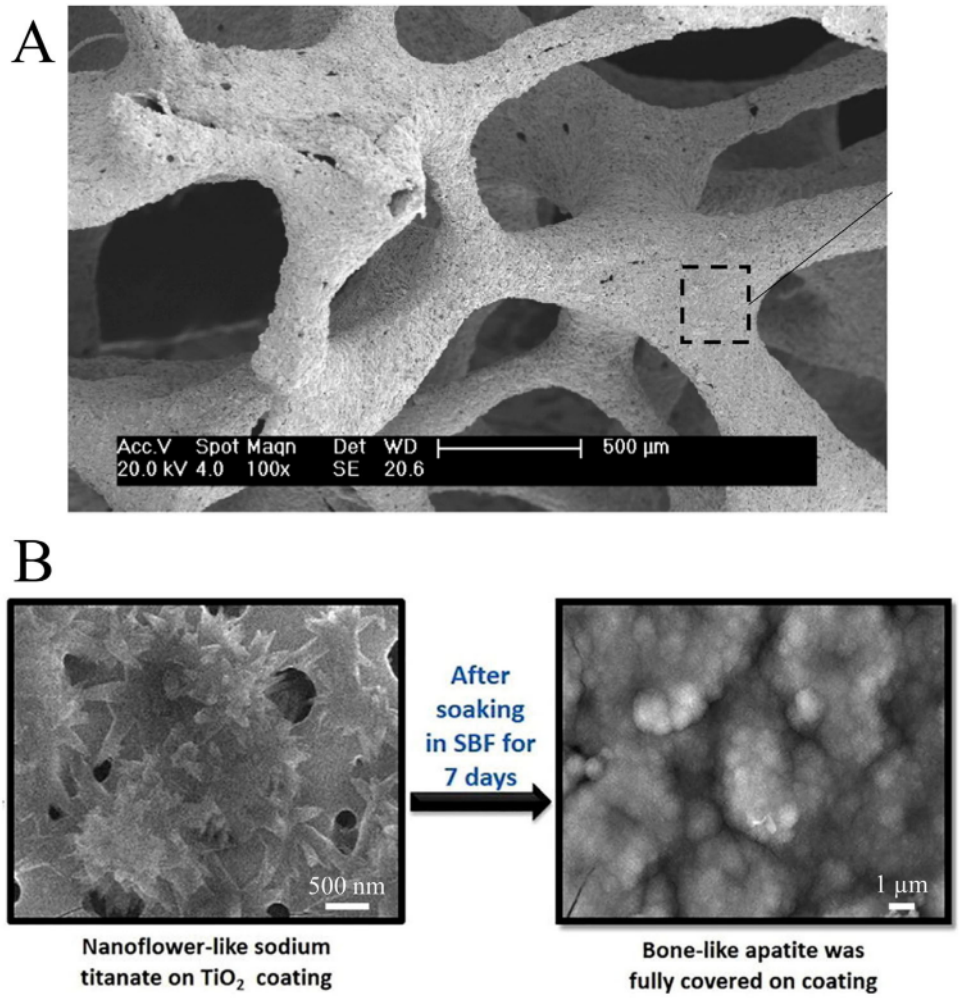

Figure 13. (A) SEM micrograph of hydrothermally treated porous TiNbZr scaffolds. Reprinted from Rao et al. [157] with permission from Elsevier; (B) Formation of nanoflower-like sodium titanate on a TiO_2 coating via anodic oxidation. Reprinted from Lee et al. [158] with permission from Elsevier.

uptake and bonding. The titanate-containing silk generated a greater response compared to silk alone, due to the negatively charged titanate nanosheets interacting more with water [160].

Nano-grid titanate geometries have been produced by anodising Ti foil, such as by Zhang et al., which additionally introduced zinc through hydrothermal incorporation and showed *in vitro* potential for anti-tumour osteosarcoma applications (Figure 14) [161]. ZnO nanorods or nano particles have been used for anti-tumour applications in the past; however, their ease of detachment from the implant results in lower efficacy, hence, loading of Zn into these nano-grid structures. Nano-grids with a Zn content of 0.15 M were found to be optimal, had affirmatory abilities to significantly inhibit UMR-106 tumour growth *in vivo* and had no impairment to the body. The geometry of these structures is of importance to biomaterial

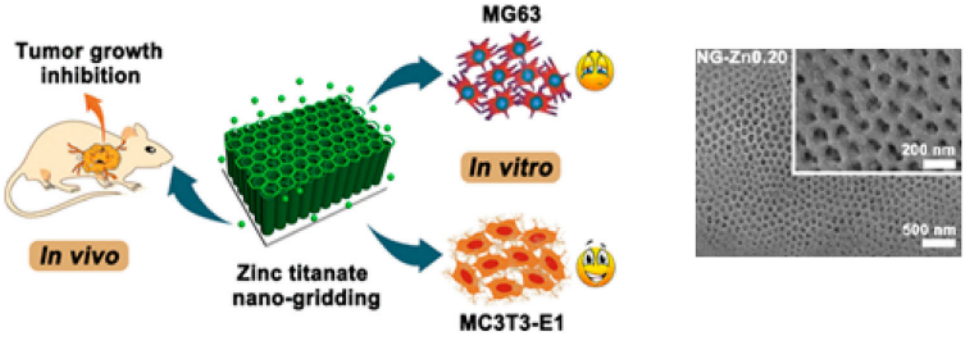

Figure 14. Schematic and surface SEM micrographs of the utilisation of zinc titanate nano-grids for the use as a treatment for osteosarcoma. Reproduced from Zhang et al. [161], with permission of the American Chemical Society.

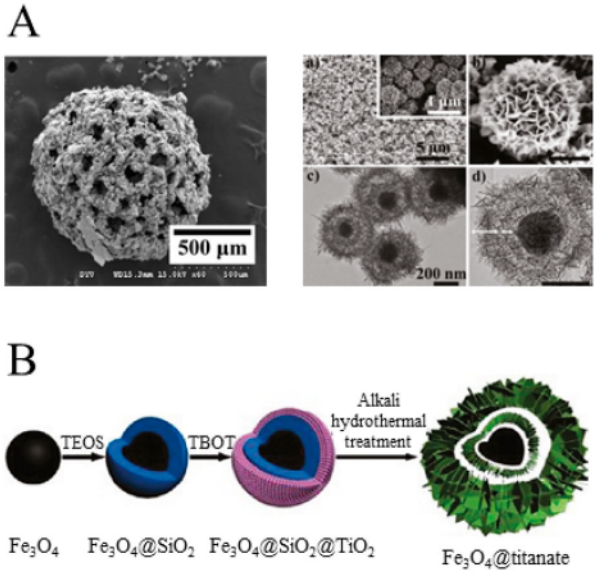

Figure 15. (A) SEM micrograph demonstrating the morphology of a titanium microsphere made porous through the use of a camphene porogen. Reprinted from Hsu et al. [163] with permission from Elsevier; (B) Schematic illustration of the formation process of the Fe_3O_4@titanate double-shelled yolk-shell microspheres. Reprinted with permission from Li et al. [165]. Copyright (2011) American Chemical Society.

applications, due to not only enhanced release of beneficial ions, but also enhanced adhesion, migration and proliferation of normal osteoblasts.

Hsu et al. developed titanate microspheres using a water-in-oil emulsion method and a non-toxic camphene porogen for titanium. Orthopaedic microspheres are often formed of Ca/P ceramic and glasses for injecting into bone, cartilage or muscle as a regenerative filler with enhanced cell infiltration [162]. Here titanate spheres contained up to 74% porosity with pore sizes up to 200 µm (Figure 15(A)) [163]. Silica- and Nb-substitution into the titanate structure was shown by Milosevic et al. to improve absorption of Ovalbumin, gentamicin and methyl blue with 1 g of titanate absorbing between 9 and 90 mg at pH 5.0–7.0 and showing desorption characteristics at pH 7.0 indicating the potential of substituted-titanate structure for protein/drug delivery [164]. Li et al. produced magnetic yolk-shell titanate microspheres of ca. 560 nm in diameter, which were produced using an Fe_2O_3 core coated with SiO_2 and TiO_2, followed by titanate formation for catalysis applications; however, their potential could be extended to MRI imaging (Figure 15(B)) [165].

Nanostructures: from nanotubes to nanograins

Nano-geometries of alkaline titanate structures are of interest since they can increase effective surface area and therefore cellular interaction rates for biomedical applications and nanotubes have been developed as a carrier material for cellular stimuli, such as proteins or delivery of therapeutic ions owing to the ease of functionalisation. In 1998, Kasuga et al. first reported synthesised nanotubes of ca. 8 and 100 nm in diameter and length, respectively, with surface areas of ca. 400 $m^2\,g^{-1}$ from sol–gel produced TiO_2 powders via a hydrothermal reaction at 120 °C [166]. Nanotubes and nanosheets of $Na_2TiO_3O_7$ have been formed using a commercially available P25 TiO_2 nanoparticle precursor. TiO_2 powders (21 nm diameter) treated in NaOH solutions at temperatures up to 150°C exhibited increased surface areas from 66 to 337 $m^2\,g^{-1}$ due to the resultant formation of 50 nm diameter tubes, that were hundreds of nm in length [167]. Similar tubes were electrochemically deposited onto Si substrates for use as optical/semiconductor films by Kim et al. [168] while other manufacturing modifications have successfully produced elongated tubes by rotating particles at up to 20 $rev.min^{-1}$ during synthesis [169]. The P25 TiO_2 hydrothermally-derived titanate nanotubes were tested with rat cardiomyocytes and were shown to be cytocompatible over 24 h, despite reporting endocytosis and diffusion of particles into the cell, suggesting potential future cardiovascular applications (Figure 16) [170]. The authors went a step further by exploiting the presence of negatively charged surface hydroxyls to bond polyethylene glycol (PEG) and polyethylene imine (PEI) for therapeutic and gene therapy applications also showing no cytotoxic effects on cardiomyocytes in concentrations up to 10 $\mu g\,mL^{-1}$ [171].

More recently, Rodrigues et al. highlighted the potential for rare earth (La^{3+}, Ce^{4+}, Pr^{3+}, Nd^{3+}, Er^{3+} and Yb^{3+}) doping of sodium titanate nanotubes generated via a microwave assisted hydrothermal method [172]. The synthesised nanotubes were then thermally treated (200, 400, 600 and 800°C, 2 h) in order to produce structural and morphological changes which ultimately can modify their optical properties. However, in the context of implantable medical devices, these materials will be significantly limited due to the toxicity of the RE elements.

Alkaline titanate nano-whiskers, specifically K_2TiO_3 and $K_2Ti_4O_9$, were found to be bioactive in SBF over a 12-d period, precipitating calcium titanate, Ca/P, and hydroxyapatite on their surface [173]. Zhao et al. formed nanowire scaffolds by hydrothermal treatment of Ti substrates, which were post coated with electrochemically deposited hydroxyapatite. They showed encouraging proliferation and differentiation of MG63 osteoblast cells after 7 days [174].

Titanate, titanium-based metallic and titanium-incorporated glasses

Another important class of titanate materials are titanate glasses. In a biomedical context, glasses have been widely used from biodegradable, bioactive coating and scaffold materials to enhance osseointegration [175], to cancer detection through fibreoptic cables [176]. The glass structure is highly modifiable through the

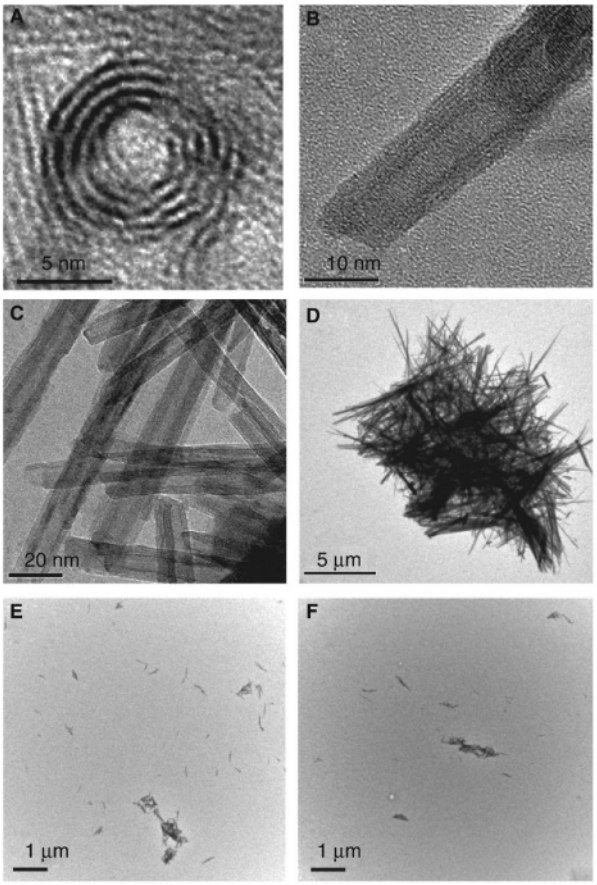

Figure 16. HRTEM images of (A) a titanate nanotube cross-section with inner cavity and spiral morphology, (B) a titanate nanotube ($TiON_{ts}$) and one of its open ends. TEM images (C,D) of $TiON_{ts}$ after hydrothermal treatment and washings to reach pH6, (E,F) of $TiON_{ts}$ after PEI_{1800} adsorption onto their surface with the following $TiON_{ts}$:PEI weight to weight ratios: (E) 1:1 and (F) 1:10. Reproduced from [170] with permission from Taylor & Francis.

incorporation of elements. For example, the bulk glass composition can be modified to illicit controllable degradation profiles [177], which can be utilised in bone repair scenarios [178]. Titanium-based glasses pose a novel alternative to presently used glasses, such that their mechanical properties are significantly higher than conventional glasses in tensile loading (1.4–2 GPa *v.* ca. 7 MPa for a typical glass [179]), as well as the ability to dope such structures with functional ions. This will enable wider use of glass structures in medical applications, such as load-bearing scenarios, which they have been limited previously. In this review, we compare titanate glasses with titanium-based metallic and titanium-incorporated glasses.

Titanate glasses were first reported by Jijian et al. in 1986 and contained up to 60 wt-% TiO_2 [180]. High-density (up to 4.5 g cm^{-3}) barium titanate glass microspheres have shown promise for high-resolution imaging of biological samples [181]. In contrast to titanate structures, titanium-based metallic glasses within the biomedical field are interesting candidates for non-corrosive, load-bearing applications. Titanium metallic glass alloys exhibit mechanical properties, such as tensile strength (ca. 1.4–2 GPa [182]) and elastic strain limit (up to 2% [183]), which supersede that of implant materials, such as Ti6Al4V (0.85–1.1 GPa [182]). Reported manufacturing routes are so far limited to melt casting of small (up to 6mm diameter) rods and spin casting of 30 µm ribbons, Qin et al. [184] and Jiang et al. [185], respectively. Titanium glasses have a relatively high glass-forming window, in compositions from $Ti_{10}Zr_{30}Cu_{60}$ [185] to $Ti_{40}Zr_{10}Cu_{36}Pd_{14}$ [184]; however, high-resolution TEM revealed nanocrystals of up to 15 nm embedded within the amorphous matrix for $Ti_{10}Zr_{30}Cu_{60}$ composition suggesting a glass-forming limit. $Ti_{40}Zr_{10}Cu_{36}Pd_{14}$ glasses can be treated in a NaOH solution to form sodium titanate prior to submerging in Hanks Balanced Salt Solution (HBSS) for 30 days to observe formation of an apatite layer, suggesting limited *in vitro* reactivity [184].

Another approach is to use TiO_2 inclusions in phosphate-based glasses (PBGs). Examples include 25 mol-% TiO_2 to improve network connectivity by increasing ionic cross-linking between phosphate units and/or positioning itself within the structural backbone to reduce the prevalence of P–O–P chains, which 'depolymerise' by hydrolysis [186]. Alternatively, Das et al. melt quenched anti-wear strontium bismuth titanate borosilicates glasses, using post-heat treatment for crystallisation of wear resistance ceramic phases, attributing TiO_3 units as effective nucleation sites for crystallisation [187].

Piezoelectric biomedical titanates

The interest in biomaterials that are piezoelectric stems from the piezoelectric properties of human bone (coefficient of ca. 0.7 pC/N) [188], which have been known to stimulate osteogenic cells to facilitate bone remodelling [189,190]. In particular, barium titanates ($BaTiO_3$) [191,192] have potential uses in piezoelectric medical composites, in particular, in medical imaging, due to its high refractive index (ca. 2.1) increasing imaging resolution by a factor of three [193]. To achieve sufficient electrical polarisation, 80 vol% $BaTiO_3$ has been desirable in orthopaedic structures [194]; below 70%, no measurable piezoelectric properties where found [195]. Bowen et al. [195] hypothesised the reason for the reduction in the piezoelectric properties was due to 'mechanical clamping' of the $BaTiO_3$ materials due to the stiffer HA matrix preventing adequate strain to be generated during poling. Further to the work by Bowen et al., Vouilloz et al. formed $BaTiO_3$-$Ca_{10}(PO_4)_6(OH_2)$ structures containing 20–80 vol% $BaTiO_3$. The produced structures demonstrated both cytotoxic and cytocompatible responses, depending on the level of $BaTiO_3$ used; the 80% $BaTiO_3$-HA sample was the only non-

cytotoxic composition after 72 h incubation [190]. Ions of Ba^{2+} were released, ca. 582–826 ppm by 72 h, due to the reactivity of less stable ceramic phases produced during the sintering process. However, less soluble composites, such as the 80% $BaTiO_3$-HA composite (244 ppm Ba^{2+}) formed non-soluble secondary phases ($CaTiO_3$ and $Ca_3(PO_4)_2$) and remained cytocompatible [190].

Generating porosity in such scaffolds adds to the potential medical application of these structures, since enhanced bone ingrowth combined with piezoelectric properties draws on the natural properties of bone. HA-coated $BaTiO_3$ porous scaffolds were generated by Etherami et al. and produced by the ceramic slurry coating of a polyurethane template (burned out in a post process) and dip coated with a Gelatine/HA layer. Gelatine was used to enhance the mechanical stability of the scaffolds, since it has been known to exhibit microscale crack-bridging properties, which leads to potential enhancement of the toughness of the scaffold, similar to collagen fibres in bone. The composite exhibited cytocompatibility with seeded MG63 osteoblast cells for up to 7 days, successfully adhering to and incorporating through the porous ceramic network, while the crystalline structures exhibited piezoelectric properties of 4.5 pC/N [189].

Other approaches to generate and improve medical piezoelectric materials include modifying $BaTiO_3$ structures with elements such as Ca, Sr, Zr and C, to improve electrical characteristics, mechanical properties and cellular cytocompatibility. Sr^{2+} ions have been reported to improve and suppress osteoblast and osteoclast proliferation, respectively, while increasing the dielectric constant in piezoelectric titanates; the increase is due to Sr^{2+} decreasing the oscillation space of Ti and distorts the structure of the ferroelectric domain [196]. Phromoyoo et al. added zirconia to increase the piezoelectric coefficient in egg shell synthesised β-TCP/$BaTiO_3$/Zr (β-TCP/BZT) composites showing enhanced mechanical hardness, due to the shift from intergranular to predominantly intragranular fracture, with >80 vol% needed to produce piezoelectric properties [188]. $BaTiO_3$ was electrodeposited by Rahmati et al. onto Ti6Al4V surfaces for their use as osteoinduction/piezoelectric coatings in load-bearing orthopaedic implants, such as hip stems or dental implants. *In vitro* bioactivity was confirmed by apatite formation 7 d post-submersion in simulated body fluids (SBF) [197].

Composite approaches have also been used, such as Beta-Tri Calcium Phosphate (β-TCP)/Sr-doped $BaTiO_3$ composites were 3D printed using polyvinyl chloride (PVC) as a binder to form Ca/P leaching osteogenic scaffolds. Other applications include fixation bone cements. Tang et al. mixed graphene and $BaTiO_3$ (30–80 vol%) into polymethyl methacrylate PMMA suggesting that 0.5 vol% graphene increased electrical conductivity and reduced the relative required proportion of $BaTiO_3$ to 60 vol%. Without graphene, they obtained a compromise between piezoelectric performance (achieving 0.33 pC/N at 60 vol% $BaTiO_3$) and compressive strength (ca. 85.3 MPa) showing similar strength to natural human bone. Graphene inclusion increased piezo performance to 0.8 pC/N attributed to improved charge transfer and remaining cytocompatible [198]. A comparative look at the various piezoelectric, material and chemical properties of alkaline titanate materials described within the literature, in comparison with human bone, has been compiled in Table 3.

Pre-modification: the potential for multifunctional surfaces with peroxide pre-treatment

A study by Janson et al. [208] has developed dual-functionality surfaces that incorporate titanate structures. This work, following on from previous work by Tengvall et al. [209], looked into the generation of a titanium-peroxy gel layer; suggested by Tengvall et al., to be:

$$[Ti^{4+}(OH^-)_xO_2^{2-}] - [Ti^{4+}(OH^-)_yO_2^-] - [Ti^{4+}(OH^-)_4] - TiO_2 \cdot n \cdot H_2O$$

where a hydrogen peroxide (H_2O_2) treatment of titanium has potential bactericidal properties. By combining a hydrogen peroxide treatment (30 wt-%, 80°C, 1 h), with subsequent sodium (5 M, 15 min) and calcium hydroxide (0.1 mM, 15 min) treatments, these surfaces demonstrated bactericidal effects (reduced viability by 93%) on *Staphylococcus epidermidis* through direct and biofilm inhibition tests, while ensuring cytocompatible surfaces to MC3T3 human dermal fibroblast cells [208]. Reduced soaking times in alkali media were utilised to lessen reactive oxygen species (ROS), which are toxic to both bacteria and potentially human cells. This approach's objective reduced the release of ROS species to prevent cytotoxicity, while maintaining bactericidal properties; this compromise is prevalent in many elution-based bactericidal materials, since human cells tend to be more susceptible compared to bacteria.

H_2O_2 pre-treatment is also effective for the formation of apatite on sodium titanate-treated NiTi alloys surfaces by Cheng-lin et al. [139]. It was found that H_2O_2 pre-treatment led to the creation of more Ti–OH groups, as well as reducing the amount of Ni_2O_3, Na_2TiO_3 and remnant NiTi phases. As a result, the induction period of apatite formation is shortened from >24 h to 12 h by the slow kinetic formation process of Ti–OH groups via the exchange of Na^+ ions from Na_2TiO_3 with H_3O^+ ions in SBF.

Table 3. Comparison of piezoelectric properties of various titanate materials compiled from literature, with particular emphasis on processing, microstructure, phase, porosity, mechanical, electrical and multifunctional properties, and the factors that affect them.

Material	Titanate content	Authors	d_{33} Piezoelectric coefficient (pC/N) (% = Titanate content)	Processing technique/parameters	Microstructure/Phase quantification	Porosity (%)/Density (g/cm^3)	Comments on mechanical/electrical/ multifunctional properties	Ref.
Human bone	0%	Anderson and Eriksson Phromyoo et al.	0.45–0.70	Dry and wet bone specimens	N/A	N/A	Bone is a naturally occurring piezoelectric material, which is purportedly the mechanism behind bone growth.	[188,199]
HA–$BaTiO_3$ composite	0–100%	Bowen et al.	<80% = 0 95% = 6–20 100% = 70–85	Pressure-less sintering: Ball milling in zirconia media plus binder, then cold pressed at 100 MPa. Sintered at 1300°C (2 h).	Two insulting phases: Pure $BaTiO_3$ and HA.	N/A	Stiffer HA matrix 'clamps' $BaTiO_3$ causing mechanical depolarisation and loss of piezoelectric properties. >90% $BaTiO_3$ required to achieve 6 pC/N (d_{33}).	[195]
$Ba(Ti_{1-x}Zr_x)O_3$	x = 0–0.3	Yu et al. Nanakorn et al.	N/A (Preliminary studies to the Phromyoo et al. paper)	Solid state/mixed oxide reaction: $BaCO_3$, TiO_2 and ZrO_2 powders were calcined at ca. 1200°C (2 h), then pressed into discs before sintering at ca. 1500°C.	Single perovskite phase with large grains (20–60 µm)	N/A ca. 5.78–5.85 g cm^{-3} (ca. 95% of theoretical density)	Incorporation of Zr into the $BaTiO_3$ structure enhances the dielectric constant. Zr is doped at the B-site, which results in lattice expansion, with decreasing grain size as Zr content increases. Furthermore, Zr doping results in reduction of the Curie point by ca. 4.5°C/(mol-% Zr) [200], which is critical since the Curie point defines the maximum dielectric constant.	[201,202]
β-TCP/ $Ba(Zr_{0.07}Ti_{0.93})O_3$ composites	0–80% BZT	Phromyoo et al.	80% = 40	β-TCP and BZT powder (both synthesised through ball milling and then firing at elevated temperatures) were ball milled followed by uniaxial pressing, before sintering at 1200–1500°C	Multiphase:β-TCP, BZT, $CaH_2O_7P_2$,$Ca_2O_7P_2$ and $CaTiO_3$	0% = 2.74 g/cm^3 60% = ca. 5 g/cm^3 80% = ca. 5.5 g/cm^3	Hardness (H_v), fracture toughness (K_{IC}) density and piezoelectric constant, all increased, and average grain size decreased, with increasing BZT concentration. Reasons: BZT (6.02 g cm^{-3}) has a higher density than β-TCP (2.74 g cm^{-3}). Mutual inhibition of grain growth, and shift from intergranular to intragranular cleavage. Piezoelectric constant is strongly dependent on phase filler, in this case, BZT.	[188]
HA–$BaTiO_3$ (Both commercial and synthesised BT and HA)	20–80%	Vouilloz et al.	80% = ca. 13 100% = ca. 37	Commercial and synthesised (mechanochemical) HA and $BaTiO_3$ powders were used. Composite powders were ball milled, hydraulically compacted, before sintering at 1250–1300°C	Multiphase: $BaTiO_3$ (with Ca^{2+} substitution), barium phosphate ($Ba_3(PO_4)_2$, and barium calcium phosphate ($Ba_{2.1}Ca_{0.9}(PO_4)_2$	20% BT = ca. 17% (ca. 3.07 g/cm^3) 40% BT = ca. 36% (ca. 2.74 g/cm^3) 60% BT = ca. 8% (ca. 4.46 g/cm^3) 80% BT = ca. 7% (ca. 5.09 g/cm^3)	Study interested in what phases form and their secondary effects on biotoxicity. High reactivity between BT and HA at higher HA compositions (>20 vol%) causes $Ba_3(PO_4)_2$ crystallisation and favours subsequent Ba^{2+} lixiviation, increasing biotoxicity. Porosity *v.* polarisation must be considered. High HA content results in a higher degree of porosity and osteoconduction; however, this inhibits polarisation due to the stiffer HA phase present.	[190]
$BaTiO_3$/HA blended scaffolds	100%	Polley et al.	3.08 ± 0.63	Blend of 68, 18 and 14 wt.% of $BaTiO_3$, HA and PEMA, respectively, was 3D printed, before sintering at 1320°C to remove the polymer and bind the powder.	Multiphase: $BaTiO_3$ (both cubic and tetragonal), as well as HA.	50% open pore porosity.	Study demonstrated lower piezoelectric constant compared to other studies in this table. The scaffold, despite showing widespread MC-3T3 cell attachment, exhibited high microporosity through weak mechanical properties. This in	[203]

(*Continued*)

Table 3. Continued.

Material	Titanate content	Authors	d_{33} Piezoelectric coefficient (pC/N) (% = Titanate content)	Processing technique/parameters	Microstructure/Phase quantification	Porosity (%)/Density (g/cm^3)	Comments on mechanical/electrical/ multifunctional properties	Ref.
							part may explain the lower piezoelectric constant seen.	
Highly porous barium titanate based scaffold coated by Gel/HA nanocomposite	N/A	Ehterami et al.	Sintering Temp. 1300°C = 3.9 1400°C = 4.5 Polarisation not possible for 1100–1200°C	BT scaffolds were prepared by using the foam replication method: green bodies of polyurethane (PU) sponge were coated with the BT ceramic slurry, before sintering at 1100–1400°C. Dip coating and in situ precipitation process were used to form gelatin and HA coating on the surface of porous scaffolds	Polycrystalline BT with HA.	Uncoated scaffold = 1.34 ± 39.86 to 1.94 ± 27.83% Coated scaffold = 83.64 ± 1.83 to 90.42 ± 1.34%	Increasing the sintering temperature to 1400°C, increased the grain size, density of the material and reduced the number and size of air voids which increased the dielectric and piezoelectric properties of the piezoelectric barium titanate scaffolds. The coating did not impede the piezoelectric properties. Cellular density was higher for the coated scaffold, since the coating enhanced the attachment and subsequent proliferation and viability of seeded cells.	[189]
HA/$BaTiO_3$ ceramics	90%	Baxter et al.	57.8 ± 10.8	Pressed, sintered (1300°C, 2 h) discs.	Multiphase: $BaTiO_3$ and HA confirmed, with the possible addition of β-tricalcium phosphate, barium phosphate, calcium barium hydrogen phosphate and barium titanium phosphate	N/A	Saos-2 human cell line was used. No significant difference was noted between the 90% BT and 100% HA samples.	[194]
HA/$BaTiO_3$ composites with aligned lamellar porous structures	90%	Liu et al.	50% = 5	Ice-templating method (described by Zhang et al. [204]). Mixed slurry was freeze-cast in a PDMS mould, followed by freeze-drying before sintering at 1250°C. Polyamide fibres were used as structural templates to construct macro- and lamellar pores.	N/A	40, 50 and 60%	No significant differences of cell proliferation and differentiation were found between the polarised and non-polarised groups indicating that polarised piezoelectric HA/$BaTiO_3$ could not promote osteoblast proliferation and differentiation distinctly without acting load.	[205]
HA/$BaTiO_3$ composites	0, 80 90, and 100%	Tang et al	0% = 0 80% = 1.3 90% = 2.7 100% = 6.8	Slurry was added to plaster cylinders, prior to sintering at 1250°C (2 h).	Mixture of HA and $BaTiO_3$ phases.	N/A	Under static non-loading conditions, pure HA had better biocompatibility and bioactivity than HA/$BaTiO_3$ (low significance except ALP activity). However, cyclic loading caused the converse. Reasons: Electric charge on the surface attracted Ca^{2+} preferentially, induced by the piezoelectric properties. Piezoelectric materials can generate free charge on the surface, inducing microenvironment effects (↑ bone formation protein, β growth factor, Shima II, osteoblast proliferation and growth) The optimal polarisation process was obtained for the polarisation time of 30 min, polarised electric field intensity of 1.2 kV·mm^{-1}, and polarisation temperature of 130°C. Reasons: At 30 min, interfacial polarisation, ion displacement polarisation, inversion of the 180° domain, and shift of the 90° domain were completed. The high electric field intensity could decrease	[206]

							the direction changes of the electric domain; hence, a lower limit of the electric field intensity exists 130°C is the Curie point temperature of $BaTiO_3$	
Graphene (G)/BT ($BaTiO_3$)/PMMA composites	30–80% vol. (0.5–2.5% vol. graphene)	Tang et al.	*No Graphene* <50% = ca. 0 60% = ca. 0.33 70% = ca. 0.77 80% = ca. 0.83 *With Graphene (60% BT)* 0.5% = 0.45 1.5% =–0.75 2.5% = 1.5	BT/PMMA solid phase mixture. MMA liquid phase added, solidified in 100% humidity (37°C). Graphene added via dispersive addition.	BT and graphene as reinforcement to the PMMA solid matrix.	N/A	Rise in d_{33} value at 50% BT is likely due to formation of a barium titanate network. Compressive strength dropped at ca. 60% BT (85.3 MPa to ca. 25 MPa at 90% BT), due to low PMMA content providing stable adhesion for BT powders. 0.5% graphene increased the compression strength to 89.5 MPa due to crack deflection; however, higher graphene content reduced the compressive strength due to cracks extending forward through the PMMA. Graphene enhanced the charge transfer through to the surface of the material, which increased the material's piezoelectric coefficient	[198]
Porous barium titanate/HA composites	50, 70 and 90 vol% BT, solid loading 10–40 vol%, with 0–60 vol% of PA fibres	Zhang et al.	*Values for 20% solid loading (S.L.)* 50%BT = 0.3 70%BT = 1.2 90%BT = 2.8 *Values for 90%BT and 15% PA* 30%S.L. = 2.6 40%S.L. = 3.1	Mixed slurry (HA/BT) was freeze-cast in a PDMS mould, followed by freeze-drying before sintering at 1250°C. Polyamide fibres were used as structural templates to construct macro- and lamellar pores.	Multiphase: BT and HA	Values for 20% solid loading (S.L.) 50%BT = 57.4% 70%BT = 58.9% 90%BT = 57% Values for 90%BT and 15% PA 30%S.L. = 2.6 40%S.L. = 3.14%	The increase of solid loading led to a reduction of porosity, smaller lamellar pore width and thicker lamellar ceramic wall resulting in the increase of the active piezoelectric ceramic phase in the HA/BT composite. Despite lower mechanical properties, the porous scaffolds with larger pore sizes (>100 µm) are more suitable for tissue ingrowth, while those with small pores sizes (≤100 µm) can provide good mechanical properties and facilitate the nutrition and fluid transport through pore channels in the aligned graded porous structures.	[204]
Polycaprolactone/barium titanate composites	5–40 vol%	Liu et al.	15% = 0.1 35% = 1.25 40% = 3.9	PCL and BT particles were dissolved in tetrahydrofuran, (1.5 h). The mixture was poured into ethanol to precipitate the composite flocs and were then filtered. Flocs were moulded on a flat vulcanising machine (5 min, 15 MPa, 70°C).	BT dispersed in a PCL matrix	N/A	At vol fractions of less than 40%, any induced charge is blocked by the insulative matrix, hence the lower d_{33} values. At 40%, a network is formed, bridging the insulative matrix. The addition of BT to the PCL matrix improves cellular adhesion, due to strong interaction with surface charge (irrespective of whether positive or negative).	[207]

Limitations of first-generation sodium titanates

Before discussing some of the exciting flexible titanate structures in Section Modifiable titanate structures based on ion-exchangeability *in vitro*, it is worth exploring some of the limitations of the first-generation sodium titanate structures.

Ca reagent contamination, its effects on apatite formation and shelf-life assessment

Kizuki et al. [210] demonstrated that even 0.0005% of Ca ions present within the initial NaOH solution used, will preferentially enter into the sodium titanate layers formed, inhibiting apatite formation (Figure 17; above 1.5 ppm Ca concentration apatite nucleation is inhibited), since the sodium ions diffusion is reduced due to partial replacement of Na^+ with Ca^{2+} in the surface structure. Generally, the reduction in apatite formation was a direct correlation to greater NaOH volumes used, i.e. a larger availability of Ca^{2+} ions. It was found that just 1.5 ppm of Ca^{2+} was enough to reduce Na^+ release from 1.21 to 0.87 ppm (Figure 18) [210]. Fundamentally, there is a need for very careful planning of the type of reagent used, since contamination on this scale can be considered negligible depending on the application.

The lack of stability of sodium titanate structures in humid environments is also a concern [211]. Humid environments (Kawai et al. assessed for 1 week at 80°C and 95% humidity [211]) inherently contain H_3O^+ within the water vapour [212], ion-exchange reactions can still persist, causing a decrease in the sodium content and hence reduced apatite formation in implantation. This is a significant issue for medical implants, since there is a substantial wait between manufacture, shelf-life and implantation, so careful inert packaging is required. This effect must also be considered during all stages of production from preparation and handling of these materials, characterisation and validation and storage.

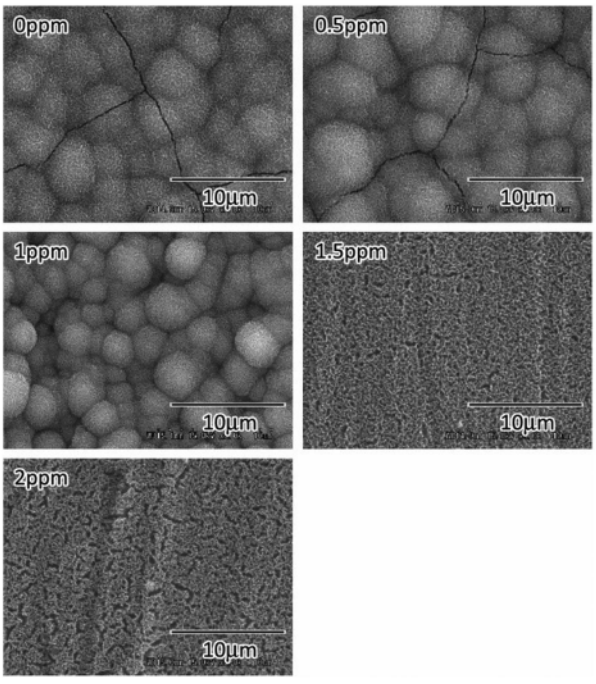

Figure 17. SEM images of the Ti specimen surface after the NaOH and heat treatments as a function of the Ca concentration in the NaOH solution. Apatite growth occurs between 0 and 1 ppm, with 1.5 ppm and above showing no apatite nucleation. Reprinted from Kizuki et al. [210] with permission from Springer Nature.

Inability to produce titanate surfaces on certain Ti alloys

Alkali-treatments are not so effective to produce apatite on Ti–Zr–Nb–Ta alloys [213]. Specifically, the Ti–15Zr–4Nb–4Ta alloy utilised had the advantage of having high ultimate tensile strength (ca. 453 MPa) [214], but the inclusion of Nb and Zr inhibit apatite formation, as illustrated by Cho et al. [215] and Niinomi [216]. If the mass% of Nb and Zr in the alloy is less than 10%, it is postulated that apatite formation is possible on NaOH-treated alloys when the number of sodium titanate molecules on the surface is sufficient to nucleate apatite. Sodium niobate can also form and there is a delay in the ion-exchange of Na^+ with H_3O^+, likely due to stronger interaction between Nb–O and Na^+. Also, Zr has higher corrosion durability in NaOH solution compared to Ti, which forms a thin Na-free zirconia hydrogel, where OH^- formation is rare; further inhibiting sodium titanate and subsequent apatite formation. Therefore, additional or modified steps are required in order to confer apatite-

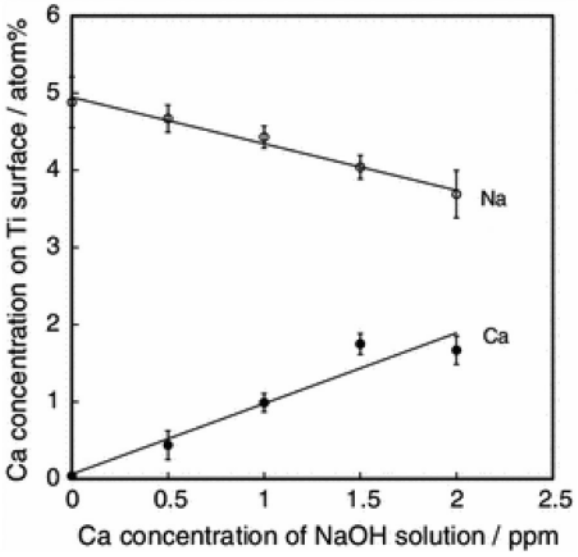

Figure 18. Na and Ca concentrations on the Ti specimen surface after the NaOH and heat treatments as a function of the Ca concentration in the NaOH solution. Reprinted from Kizuki et al. [210] with permission from Springer Nature.

forming titanate structures not just non-Ti-containing materials, but also many Ti alloys [216].

Modifiable titanate structures based on ion-exchangeability *in vitro*

The limitations outlined in Section Pre-modification: the potential for multifunctional surfaces with peroxide pre-treatment, can be overcome by the flexibility of the titanate structure, enabling facile ion-exchange. Here we consider approaches to improve biocompatibility and impart bacterial resistance.

Bioactive titanates

The majority of studies regarding titanate surfaces for biomedical applications focus on their bioactive potential both *in vitro* and *in vivo*. The development on the original sodium titanate surfaces, to incorporate ions such as calcium, magnesium, strontium, through ion-exchange reactions, has seen many alternative produced surfaces for biomedical implants.

Calcium titanate

Calcium as an element has been incorporated in a number of coatings and materials designed to be bioactive and is essential in biomineralisation of bone; 99% of the calcium in the body is found within hydroxyapatite [217] and has been incorporated into various materials in order to aid bone growth and osteoblast proliferation [218,219]. Studies of calcium titanate ($CaTiO_3$) coatings have demonstrated increased osteoblast adhesion [220], apatite-forming ability [221] and improved osseointegration in a rabbit model [222] compared to untreated or roughened Ti. By incorporating an additional step into the hydrothermal treatment, which soaks the sodium titanate-converted samples in a calcium-rich (saturated Ca$(OH)_2$) solution (36.5°C, 24 h), Rakngarm et al. demonstrated the ability of sodium titanate surfaces to incorporate alternative ions (Ca^{2+}) into the structure on Cp-Ti and Ti–6Al–4V alloys, enabling faster apatite generation; HA deposition within 24 h immersion in SBF, and complete coverage within 7 days, compared to only sodium titanate treatment (up to 1 month) or acid treatment (10 days) [223]. Kizuki et al. [19,224] improved the apatite-forming ability (no apatite nucleation pre-water treatment, with total apatite-surface coverage following water treatment) of calcium titanate surfaces, as well as scratch resistance by incorporating a heat treatment at 600°C, followed by submersion in H_2O at 80°C for 24 h (<10 mN for pre-heat treatment; 48 mN following heat treatment; 54 mN following subsequent water treatment). The increase in scratch resistance due to the conversion of $Ca_xH_{2-2x}Ti_3O_7$ to $CaTiO_3$ post-heat treatment also stopped apatite formation in SBF, no apatite nucleation observed by SEM, due to the suppression in Ca^{2+} leaching from the calcium titanate layer. Therefore, an additional hot water treatment stage (80°C for 24 h) is required to generate a calcium-deficient titanate layer on the surface due to ion-exchange with H_3O^+ ions, facilitating calcium release. Due to this initial release (0.15 ppm), subsequent apatite formation through ion-exchange reactions detailed previously can occur [19,224]. This identical hot water treatment is effective at generating apatite formation on Ti–Zr–Nb–Ta alloys, which had previously not been achieved without this additional treatment [225,226].

Bone bonding of NaOH (5M, 60°C, 24 h), $CaCl_2$ (100 mM, 40°C, 24 h), heat- (600 or 700°C) and water-treated (80°C, 24 h) Ti metal and Ti alloys, specifically from the Ti–Zr–Nb–Ta alloys, namely Ti–15Zr–4Nb–4Ta, Ti–29Nb–13Ta–4.6Zr alloys and gum metal (Ti–36Nb–2Ta–3Zr–0.3O) were investigated by Fukuda et al. and Tanaka et al. [227,228]. Both studies demonstrated successful bone bonding without fibrous encapsulation on rabbit tibial implants (Figure 19). During detachment testing, facture occurred within the main bone portion, as opposed to the interface, meaning the interfacial bond strength is sufficient to prevent delamination; with all failure loads of the 700°C and water-treated samples exhibited failure loads > 50 N. One postulate is that by developing better bone-bonding capabilities (minimising fibrous encapsulation and enabling mature bonding) on alloys that are free of cytotoxic elements, it will result in a new generation of implant materials that can potentially replace the current generation of Ti alloys, through potentially negating any negative biological effects. In 2019, the first clinical trial of $CaTiO_3$ Schanz screws demonstrated marked improvement (median values of 25.36 Nm *v.* 16.68 Nm, respectively; $p = 0.043$) in fixation strength over stainless steel (SS) and HA, confirming its potential efficacy [229].

Magnesium titanate

Typically, calcium titanate structures are substituted with an additional cation (Mg, Zn or Sr), although multiple cations are also possible. These multi-cationic titanates not only produce titanate structures with equivalent bioactivity but also possess their own unique functionalities, which can be optimised through varying the compositional ratio [230].

Magnesium is a highly abundant element within the body, with 60% of its *in vivo* distribution being contained within bone [231]. It's essential participation as a cofactor to >300 enzymes, as well as reducing HA crystal size, without which would ultimately result in brittle bones, makes it an ideal element to incorporate within the titanate structure for biomedical applications [82]. Magnesium titanate was first produced via ion-exchange through submersion of

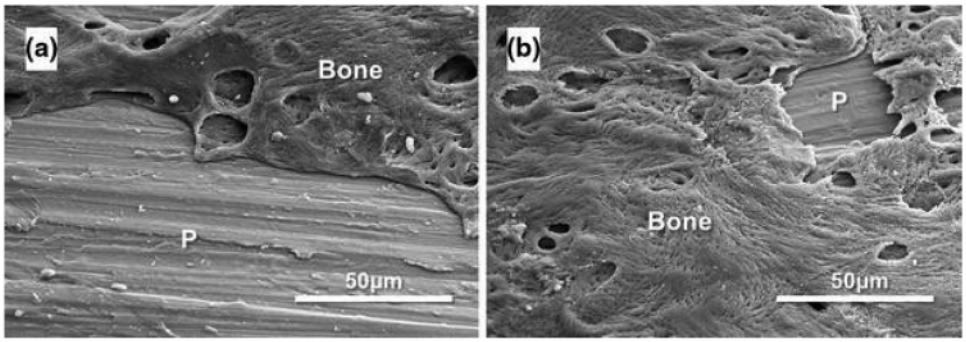

Figure 19. SEM images of the surface of an AcaHW-GM plate (defined below) after detaching tests at (A) 4 weeks and (b) 26 weeks. AcaHW-GM plates were prepared as follows: plates of gum metal were first soaked in 10 mL of 1 M aqueous NaOH solution at 60°C for 24 h. After removal they were gently rinsed with ultrapure water for 30 s and dried at 40°C. The plates were subsequently soaked in 20 mL of 100 mM $CaCl_2$ solution at 40°C for 24 h, washed and dried in a similar manner. Next, they were heated to 700°C at a rate of 5°C min^{-1} in an electric furnace in air and kept at that temperature for 1 h, followed by natural cooling, followed by soaking in 20 mL of ultrapure water at 80°C for 24 h, and then washed and dried. (A) Some bone residue (Bone) was observed on the AcaHW-GM plate (P) at 4 weeks. (B) Much more bone residue (Bone) was observed on the AcaHW-GM plate (P) at 26 weeks. Reprinted from Tanaka et al. [228] with permission from Springer Nature.

pure Ti in an $MgCl_2$ aqueous solution, by Shi et al. [232]. The resulting Mg-containing surface showed improvements in cell attachment (38% *v.* 25%) and proliferation (10×10^4 *v.* 8.5×10^4 cells/well), linked to the increased protein (16 *v.* 8 μg cm^{-2}) adsorption observed on the treated surface compared to untreated Ti. It is widely accepted that electrostatic interactions are important for protein adsorption, with Mg^{2+} acting as a cation bridge between the solution proteins and the underlying Ti surface. Higher protein adsorption aids in cell proliferation due to the increasing expression of integrins that mediate cellular adhesion. Yamaguchi et al. demonstrated an Mg-containing $CaTiO_3$ using a $CaCl_2$–$MgCl_2$ mixture following an initial NaOH solution treatment. Ca/Mg ratios between 1:0 (pure calcium titanate) and 0:1 (pure magnesium titanate) were investigated [21]. The apatite-forming ability of the Ca/Mg titanate compositions required additional heat treatment (600°C, 1 h), as well as subsequent H_2O (80°C, 120 strokes min^{-1}, 24 h) or $MgCl_2$ (1 M, same conditions as H_2O treatment) solution treatments due to the issues described previously in Section Calcium titanate. Inductively coupled plasma (ICP) analysis revealed H_2O treatments allowed greater Ca^{2+} release (0.35 *v.* 0.24 ppm), while samples with the additional $MgCl_2$ solution treatments showed an increase in Mg^{2+} release (0.29 *v.* 0.02 ppm), even after 7 days, with no apatite nucleation occurring on the non-water-treated samples [21]. Okuzu et al. showed Ca-containing $MgTiO_3$ samples demonstrated superior results to $CaTiO_3$ materials alone. With Ca-containing $MgTiO_3$ showing higher cell viability; as well as greater expression of β catenin, integrin 1β, cyclin D1, ALP and Opn over 7 days (see Figure 20 for corresponding values). Furthermore, Ca-containing $MgTiO_3$ showed greater failure loads and a higher bone–implant contact through a 24-week rabbit tibial *in vivo* test, supporting the biological markers found *in vitro* [233].

Another approach is to fully substitute $MgTiO_3$ by excluding $CaCl_2$. $MgTiO_3$ exhibited apatite formation after heat treatment without needing additional water or aqueous solution treatments, and that the apatite-forming ability was greater than $NaTiO_3$, as well as increased albumin adsorption, higher MC3T3-E1 cell attachment, spreading and faster proliferation over 7 days. This was due to the greater electrostatic attraction between the divalent Mg^{2+} ions and negative albumin over Na^+ or $Ti–O^-$ [234].

Strontium titanate

Strontium has been shown to regulate bone regrowth, by activating osteoblast activity and reducing osteoclastic activity and hence has been a popular choice as a bioactive agent [235]. Initial work on ion exchange of Sr by Yamaguchi et al. [236] demonstrated Sr-containing $CaTiO_3$ did not exhibit apatite-forming ability until a further H_2O or $SrCl_2$ treatment was employed, which showed higher Ca^{2+} release (0.05 ppm) and lower Sr^{2+} release (0.06 ppm), compared with $SrCl_2$ treatment alone (0.01 and 0.92 ppm, respectively over 7 days) [236]. Okuzu et al. also found higher cell viability, greater expression of β catenin, integrin 1β, cyclin D1, ALP and Opn, as well as higher ECM mineralisation and Ocn expression over 7 days for Sr-containing $MgTiO_3$ (Figure 20), compared to Ca-doped titanate alone. Greater failure loads (32 *v.* 22 N at 24 weeks) and higher bone–implant contact (40 *v.* 36%) was also achieved in the Sr-containing $MgTiO_3$ compared to Ca-doped titanate alone, through the same rabbit tibia model (Figure 21) [233].

The $SrCl_2$ ion-exchange treatment has been used on selective laser sintered (SLS) Ti–6Al–4V scaffolds by Shimizu et al. [237]. The chemical process

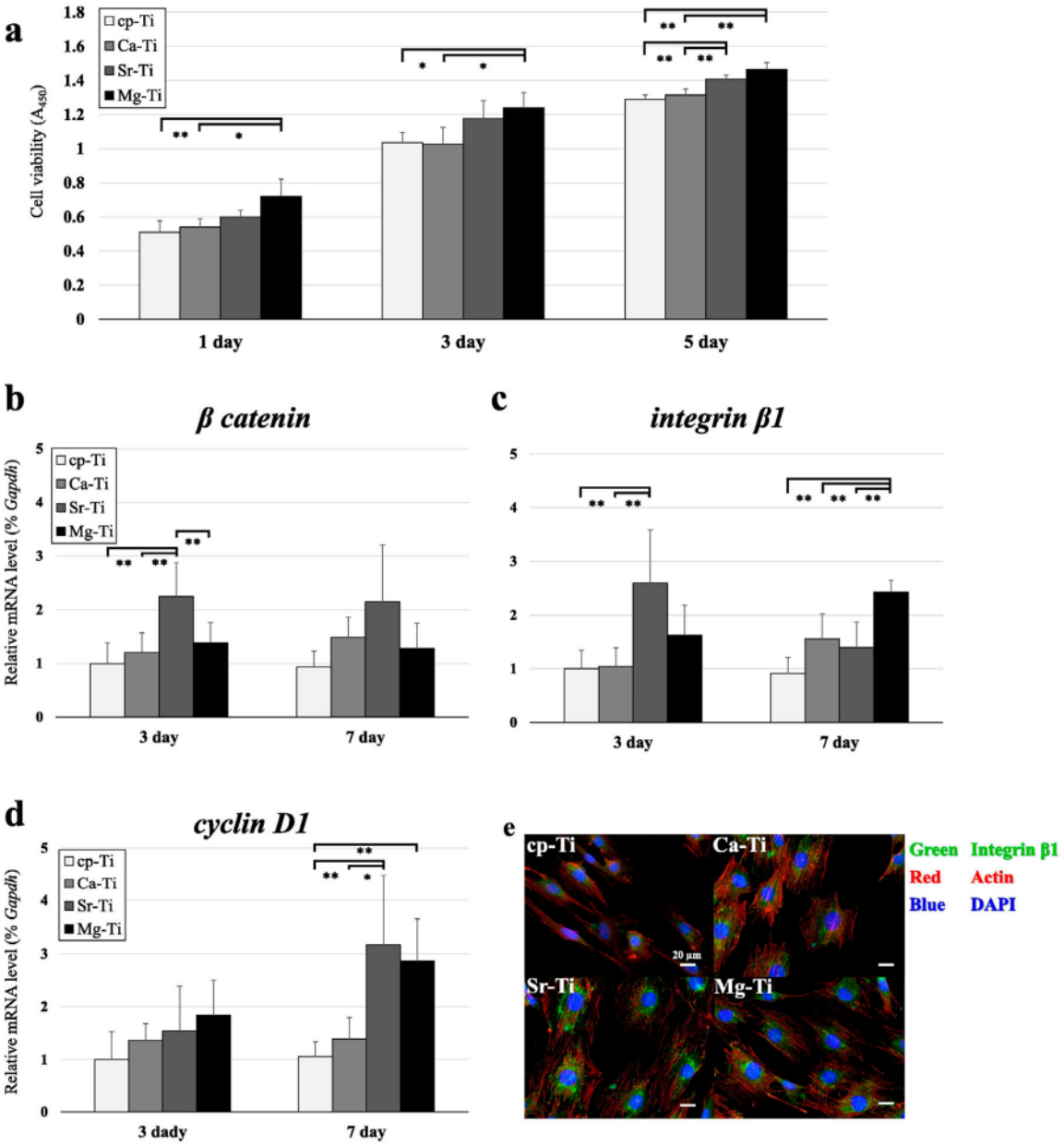

Figure 20. Cell viability, gene expression of β-catenin, integrin β1, and cyclin D1, and immunofluorescence staining of integrin β1 of MC3T3-E1 cells cultured on each sample type: Cp-Ti, Ca–Ti (Ca-doped titanate), Sr–Ti (Ca and Sr-doped titanate), Mg–Ti (Ca and Mg-doped titanate). (a) Cytotoxicity of the three treated sample implant types as assessed by cell viability ($n = 4$) (b–d) Relative gene expression of the indicated genes in the three treated samples and cp-Ti as measured by RT-qPCR. Gapdh was used as an internal control. ($n = 5$) I Cells on Sr- and Mg–Ti showed good cellular extension as well as higher expression and more extensive distribution of integrin β1 than those on Ca–Ti and cp-Ti. *$p < 0.05$, **$p < 0.01$. Reproduced from Okuzu et al. [233], with permission from Elsevier.

successfully imparted the nanostructure of titanate on the microscale roughness of the scaffold. XTT cell viability showed no significant difference between titanate and untreated scaffolds, but the $CaTiO_3$- and $SrTiO_3$-modified scaffolds showed higher ALP and integrin 1β gene expression *in vitro*. *In vivo* testing in a rabbit model further detailed enhanced failure loads and bone–implant contact (ca. 35% *v.* 27% for $SrTiO_3$ and $CaTiO_3$, respectively) at 2 and 4 weeks, with $SrTiO_3$ (51.3 and 103.6 N for 2 and 4 weeks, respectively) outperforming $CaTiO_3$ (51.3 and 103.6 N for 2 and 4 weeks, respectively) [237]. The $SrTiO_3$-modified scaffolds also contained Ca ions, which may have led to a synergistic behaviour observed when both ions are delivered, increasing osteogenesis; however the underlying molecular mechanism and the various factors affecting this is still unclear [238].

Barium titanate

Zhou et al. [239] described the formation of barium titanate films, which were subsequently doped with strontium (Sr) ions, for improved bioactivity for osseointegration enhancement; Sr has been shown to

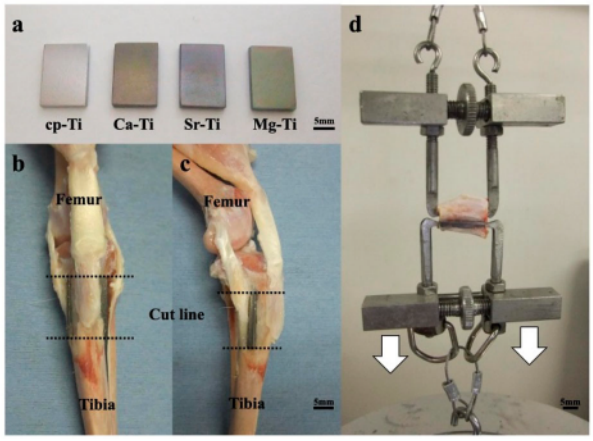

Figure 21. Sample appearance, implantation into the tibia, and the biomechanical test used in the in *vivo* study. (A) Cp-Ti and surface-treated Ti plates. (B,C) Representative images of the knee after sample explanation. (d) Detachment test to measure the bone-bonding strength of the implant. Reprinted from Okuzu et al. [233] with permission from Elsevier.

activate various signalling pathways in osteoblasts and osteoclasts, such as the calcium-sensing receptor, inositol 1,4,5 triphosphate, MAPK-ERK1/2 and Wnt/NFATc, enabling bone stem cell osteogenic differentiation and inhibiting osteoclast activity. Due to Sr and Ba having similar ionic radii (1.12 and 1.34 Å, respectively [240]) and electronic structures, substituting Sr into the barium titanate structure is a logical step to not only modify the piezoelectric properties of barium titanate, but to also improve the bioactivity. With Sr substitution, the morphology becomes rougher with a micropore structure (ca. 30–300 μm), and the water contact angle (WCA) ($BaTiO_3$ = ca. 50° *v.* Sr-$BaTiO_3$ = ca. 40°), elastic modulus and hardness ($BaTiO_3$ = ca. 1 GPa *v.* Sr-$BaTiO_3$ = ca. 0.75 GPa) decreased. The film exhibited a sustained release of Sr ions (3 ppm day 1, 4 ppm day 14) and proved beneficial for *in vitro* cell adhesion, osteogenic differentiation, *in vivo* osteogenesis and osteointegration. The benefits of lower mechanical properties (benefit cellular proliferation and osteogenesis) and WCA between 40° and 60° (enhance cell adhesion), combined with the properties highlighted above for Sr inclusion, demonstrate the improved properties for Sr-doped structures over $BaTiO_3$ alone.

The link between bioactivity and piezoelectric/ferroelectric material properties is complex since bone growth is heavily dependent on multifactor processes. It has been suggested that localised stresses are detectable by osteocytes, which results in enhanced bone remodelling at areas of higher stress. Furthermore, electrical polarisation may induce specific cellular pathways that can lead to enhanced bone growth. Further studies on barium titanate ceramics have demonstrated apatite-forming ability being dependent on the polarity or partial charge of the surface, with positively charged surfaces showing no bioactivity while negatively charged surfaces were able to bond cations such as Ca^{2+}, subsequently allowing the typical process of apatite formation of chemically derived titanates to occur [33,241–243]. Furthermore, although not covered in this review, the use of barium titanate materials for medical sensing applications is becoming an increasingly attractive research area [244–246].

Zinc titanate

Zinc is another essential element within the body, being the second most abundant metal after iron. Its functions in the body are numerous, but can be divided between structural roles, catalytic functions and regulatory functions, and are essential to growth and repair mechanisms *in vivo*, such as promotion of bone formation [247,248]. Initial work by Yamaguchi et al. used a mixture of $Ca(CH_3COO)_2$ and Zn $(CH_3COO)_2$ at 40°C for 24 h to exchange Na^+ ions in $NaTiO_3$. The initial Zn-containing $CaTiO_3$ (sodium hydrogen titanate was isomorphously transformed into zinc-incorporated calcium hydrogen titanate, $Zn_xCa_yH_{2-2(x+y)}Ti_3O_7$) exhibited apatite nucleation after SBF submersion (3 days) but had low scratch resistance (0.9 mN). Again, heat treatment (600°C; forming $Zn_xCa_{1-x}Ti_4O_9$) improved scratch resistance (41.7 mN; likely due to the dehydration and further crystallisation), but reduced apatite formation in SBF. Acetic acid treatment returned apatite formation, via the partial exchange of Ca^{2+}, which was not possible with water, due to the presence of Zn. This acetic acid-treated Zn-containing $CaTiO_3$ released both Ca^{2+} and Zn^{2+} ions, though Zn release was very low at 0.03 ppm after 12 days while Ca release was higher at 0.24 ppm, and restored apatite nucleation in SBF. It was suggested that the Zn ions present inhibited Ca release from the titanate surface, and hence inhibited apatite formation [248].

Antibacterial titanates

In addition to bioactive ion incorporation into alkali-titanate structures, antibacterial ions have also been considered to negate issues regarding implant infection rates, while avoiding antibiotics overuse. Additionally, it allows scope for generating multifunctional interfaces, whereby bioactive and antibacterial properties are combined in one surface [249].

Silver titanate

One of the main antibacterial ions, which is widely prevalent in the literature, is silver (Ag) [250,251]. Studies by Inoue et al., Lee et al. and Kizuki et al. investigated the ion-exchangeability of Ag^+ with Na^+ in the titanate structure [224,252,253]. The initial study by Inoue et al. described the formation of titanate nanotubes through 10 M NaOH treatment at 160°C for 3 h, followed by heat treatment at 300°C

for 1 h. The nanotubes were submersed in 12 mL, 0.05 M silver acetate, generating nanostructured silver titanates with loaded silver nanoparticles (metallic colloids; see Figure 22).

The surfaces produced also generated an antibacterial effect that was shown to be due to Ag-ion elution which, due to the faster elution speed of Ag^+ (82 ppm for Ag^+ *v.* 7.9 ppm for Ag(0)), could possibly be more potent against Multidrug Resistant *S. aureus* (MRSA) than metallic silver alone [252]. Kizuki et al. expanded the study by Inoue et al. to produce a silver titanate layer, on Ti and a Ti–15Zr–4Nb–4Ta alloy, without forming metal colloids on the surface, as well as investigating the effect on apatite-forming and bone-bonding abilities of the resultant products [224]. All samples experienced an $AgNO_3$ solution step at varying molarities (0.01–25 mM) following previous NaOH, $CaCl_2$ (optional), and heat- and water treatments. Despite excellent *in vitro* antibacterial activity against a wide range of bacterial types (*S. aureus, E. coli,* etc.), *in vivo* activity was insufficient due to the very low incorporation of Ag into the Ti surface as a result of its cytotoxicity [254–257].

A different approach by Shuai et al. [258] involved the functionalisation of polydopamine-coated $BaTiO_3$ nanoparticles with a silver ammonia solution. The co-benefits of the piezoelectric properties of $BaTiO_2$, as well as the antibacterial potential of Ag, make this an attractive future research area (Figure 23).

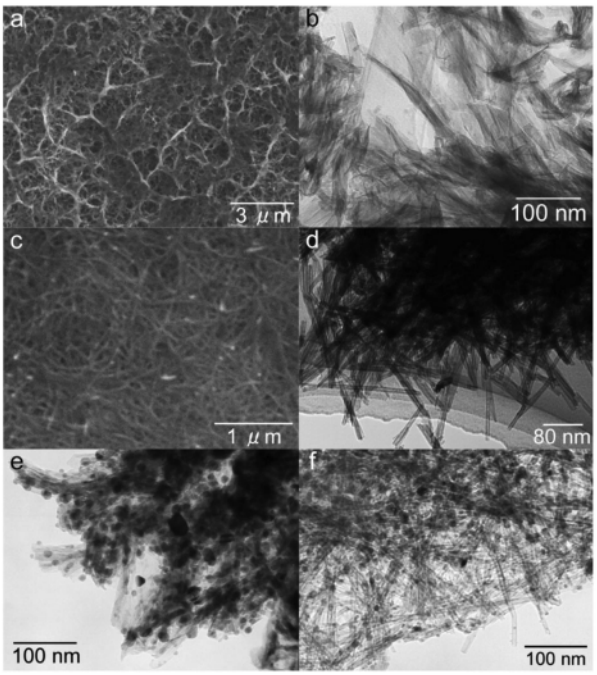

Figure 22. SEM (A,C) and TEM (B,D–F) images of NaOH-treated Ti plate (A,B), Calcined and NaOH-treated Ti plate (C,D), and silver acetate-treated of the NaOH-treated (E) and Calcined (F) samples, respectively. Exact sample methodology detailed by, and figure reprinted from Inoue et al. [252] with permission from John Wiley and Sons.

Gallium titanate

Gallium (Ga) has been previously reported to be an ideal substitute for Ag in the antibacterial setting [259,260]. Its history in the field of medicine is expansive, having been notably used in chemotherapeutic drugs [261]. Its similarity to Fe(III) in ionic radius and charge, allow replacement within target molecules, which has resulted in an ideal antimicrobial agent, whose presence can cause Ga(III)-induced bacterial metabolic distress through a 'Trojan horse' mechanism (Figure 24) [259,262]. Furthermore, inhibition of bone resorption through reduced Ca^{2+} release from bone makes it an ideal element for incorporation in orthopaedic devices [263]. Cochis et al. incorporated gallium into the surface of titanium through electrodeposition [260]. These surfaces are antibacterial against *Acinetobacter Baumannii* (MRAB12); a multi-drug resistant (MDR) nosocomial pathogen, which is rapidly emerging in implant-associated infections, with a higher efficacy compared to silver [264].

Only three biomedical studies have focussed on the incorporation of gallium into the titanate structure for antibacterial applications. Yamaguchi et al. [249] demonstrated the successful incorporation of gallium into the calcium titanate structure through a mixture of $CaCl_2$ and $GaCl_3$, as well as purely $GaCl_3$ treatments (with additional water treatments post-heat treatment), generating Ga-doped calcium titanate and gallium titanate surfaces, respectively. Both Ga-containing calcium titanate and gallium titanate surfaces killed *A. baumannii*, with Ga^{3+} release rates of 0.35 and 3.75 ppm, respectively, while also producing apatite in SBF. *A. baumannii*, however, is susceptible to Ga ions, requiring only 2–100 μM to produce an inhibitory affect compared to *S. aureus* (0.32–5.12 mM) [259,265].

Wadge et al. [266] assessed the potential viability of Ga-ion-exchanged titanate, produced using a 4 mM $Ga(NO_3)_3$ ion-exchange solution (more biocompatible compared to $GaCl_3$; FDA approved for cancer-associated hypercalcemia treatment), against *S. aureus,* a less susceptible pathogenic species. The Ga titanate structures tested would not leach enough Ga^{3+} ions (4–40 μM) into solution to have an antibacterial effect on *S. aureus* (Figure 25). To demonstrate both a bioactive and broad-spectrum antibacterial effect requires further work. It was also found that without subsequent heat treatment, gallium titanate surfaces present a cytotoxic effect on MG63 cells (cell viability 24.2%), due to the higher release rate of Ga^{3+} ions into the surrounding solution; heat treatment was necessary to enhance the coating stability.

Similar to the study by Wadge et al., whereby Ga $(NO_3)_3$ was used, Rodríguez-Contreras et al. [267] highlighted the further potential of using non-toxic $Ga(NO_3)_3$ at higher concentrations; 100 mM, to produce gallium-doped calcium titanate coatings on

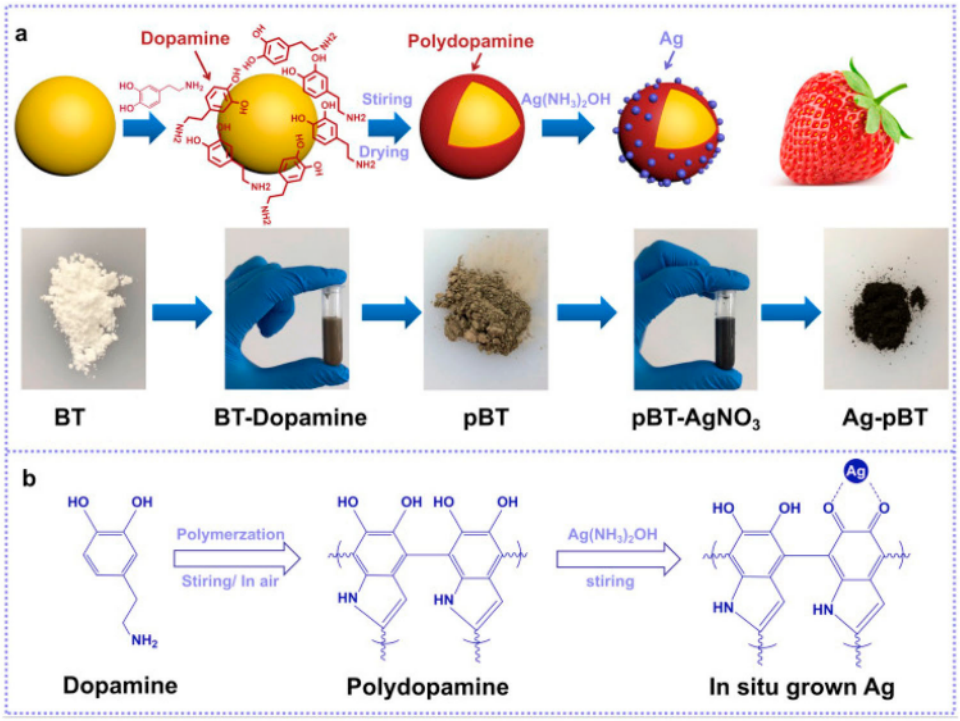

Figure 23. Preparation process (A) and reaction mechanism diagrams (B) of *in situ* growth of Ag nanoparticles on $BaTiO_3$. Reprinted from Shuai et al. [258] with permission from Elsevier.

porous (macroporosity of 347 ± 1 μm and a microporosity of 8.6 ± 0.2 μm) additively manufactured Ti structures (Figure 26). It was found that the higher gallium nitrate concentration resulted in the formation of a thicker apatite layer, indicating accelerated nucleation. Furthermore, no cytotoxicity (cell viability >70%) was seen for both the 5 and 100 mM treated samples. The gallium-treated samples, irrespective of Ga concentration used, resulted in an inhibition halo for *P. aeruginosa*. However, no inhibition halo was noted for *S. aureus* or *S. epidermidis*, while *E. coli* required the highest concentration (100 mM $Ga(NO_3)_3$) to exhibit an inhibition halo. Therefore, it is still not clear whether

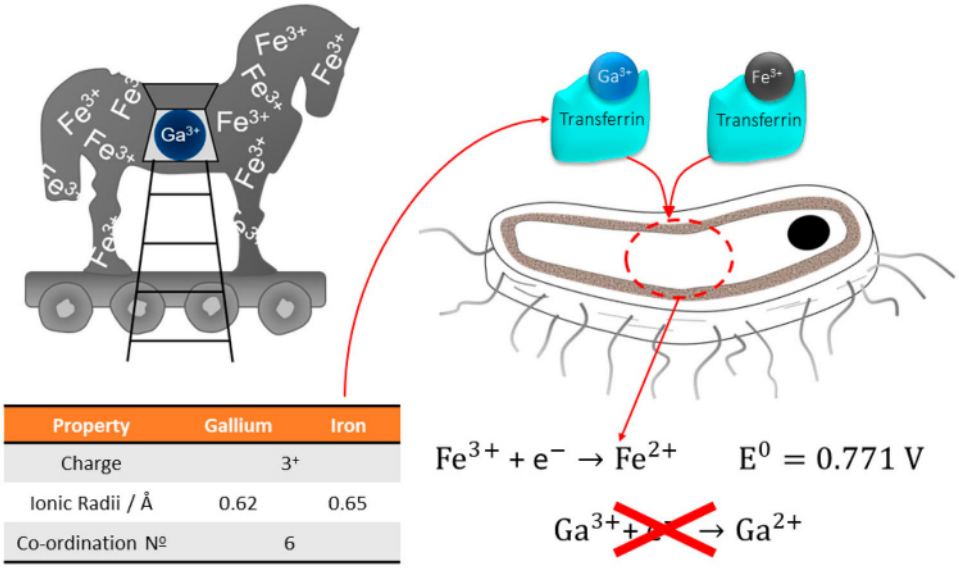

Property	Gallium	Iron
Charge	3+	
Ionic Radii / Å	0.62	0.65
Co-ordination №	6	

Figure 24. Diagram demonstrating the similarity between Ga and Fe ions and how the 'Trojan Horse' mechanism functions. Due to the similarities shown, and the process by which both ions are transported via transferrin, results in bacteria being unable to distinguish between Ga^{3+} and Fe^{3+}. Once the ions have been transported, the inability for bacteria to reduce Ga^{3+}, which is the normal process for Fe^{3+} in order to generate energy via metabolic processes, results in Ga-induce metabolic distress, and eventually bacterial death.

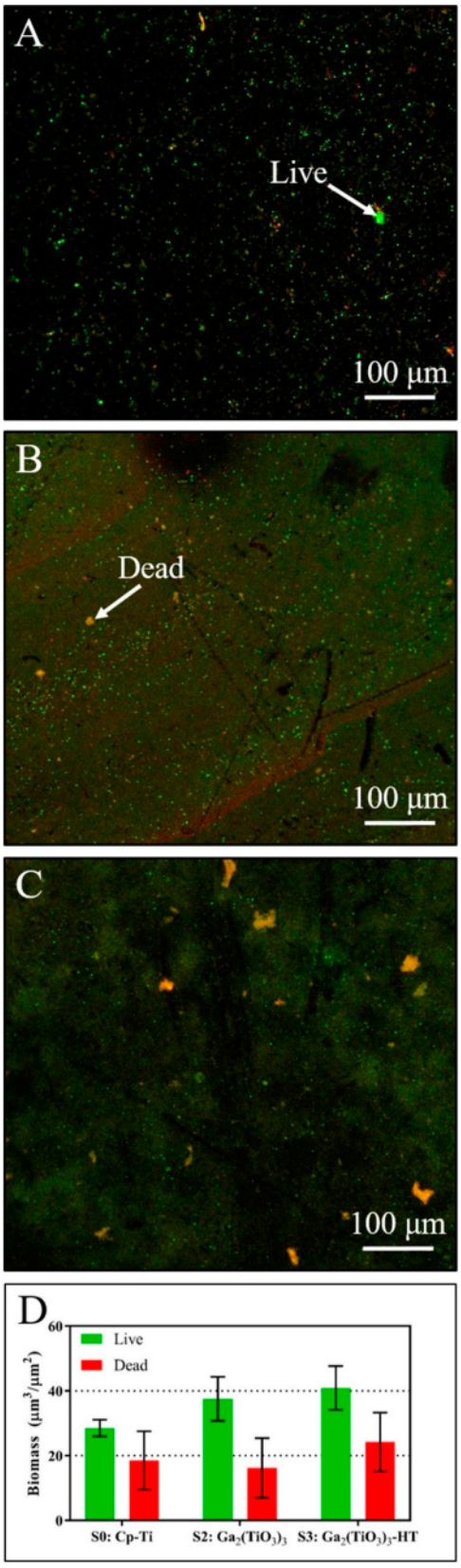

Figure 25. (A–C) LIVE/DEAD staining maps for pure Ti (S0: Cp-Ti), gallium titanate surfaces (S2: $Ga_2(TiO_3)_3$), and heat-treated gallium titanate surfaces (S3: $Ga_2(TiO_3)_3$-HT), respectively. Live bacteria are stained green, with dead bacteria stained red, as indicated. (D) Live and dead biomass from a 3-day culture of *S. aureus* analysed via COMSTAT. There is no significant difference between the live or dead values between the samples (2-way ANOVA). The experiment was repeated and the same trends observed (n = 3; error bars in S.E.M.). Reprinted from Wadge et al. [266] with permission from Elsevier.

Ga-doped titanates are capable of broad-spectrum antibacterial effects, compared to Cu or Ag.

Zinc and other heavy metals

Ag and Ga are heavy metals with high atomic weights and are believed to elicit an antimicrobial effect due to their interaction with proteins. There is evidence that heavy metals bind to sulphur atoms in cysteine molecules (an amino acid commonly present in a wide variety of proteins) or to amine groups which causes an 'oligodynamic effect' [268]. Due to the large size of the binding heavy metal ion, the shape of the protein becomes distorted and cannot perform the same biological functions [269]. Zinc (Zn) and copper (Cu) are both heavy metal ions that have also been investigated as potential antimicrobial ions in biomaterial contexts. ZnO-TiO_2 systems are prevalent in the chemical industries in gas sensors, catalysts and anode materials [270]. The delivery of zinc ions has been investigated in attempts to demonstrate antimicrobial effects; either as zinc nanoparticles, zinc oxide or zinc salts [271,272]. Zinc oxide is used extensively in bone cements and periodontal dressings. $ZnTiO_3$ has been proven to have bactericidal effects against *Escherichia coli* by Stoyanova et al. when prepared as sub-micron sized particles [273].

Copper is also widely known as both an antimicrobial and antiviral (especially pertinent with the current SARS-CoV-2 (COVID-19) pandemic [274]) ion which has successfully been incorporated into titanate nanotubes using ion-exchange methods. Compared to Ag-doped titanate nanotubes, the antimicrobial activity of the Cu-doped titanates was effective against a smaller range of pathogens but the samples did successfully release Cu ions which were able to elicit antibacterial effects [275].

Iodine-doped titanate

Iodine's broad antibacterial spectrum makes it ideal for generalised disinfectants and is regularly seen in surgical settings as a topical disinfectant under the name Povidone-iodine (PVP-I) [276]. Up to 10.5% could be loaded into a calcium-doped titanate surface, with sustained release of 5.6 ppm over 90 days, >99% reduction over the same time period (reduced to 97.3% after 6 months demonstrating some bacterial regrowth) and produced no cytotoxicity while simultaneously generating apatite with 3 days in SBF [277].

Ikeda et al. [278] also demonstrated iodine-doping into a calcium titanate surface (5M NaOH, 60°C, 24 h; 100 mM $CaCl_2$, 40°C, 24 h; 600°C heat-treat, 1 h; 10 mM ICl_3, 80°C, 24 h). From the XRD, a shift in the calcium titanate spectral peaks indicates the incorporation of I into the crystal structure. It was also shown that ALP, Ocn, Opn, Integrin β1 and Col1a1 expression, as well as MC3T3-E1 cell proliferation, viability and morphology was not significantly affected

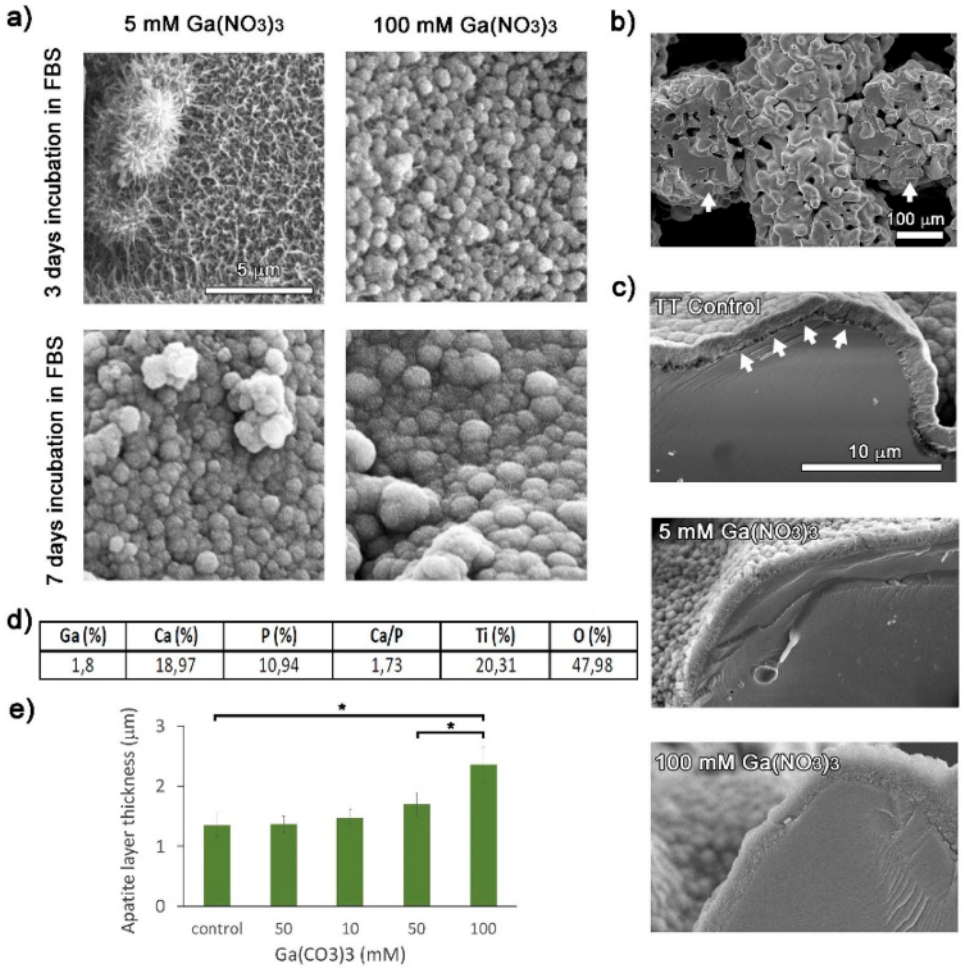

Figure 26. (A) Field Emission SEM (FESEM) micrographs (×10k) of Ti surfaces treated with 5 mM and 100 mM gallium nitrate and immersed in Fetal Bovine Serum (FBS) for 3 days and 7 days. (B) FESEM micrograph (×200) of the cross-section of the porous Ti structures. Arrows indicate the examined cross-section areas. (C) FESEM micrographs (×10k) of the cross-section after immersion in SBF for 7 days: Treated Ti by TT without Ga (control), surface treated with 5 mM gallium nitrate, surface treated with 100 mM gallium nitrate. Arrows in the control sample indicate the discontinuity of the apatite-surface interface (D). EDS analyses (atomic%) of the coating formed on a Ti surface treated with 5 mM gallium nitrate by SBF immersion during 7 days (E) Apatite layer thickness after 7 days in SBF with respect to the gallium nitrate concentration applied in the thermochemical treatment. Values showing significant differences ($p < 0.05$) are indicated with an asterisk. Reprinted from Rodríguez-Contreras et al. [267] with permission from Elsevier.

due to the presence of iodine; however, iodine-doping significantly reduced the number of *S. aureus* (methicillin-susceptible: MSSA) compared to $CaTiO_3$ alone *in vitro*: ca. 0.13 ± 0.18 *v.* 6.1 ± 4.1 (CFU x10^4), respectively, at 24 h. After 16 weeks of implantation, both bone–implant contact and failure load were significantly better for the iodine-doped titanate (ca. 20% and 20 N) compared to pure Ti (ca. 5.5% and 2 N), but had no significant difference compared to $CaTiO_3$ alone (ca. 26% and 24 N), indicating no adverse effects. An *in vivo* bacterial assessment demonstrated pus and thick granulation tissue for the pure Ti (5.7 ± 0.35 (CFU × 10^4/mL)), which was not observed in the iodine-doped group (0.09 ± 0.06 (CFU × 10^4/mL)). The iodine-doped sample also did not induce any renal dysfunction, nor affect thyroid hormone levels. The initial preliminary trials for iodine-doped calcium titanates are extremely promising and demonstrate a step forward in multifunctional titanate structures.

Limitations on clinical deployment of antibacterial titanates

Despite many successful studies demonstrating the antimicrobial efficacy of loaded-titanate structures, limitations still exist, jeopardising their commercial exploitation. To date, there is no commercially available antimicrobial surface for orthopaedic and dental applications. Translation from 'bench-to-bedside' is complex and requires the navigation of significant hurdles (cost, regulatory, ethics) [279]. Presently, getting a novel drug from first testing through to FDA approval and finally to market, takes more than 13 years, and 95% of drugs entering human trials fail. The usual issues are due to misleading, non-reproducible claims of efficacy of the initial pre-clinical trials.

Particularly in *in vitro* trials, where failure to replicate the implanted environment, as well as understanding not only the effect of the material but also unexpected side effects, is a significant issue that inhibits further clinical efficacy. In the case of antibacterial titanate structures, there are several possible limitations that can prevent its further translation. The antibacterial properties of the material rely on elution of cations, so there is a finite concentration that can be achieved pre-implantation, and therefore can only generate short-term antibacterial effects often with a burst release of the active cation upon implantation. There is also potential for encapsulation due to the deposition of a protein conditioning layer or the antibacterial release may not prevent biofilm formation. Such layers may inhibit the effective release of the active agent, reducing its efficacy further.

The authors postulate that the formation of transient degradable coatings and/or protective coatings, in combination with titanate surfaces, can address these issues. If a degradable coating is applied on top of the titanate surface, not only can this be modified to release additional antibacterial agents, but also the transient nature of the coating will inhibit bacterial attachment in the short-term. Once degraded, the titanate surface will be exposed, enabling longer-term multifunctional cation release, which can sustain the antibacterial effects, while improving bioactive properties. This is further discussed in the future outlook section (Combinatorial material approaches for a wide-range of applications). Another approach is to directly load antibiotics into the sodium titanate structure, Yilmaz and Türk [280]. They demonstrated that following the NaOH treatment (10 M, 60°C, 24 h) of pure Ti plates, a gentamicin sulphate solution (50 mg mL^{-1}; a broad-spectrum aminoglycoside antibiotic, which targets both Gram-positive and -negative bacteria) could be used to load the titanate surface. Cell viability remained high (85%) for the antibiotic-loaded sample, with apatite nucleation measured in as little as 3 days, as well as ca. 90 wt.% of the drug being released within 125 min (57% after 15 min). The rapid release inhibited bacterial invasion and prevented early contamination of the sample. For long-term usage, not only is burst release of the antibiotic critical to inhibiting biofilm formation but also retention of some of the drug over longer periods is necessary to inhibit subsequent infections. Therefore, antibiotic-loaded-titanate structures are a promising area for trialling long-term antibacterial studies.

Critical comment

It is clear that a number of possibilities exist regarding the use of substituted-titanate structures for orthopaedic implant applications. However, not only is there a complex interplay between various ions in the extracellular environment, which are continuously being replenished/controlled, but also the presence of various proteins, cells, bacteria and micromotion during movement. It is also essential to understand how various ions affect cells and bacteria, depending on their concentration, speed of elution and potential for reacting with other ions in solution to form compounds and complexes, and in extension, their effects once formed. Usually, there is a trade-off between killing bacteria and having cytotoxicity towards cells; bacteria tend to be more resistant than cells, and hence to attain bactericidal levels, some cells will die, so finding an acceptable window, if that exists, is key.

Co-release or multi-release coatings, where each doped element possesses a different mechanism or mode of action, offer a significant advantage over single-release coatings due to reduced bacterial resistance, and potentially synergistic effects of the doped elements. Yamaguchi et al. [21,236,248] have highlighted the potential for such co-doped titanate structures, such as Mg, Zn or Sr being modified into the $CaTiO_3$ structure to allow dual-bioactive ion potential. Similarly, doped $CaTiO_3$ with Ag and Ga enable the potential combinatorial approach of bioactive and antibacterial properties [249], opening up scope for multifunctional, tailorable biomedical surfaces. The authors suggest that multi-layered, multi-component structures offer a broader, multifunctional, and more promising option to the present structures, as suggested in Section Limitations on clinical deployment of antibacterial titanates and discussed further in Section Combinatorial material approaches for a wide-range of applications. Silver has long been the most successful and widely used antibacterial element in modified coatings; however, gallium or iodine show promise to provide broad-spectrum antibacterial properties, with combined bioactivity. By combing these elements in titanate structures, which offer enhanced surface area due to their nanoporosity, with exfoliating layers such as Mg or similar, multiple doped coatings can be utilised to meet the challenge of perturbing bacterial growth, increased capacity and longer-term antibacterial action and improved bone bonding.

If antibacterial titanate structures are to be successful, they must address the issues raised in Section Limitations on clinical deployment of antibacterial titanates of long-term antibacterial efficacy, while ensuring limited burst release of the active agent. This is critical to attaining clinical success. To achieve the understanding of how titanate structures, with additional materials/drugs, behave *in vivo* requires *in vitro* use of co-cultures of bacteria and cells and the presence of appropriate proteins. Additionally, understanding how combinations of various bioactive and

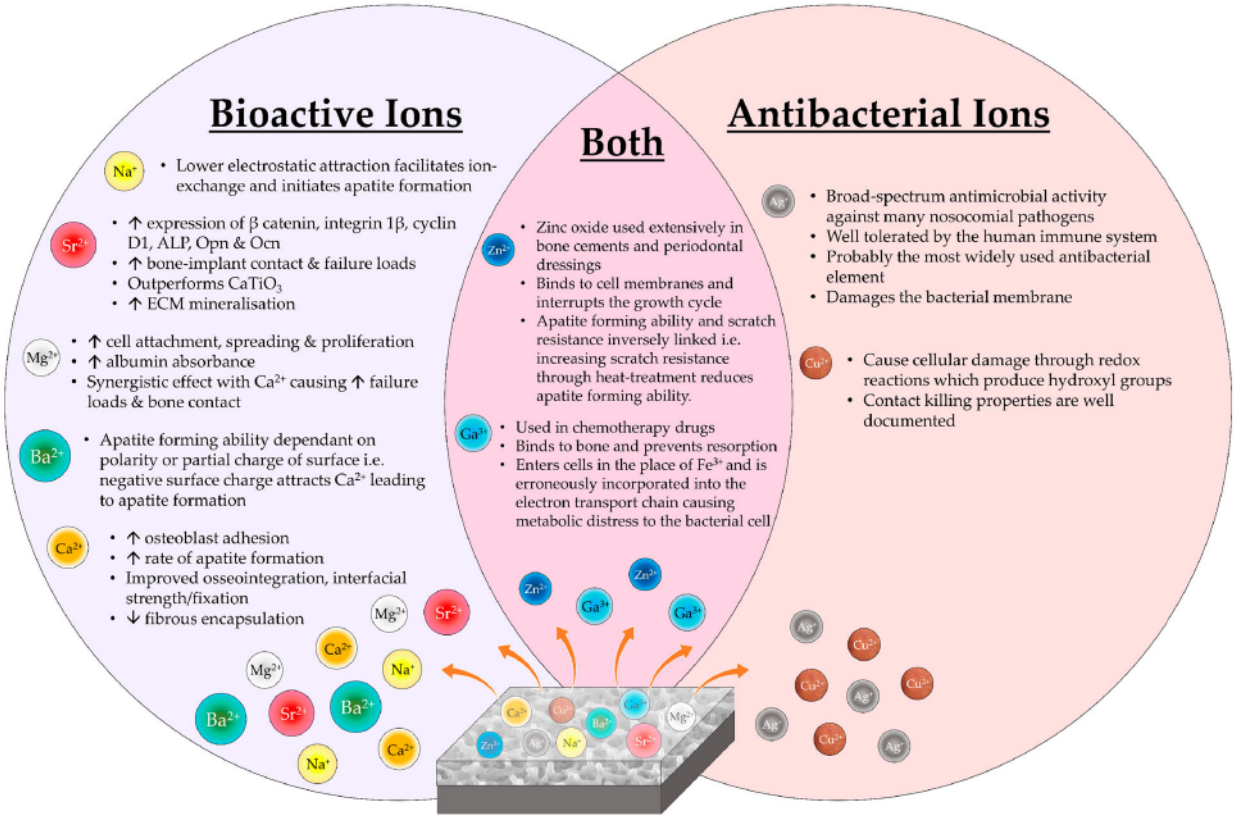

Figure 27. Bioactive and antibacterial effects of specific cations that have been incorporated into titanate structures for biomedical applications.

antibacterial cations affect the chemical, structural and biological properties of the titanate surface is key to finding optimal modes of action against various bacterial types. Figure 27 has been included as it summarises the bioactive, antibacterial and multifunctional cations, which can be utilised in combination to generate effective multi-ion surfaces for a broad range of medical applications.

In vivo trials & subsequent clinical deployment

There have been a small number of *in vivo* studies of implanted alkali-titanate surfaces of biomaterials, demonstrating their clinical potential.

Hip stems

Yan et al. studied the effect of NaOH (4 M, 60°C, 24 h) and heat-treated (600°C, 1 h) Ti implants (Figure 28) through implantation into rabbit tibiae, which were harvested 4, 8 and 16 weeks post-implantation [281]. At 16 weeks, the failure load of the treated implants was ca. 45 N, compared to 14 N for untreated Ti; a marked increase in bone bonding, with no adverse tissue response. There was no significant difference between alkali-treated samples and SBF apatite-formed Ti samples, indicating that the titanate samples can generate apatite *in vivo* and are equivalent to *in vitro* grown apatite surfaces. A similar study by Fujibayashi et al. also exhibited corroboratory results [282].

Further studies by Nishiguchi et al. on alkali-treated Ti [283–286]; and Ti–6Al–4V, Ti–6Al–2Nb–Ta and Ti–15Mo–5Zr–3Al alloys [285,287], showed the alkali-treated Ti metal inserted into rabbit femora and tibiae had failure loads which were significantly higher than that of untreated Ti at 3, 4 and 12 weeks post-implantation (e.g. for rabbit femora, the failure loads were 72.2 ± 41.8 and 411.7 ± 70.6 N, respectively, at 12 weeks) [283,285,287]; and 8 weeks (0.02 ± 0.03 and 2.7 ± 1.5 kgf, respectively) and 16 (0.3 ± 0.4 and 4.1 ± 1.3 kgf, respectively) weeks in the proximal metaphyses of tibiae [284], due to enhanced bone bonding. All alkali-treated alloys exhibited no fibrous tissue intervention at the interface between the bone and implants [287]. Removal of the alkali-treated implants resulted in detachment of bone from the surrounding area, demonstrating that the bone–implant interface exhibited stronger interfacial strength than the surrounding bulk bone.

Regarding total hip replacements, the alkali treatment (5 M NaOH, 60°C, 24 h; followed by 600°C, 1 h heat treatment) has been employed on a Ti–6Al–2Nb–Ta acetabular shell and femoral stem. Implantation of 70 prostheses in 58 patients was performed at two different university hospitals between 2000 and 2002. Follow-up of these uncemented hip

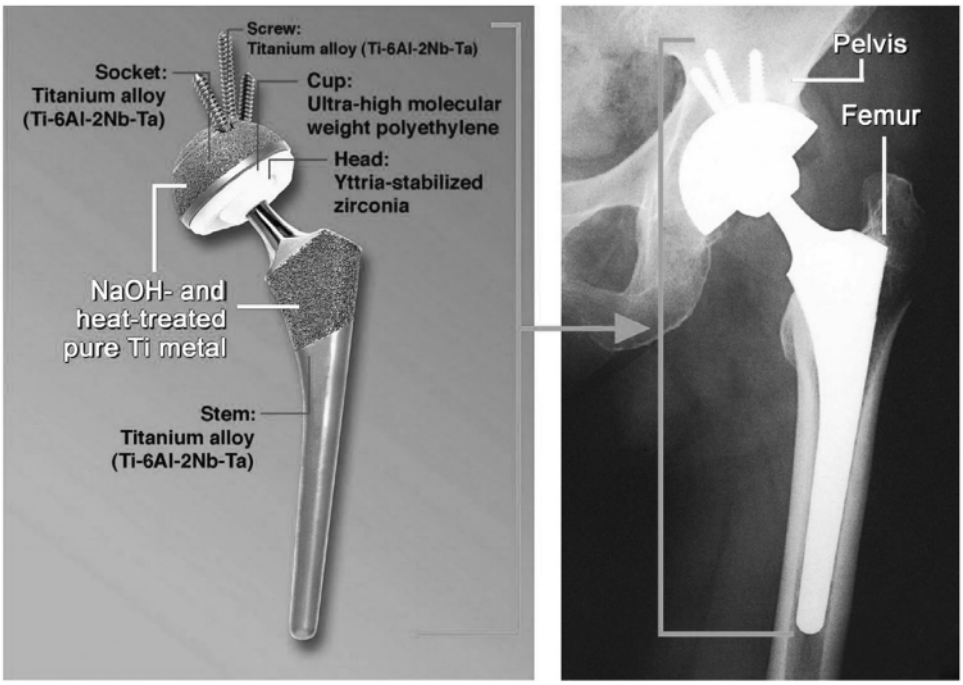

Figure 28. Application of the NaOH and heat treatments to titanium alloys in a clinical hip joint system. Reproduced from Kokubo and Yamaguchi [26], with permission from Wiley.

replacements showed that none of the implants required revision during an average follow-up period of 57.5 months (ca. 4.8 years) [288]. The average JOA score (Japanese Orthopaedic Association score: calculated from pain (/40), range of motion (/20), ability to walk (/20), ability to carry out daily activities (/20), which is quantified by an orthopaedic surgeon; however, it is unclear whether an independent surgeon was used [289]) improved from 46.9 for preoperative assessments, to 91.0 at the final follow-up; a significant increase. No observed osteolysis occurred in the 70 implanted hips, with all gaps closing within 12 months radiologically. These results demonstrated the efficacy of this surface modification in a clinical setting during a relatively short observation period [288]. The devices were made commercially available in 2007 [16].

Longer-term survival rates (min. 8 years; average 10 years) were reported by So et al. [290] and Kawanabe et al. [288]. The overall revision rate was 98% at 10 years, with no radiographic signs of loosening in any of the retrieved implants, as well as no radiographical gaps in any patient 12 months post-operation; survival rate was defined as revision occurring for any reason, with 2 patients requiring revision at 2 weeks and 8 years post-operation due to a periprosthetic femoral fracture and infection of the femoral component, respectively. Bone was found histologically in the pores of the implant within the first 2 weeks (retrieval of a fractured implant), with deep bone bonding in the pores by 8 years from the other implant. Limitations do exist, however, as alternative studies on total hip arthroplasties have shown, as highlighted in Table 4, that the samples size and study length should be increased to confirm alkali-treated implant superiority [290].

Spinal fusion cages

Spinal fusion cages (Figure 29) have also been considered; however, the level of osteoinductivity from alkali-treated surfaces alone was lower than necessary for such a device; indeed, most spinal devices require an autograft in order to induce bone growth. Therefore, a combinatory surface treatment was employed in order to improve the osteoconduction and osteoinduction of such surfaces for spinal fusion devices. NaOH treatments (5 M NaOH, 60°C, 24 h) subjected to water- (ultrapure, at 40 or 80°C for various periods up to 48 h) and heat treatments (600°C, 1 h) formed a Na-free titanium oxide onto pure Ti (>99.5%), which was also found to bond to living bone [301]. The premise for such a treatment is that the conversion from the sodium titanate gel into anatase should confer a more effective apatite nucleating surface, based on compositional and structural studies conducted by Uchida et al. and Wei et al. [302–304]. For example, apatite formation requires appropriate crystallographic matching between the apatite crystal and the material surface; the apatite (0001) plane matches better to the (110) anatase plane compared to the (101) rutile plane. Similarly, apatite formation is inhibited if the titania gel is amorphous. By conducting water treatments, a higher quantity of Ti–OH groups are found on the surface, which enhances apatite nucleation. Fujibayashi et al. discovered that such surfaces formed on porous sintered pure Ti ($5 \times 5 \times 7$ mm^3,

Table 4. Review of selected articles studying the successfulness of cementless total hip arthroplasties.

Author	No. of total hips/revisions	Average follow-up period (years; range)	Material/Surface modifications	Survival rate (%)
Garcia-Cimbrelo et al. [291]	124/11	11.3 (10–13)	Alloclassic Zweymüller stem (Ti–6Al–7Nb) with a pure Ti Zweymüller threaded cup. Average roughness (R_a) of 3–5 µm Grit-blasted	94.1*
Shetty et al. [292]	134/6	14.2 (13–15)	JRI Furlong hydroxyapatite-coated prosthesis	99*
de Witte et al. [293]	102/3	11.8 (10–17)	CementLess Spotorno (CLS) system: titanium press-fit femoral stem and a cementless titanium alloy (Ti–6Al–7Nb) expanding acetabular cup. 150–250 mm thick hydroxyapatite-coated surface	92.2*
Sariali et al. [294]	131/11	10 (8–11)	Symbios SPS anatomic proximally hydroxyapatite (HA)-coated stem	96.8*
Nourissat et al. [295]	90/7	9.2 (8–10.2)	Stryker ABG II cementless hydroxyapatite (HA) coated stems. The ABG II hemispherical acetabular components made of titanium alloy (Ti–6Al–4V) and totally HA-coated.	94.2[b]
So et al. [290]	67/3	10 (8–12)	AHFIX Q System; KYOCERA Medical Corporation, Japan cementless metaphyseal prostheses made from a titanium alloy (Ti–6Al–2Nb–1Ta–0.8Mo). All underwent alkaline (5M NaOH, 60°C, 24 h) and heat treatments (600°C, 1 h) on a 700 µm thick circumferential porous surface made by pure titanium plasma-sprayed coating. The pore size was 350–450 µm. The acetabular shell was completely coated, but only the proximal third of the femoral stem was coated circumferentially.	98[a]
Wittenberg et al. [296]	204/9	4.9 (2.9–7.1)	Metha Short Hip Stem cementless implant with modular titanium adapters. 0.35 mm Ti coating and 20 µm dicalcium phosphate coating	96.7[c]
Jameson et al. [297]	35,386/448	5 (no min. stated–max. 7.5)	Corail stem is a fully hydroxyapatite(HA) coated non-porous forged titanium alloy stem with atrapezoid cross-section proximally and a quadrangular cross-section distally	97.6[a]
Mäkelä et al. [298]	Total study (347,899/16,500) Cementless (71,454/3,539)	4.9 (0–17)	Large Nordic study on all hip replacement types	92.6[a] (10 years) 85.3[a] (15 years)
Noiseux et al. [299]	493/6	3.5 (2–10)	Porous tantalum acetabular components	98.8[a]
Hoskins et al. [300]	41,265/551	13	Corail stem is a fully hydroxyapatite(HA) coated non-porous forged titanium alloy stem with atrapezoid cross-section proximally and a quadrangular cross-section distally	97.6[a]
National Joint Registry Annual Report [2]	410,296/38,568 (Data from Apr. 2003 and Dec. 2018)	15 (N/A)	All uncemented, various implants used	90.6[a]

[a]End point was set at revision, regardless of reason.
[b]End point was reoperation, regardless of reason.
[c]Kaplan–Meier revision rate was calculated. Table is an update on the table presented by So et al. [290]. Material and surface modification details are provided where possible.

porosity = 40–60%, pore size = 300–500 µm), also inherently bonded to bone *in vivo*, as well as work from Fujibayashi et al., Takemoto et al., Fukuda et al. and Tanaka et al., confirming both osteoinductive [305–307] and osteoconductive [308] properties.

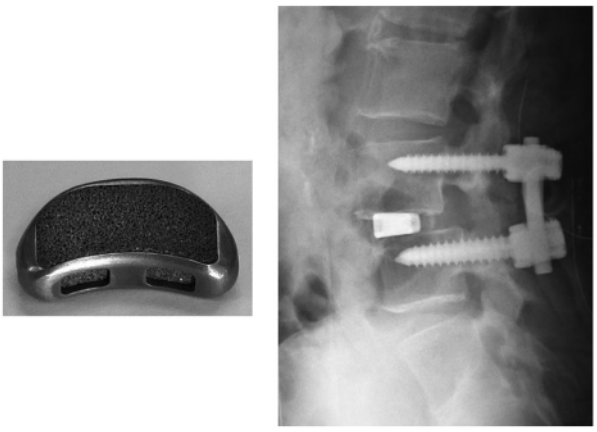

Figure 29. Spine fusion device of porous Ti metal subjected to NaOH, HCl and heat treatments (left-hand side) and its clinical application (right-hand side). Reproduced from Kokubo and Yamaguchi [26], with permission from Wiley.

To improve the osteoinductivity further, the water treatment can be replaced with 0.5 mM HCl, in particular for porous structures, where water treatments could not remove all the sodium within complex 3D structures [306]. A comparison between water and acid post-treated samples was conducted through implantation into canine muscles, with the new bone area (BA) fraction (bone growth in total pore area) and bone incidence (number of bone-induced samples/number of implanted samples) measured [306]. BA and incidence after 3 months for water-treated samples were 0.5 ± 0.6% and 1/4, respectively, with acid-treated samples exhibiting area and incidence values of 8.3 ± 2.5% and 4/4, respectively. The acid-treated samples exhibited significantly ($p < 0.05$) superior osteoinductivity at 3, 6 and 12 months [306]. Alternative HCl concentrations have been suggested by Pattanayak et al. to induce apatite formation, as well as differing heat treatment

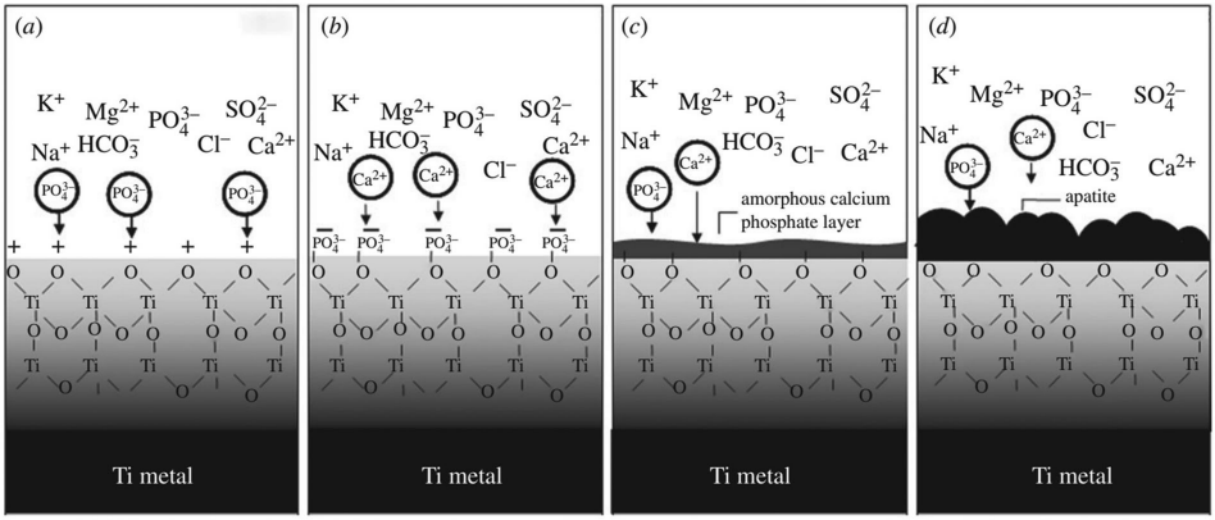

Figure 30. Process of formation of apatite on positively charged Ti metal in SBF. Apatite is formed by the process shown in (a–d). Reproduced from Kokubo et al. [315], with permission from the Royal Society.

temperatures and acid types (HCl, H_2SO_4 or HNO_3); the optimal conditions were found to be 10–100 mM (40°C, 24 h), 500–700°C (1 h), irrespective of acid type [309–311]. Another approach is to generate a titanium hydride layer (TiH_x; where $0 < x < 2$) on chemically treated Ti, which also adsorbed SO_4^{2-} and/or Cl^- ions from the solution used; a 1:1 ratio of HCl and H_2SO_4 [312]. The surface formed exhibited a micron scale roughness ($R_a = 0.99 + 0.07$ µm and $R_z = 8.87 + 0.94$ µm), compared to the nanometer scale roughness (R_a = ca. 100–200 nm from AFM [313]) exhibited by the sodium and calcium titanate surfaces. Heat treatment of this surface generated a rutile structure, with the SO_4^{2-} and/or Cl^- ions adsorbed, without morphological change. These surfaces formed apatite in SBF within 1 d via a different mechanism (Figure 30) to the described sodium titanate method (see Figure 5). Initially, the adsorbed ions (chloride and sulphates) dissociated from the surface, generating an acidic environment, which caused the Ti–O bonds to become positively charged on the surface (affirmed via zeta potential and XRD analyses). This attracted the negative phosphate ions, which following their accumulation, caused the surface to become negatively charged. This subsequently attracted the positively charged calcium ions from solution and formed an amorphous calcium phosphate. The timeline for these exchanges is suggested due to the presence of Ca and P in XPS as a function of SBF soaking time (1 and 30 min, 1, 6 and 12 h). P is seen in as little as 30 min, while Ca develops after 1 h for the heat-treated samples. Over time, this amorphous surface layer matured into crystalline apatite. Furthermore, as stated before, the acid-treated surface is not affected by humid environments; a significant issue of alkali-treated surfaces. An example of this was conducted by Kawai et al., whereby a porous Ti metal subjected to acid- and heat treatments was implanted into a rabbit femur [314]. The surrounding bone deeply penetrated into the porous structure within 3 weeks, in contrast to that of purely-acid and purely-heat-treated surfaces [314].

A canine model was set up by Takemoto et al. to establish the *in vivo* efficacy [316]. Aimed as a lumbar interbody fusion device, the structure consisted of a porous titanium construct (50% porosity; average pore size ca. 300 µm). Five devices were treated with 5 M NaOH (60°C, 24 h), followed by 0.5 mM HCl (40°C, 24 h), ultrapure water- (40°C, 24 h) and heat treatments (600°C, 1 h); another five constructs remained untreated. After 3 months, the radiological evaluation showed all treated devices achieved interbody fusion, while only 3/5 of the untreated did. Furthermore, histomorphometric evidence demonstrated the treated samples exhibited greater BA ingrowth percentage: ca. 16.7% *v.* 13.4%; as well as increased bone contact: ca. 34.9 *v.* 10.5.

Following the canine model, five spinal fusion devices were implanted into patients in Japan between 2008 and 2009 [317]. Not only did bone union occur in all of the patients, but there was no need for autologous iliac crest bone grafting, an ideal advantage for such a device. All clinical results improved from pre- to post-operatively, with no adverse effects occurring during all follow-ups tested. However, a further, larger, longer-term study is required to fully evaluate its efficacy [317]. For example, the leaching of ions in a confined volume may rapidly alter the local pH, which may result in adverse effects on living cell activity in small pores of porous structures, which should also be assessed.

Bone screws/dental root-shaped implants

Despite their success in clinical trials, the initial consensus for wet-chemically derived titanate structures

was that their application should be limited due to the lower torsional shear stress (9.5 MPa [318]) they can withstand. The torsional moment in these applications can exceed 50 lb.-in (>5.6 Nm) [319]. However, more recently, modifications have been made to the original treatment methods (5 M NaOH, 60°C, 24 h) in order to confer titanate structures onto bone screws, with the intention of withstanding the forces during insertion.

For example, Zhu et al. [320], used a pre-treatment of 2M H_2O_2/0.1M HNO_3 on Ti–6Al–4V screws, followed by a relatively low concentration of NaOH treatment (1 M, 383 K, 4 h). Furthermore, the subsequent calcium treatment utilised calcium acetate (0.04 M, combined with NaOH), rather than $CaCl_2$ or CaO. The screws were then implanted into rabbit femoral condyles, with the $CaTiO_3$-coated screws exhibiting greater ALP activity and cell proliferation than the untreated screws at 7 days. After 12 weeks of implantation, the untreated screw showed no differences at the bone-screw interface, with no physical bonding. However, the $CaTiO_3$-coated screw demonstrated a combination with bone tissue in as little as 2 weeks. These observations are likely due to the $CaTiO_3$ promoting cell adhesion and proliferation, chemical bonding between bone and the Ca-rich coating, as well as high surface roughness, increasing the bone contact area.

Wang et al. [321] modified the temperature of synthesis conditions with subsequent 5M NaOH and 0.05 mM $CaCl_2$ solutions both held at 160°C with dwell times of 10 and 24 h, respectively. The $CaTiO_3$--coated screws were compared against HA plasma sprayed screws. 12 weeks post-implantation the histomorphometric analysis showed no significant difference between the two treated screws in terms of BA percentage (78.33 ± 0.71 *v.* 79.11 ± 0.41% for $CaTiO_3$ and HA, respectively; uncoated = 42.28 ± 1.04%). However, greater strength was seen for the HA-coated screws compared to the $CaTiO_3$ coating at 12 weeks (ca. 40 *v.* 26 fixation index). The $CaTiO_3$ coating had nano-apertures (ca. 1–4 nm), while HA coating showed apertures with pore size between 100 and 200 µm. These larger apertures may explain the greater mechanical bonding.

Pure $CaTiO_3$ screws have also been investigated, such as the study by Gathen et al. [322]. In this study, four paediatric patients (2–14 years) and four cadaver tibias were used, with the comparison between $CaTiO_3$, HA and SS screws. $CaTiO_3$ screws generated a significantly better fixation index (ca. 0.81) than both the HA (ca. 0.66) and SS (ca. 0.51) screws.

Dental root-shaped implants with a sodium titanate coating have also been investigated. Dental implant treatment requires rapid healing times for clinical loading and high rates of osseointegration, which is more specifically required in elderly patients with completely edentulous jaws. Camargo et al. [5] highlighted the potential use of alkali-titanate-treated (5 M NaOH, 60°C for 1, 2, 3, 5 and 7 d), grit-blasted Ti implants for dental repair. Results showed the formation of sub-micron-structured alkali-titanate layer. *In vitro* tests showed, alkali-treated Ti surfaces had the ability to stimulate mineralisation upon soaking in SBF, while *in vivo* histomorphometrical analyses showed similar values for BA (BA%: 35.8 ± 6.9 *v.* 35.3 ± 9.0, respectively) and bone-to-implant contact (BIC%: 50.6 ± 12.8 *v.* 62.0 ± 15.0, respectively) for both commercially available, grit-blasted, acid-etched Ti implants and the alkali-treated counterpart, demonstrating their clinical potential. Overall, the collected studies highlight the potential for alkali titanates as a coating for orthopaedic screws and dental root-shaped implants, broadening the applicability of titanate materials.

Improving applicability: generating titanate structures onto non-Ti substrates

Presently, nanoporous titanate structures generated through wet-chemical conversion have been limited in their applicability to only titanium-containing materials and alloys. In order to convey the beneficial properties of titanate structures, including nanoporosity and bioactive and/or antibacterial properties, onto or embedded in alternative materials, such as polymers, ceramics and other metals/alloys, novel methodologies are needed to be considered.

One methodology which can be utilised is coating alternative materials with a layer of Ti, which is the subsequently modified using the conventional NaOH treatment (5M, 60°C, 24 h). Wadge et al. [37] investigated this, for the first time, utilising a combinatorial approach of DC magnetron sputtering Ti coatings, which are then converted (Figure 31). It was found that more equiaxed sputtered films generated thicker titanate structures due to the optimisation of surface area and the angle of growth of the titanate nanocrystals (see Figure 32). This methodology can potentially be applied to biodegradable fracture fixation devices.

Wadge et al. [323] demonstrated the potential application of sodium and calcium titanate thin films on biodegradable Mg substrates and measured the potential benefit to their corrosion resistance for biodegradable medical applications, such as fracture fixation devices, for example, bone plates. This study demonstrated that the conversion of Ti coatings into a calcium titanate structure increased the E_{corr} and decreased the i_{corr} values by 0.16 V and 0.25 mA cm^{-2}, respectively; exemplifying their potential and raising the need for further investigation (Figure 33).

A different approach is to use a sol–gel methodology generating sodium titanate structures on 316L SS (Devi et al. [324]). This also demonstrated a nanoporous

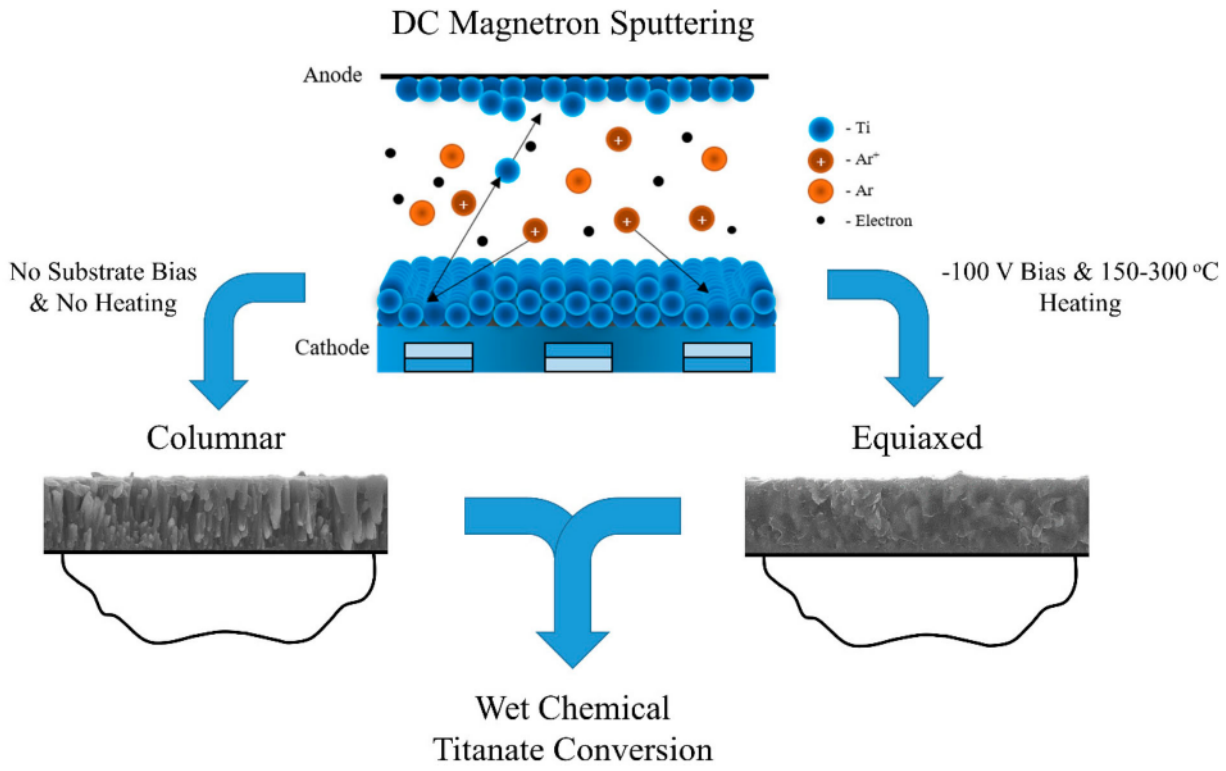

Figure 31. Methodology developed by Wadge et al. [37] for the wet-chemical conversion of DC magnetron sputtered Ti thin films in order to generate nanoporous titanate structures on alternative materials for biomedical applications.

topography, albeit with a different morphology and no chemical bond to the metal surface. The ability to generate different titanate morphologies on alternative substrates broadens the applicability of these surfaces.

Future outlook

Despite the advancements made within the medical literature to date to not only generate multifunctional

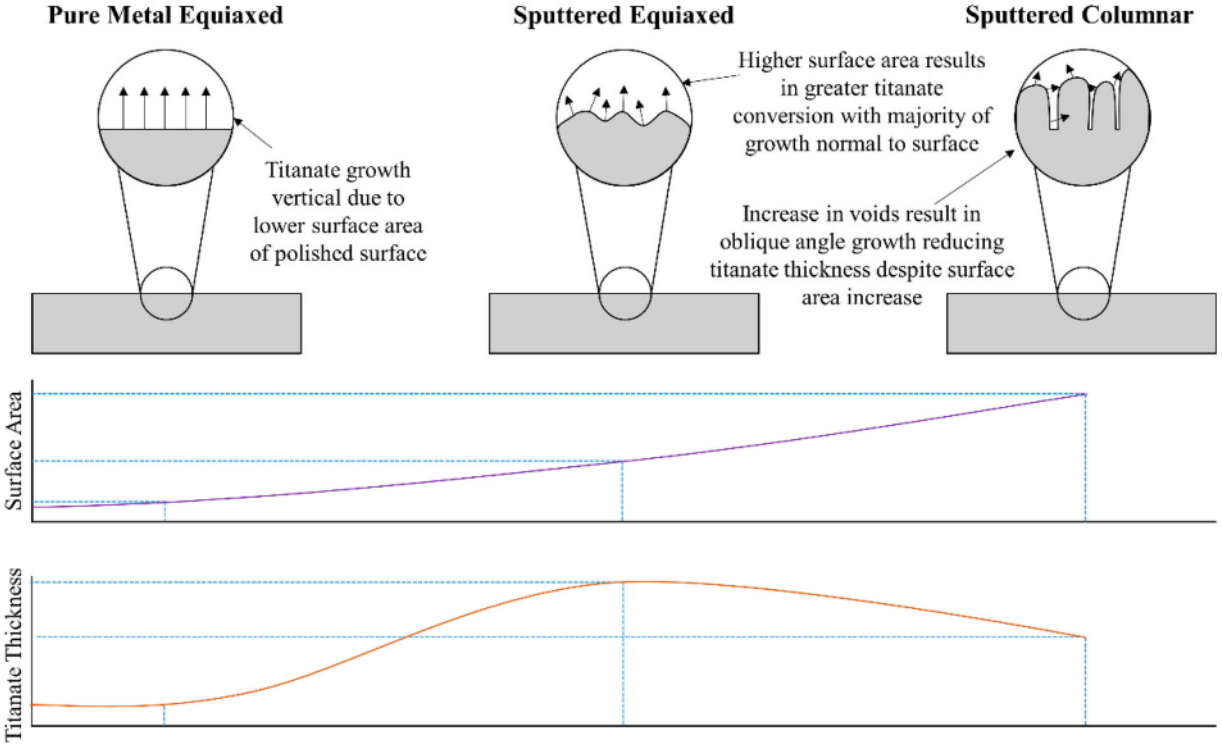

Figure 32. Relative correlation between the surface area of the sputtered Ti coating produced, and the relative effect on the produced titanate thickness in comparison to pure Ti metal conversion, as described by Wadge et al. [37]. The graphs at the bottom are purely a relative representation of the surface area and titanate thickness dependence.

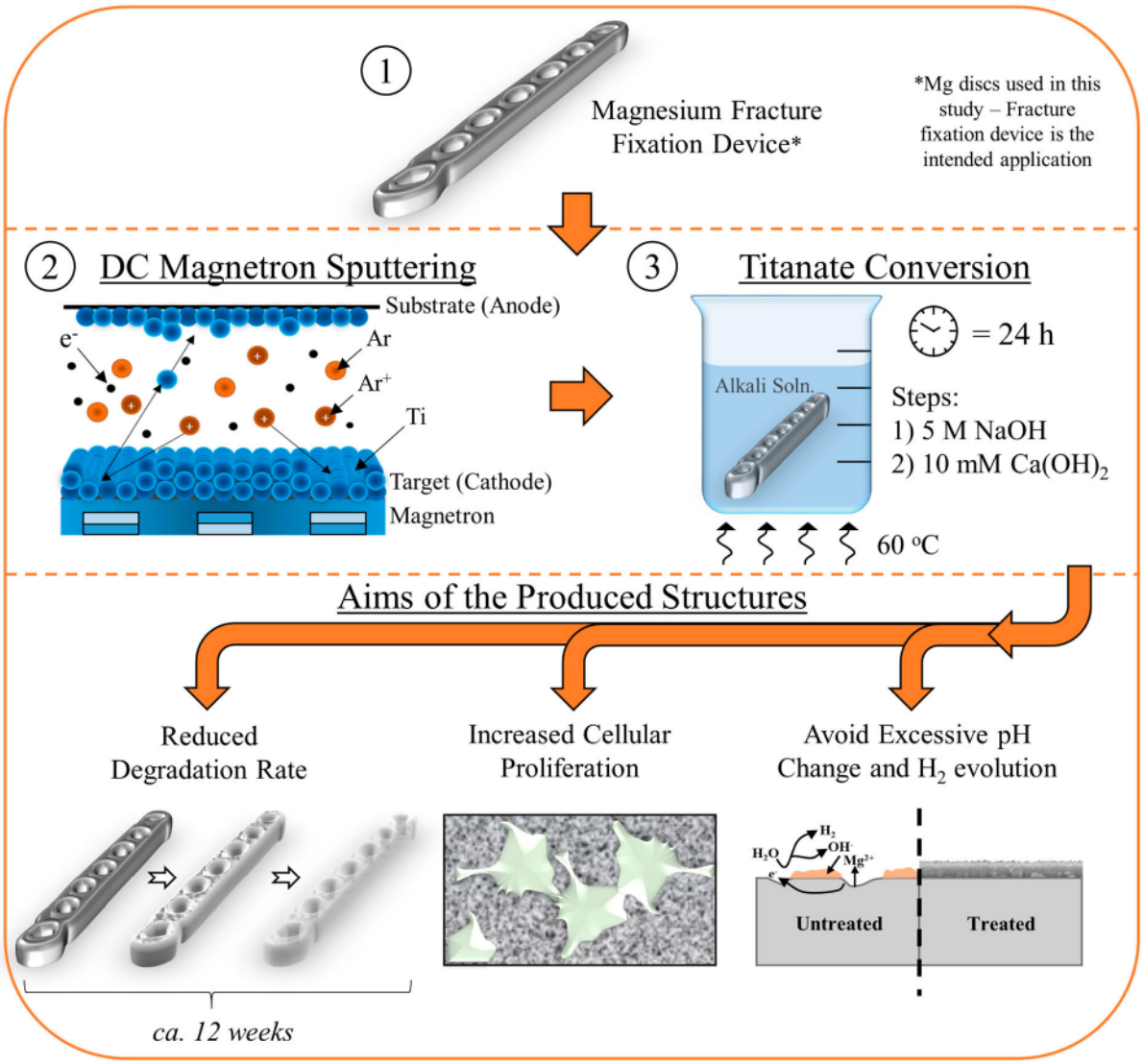

Figure 33. Schematic representation of the desired effect of titanate structures being applied to degradable Mg substrates, through the combination of DC magnetron sputtered Ti thin films and subsequent wet-chemical conversion [323].

titanate structures, with antibacterial, bioactive, and/or piezoelectric/ferroelectric properties but to also generate novel material structures/types, such as nanotubes and titanate glasses, there are still several questions that need novel solutions, as well as interesting areas which should be explored further. These are highlighted below.

Combinatorial material approaches for a wide range of applications

By utilising the advantageous properties of specific titanate structures (porosity, bioactivity, ion-exchangeability, antibacterial) and combining this with all types of materials, either through coating, embedding or multilayering, with further advantageous properties (antithrombogenic, improved radiopacity, drug eluting), novel and effective combinations can be made. For example, the combination of a titanate-converted Ti material, which is doped with a drug (for example Aspirin which is used in stent treatments, or alendronate and minodronate which are used in osteoporosis treatment), with an additional coating on top (such as PEG or gelatin), has been used in studies by Mohanta et al. [325] and Yamaguchi et al. [325,326], respectively. The potential impact of titanate materials often benefits from the generation of –OH groups on their surface, which enables connection to drugs and polymeric layers. Combining this with the porosity on the surface, drug loading and mechanical interlocking between additional coatings makes titanate structures for novel applications ideal. They key issue for future studies will be to investigate which drugs can be loaded into the structure, while providing additional multilayers that will facilitate the elution post-insertion. Ensuring appropriate bonding with the titanate structure is also critical, and potentially biodegradable multilayers may provide the added benefit of disrupting bacterial attachment and subsequent biofilm formation. These properties should then be assessed in relation to bactericidal and cellular efficacy, in both *in vitro* and *in vivo*

models, as well as understanding the elution mechanism, release profile and whether environmental factors affect these.

The path to broad-spectrum titanates, standardised testing, and 'smart' coatings

Most studies focus on small sets of bacterial types (e.g. *E. coli, Staphylococcus aureus*), and if the materials being tested can reduce/kill the bacteria, then these surfaces are branded as antibacterial, or even antimicrobial; the distinction being antibacterial is solely bacteria, while antimicrobial includes other microbes, such as fungi. This should not be sufficient to quantify a material as antibacterial and antimicrobial, since only a small subset of bacterial types are tested in each study; due to time constraints or availability of different strains. The present cut-off for most studies is sub-optimal, as well as clear differences in the type of assessment (direct *v.* indirect), bacteria used, additional factors (omission of co-culture, proteins, etc.) making clear comparison difficult. Expanding this further is key for appropriate standardisation of antibacterial assessment.

A review by Cloutier et al. succinctly sums up the current issues on antibacterial coatings, and the sub-optimal testing regimes [327]. Multipronged approaches are key to the development of next-generation antibacterial coatings, with multiple modes of action, since every bacteria has different levels of susceptibility to each mode of action (contact killing, metabolic or membrane disruption, etc.). Most *in vitro* testing does not mimic *in vivo* conditions; co-culture with cells, cultures with multiple strains, relevant proteins to specific environments, host immune responses, and biofouling, and combining this with intended applications/environments, is similarly overlooked.

A good example of the targets and goals that should be adopted by researchers in terms of the range of assessments required to provide a more complete assessment was a recent study by Ikeda et al. [278]. This study investigated the doping of iodine in the calcium titanate structure and provided the following assessments: SEM, XPS, XRD, Raman; *in vitro* cell proliferation, adhesion (SEM), fluorescent immunostaining; ALP activity, gene expression (ALP, Ocn, Opn, integrin β1, Col1a1); *in vitro* antibacterial assessment (CFU, LIVE/DEAD, crystal violet assay, SEM); and *in vivo* animal testing (biomechanical detachment, histological examination, XPS post-retrieval, blood test to test renal and thyroid function, antibacterial assessment (implant site observation, CFU, histological assessment)). Despite only one bacteria type being tested, the level of investigation has the necessary detail, and if incorporated with multiple bacteria types, and potentially co-culture *in vitro*, would be a significant step towards a standardised process. Limitations were also presented within the study which is helpful in determining future targets. For example, larger implants and larger experimental animals should be used to suitably compare to real *in vivo* scenarios. Long-term antibacterial effects and toxicity need evaluation for iodine-containing titanate surfaces. Finally, antimicrobial activity against refractory infections such as osteomyelitis (a difficult-to-treat disease causing bone destruction due to repeated inflammation) was not investigated, and hence validation using a refractory infection model is required.

Other targets include broad-spectrum and application-specific testing protocols are needed to ensure that if a surface can be claimed as antibacterial, it should satisfy a wide-range of bacterial types, with specific arrays being used for medical implants that are nosocomial, i.e. specific to hospitals, and designing appropriate protocols [328]. Standardisation of these methodologies is also paramount to avoid wastage of research effort. Longer-term stability of coatings is also a severely overlook property, and possibly one of the main reasons for the absence of studies at the clinical stage.

Specific stimuli is also an exciting target area. This includes 'On-demand' release of antimicrobial agents, such as delayed, controlled and/or sustained release, which can be triggered through pH changes, increasing/decreasing temperature, contact with specific environments (e.g. blood), exogenous stimuli (magnetic, ultrasound, etc.) and/or levels of O_2 [327]. Typically, titanate structures release cations upon suspension in aqueous environments. Therefore, to impart on-demand release, combination with additional surfaces or materials to inhibit/modify the ability for cationic release, should be targeted. For example, utilising the piezoelectric properties of some titanate materials, may allow doping of the structure, which in a particular stressed orientation could inhibit release. However, once an appropriate electrical stimulus is applied, it can distort to release the required agent. This would likely be useful in sensing applications, such as for diabetic patients, which could enable localised, controllable release of a drug or specific cation.

Interlinked titanates for scaffold generation

A key direction in the field of wet-chemical titanates will be cross-linking of titanate structures to be used as bridges or interfaces between materials, particularly in the production of scaffolds. The potential for cross-linking and bonding between titanate struts has been developed by Wadge et al. [329]. Through modification (5 M NaOH, 60°C, 24 h) of Ti–6Al–4V microspheres, interlinking between microspheres was seen, with clear densification of the titanate film (Figure 34). However, fully utilising this property in specific

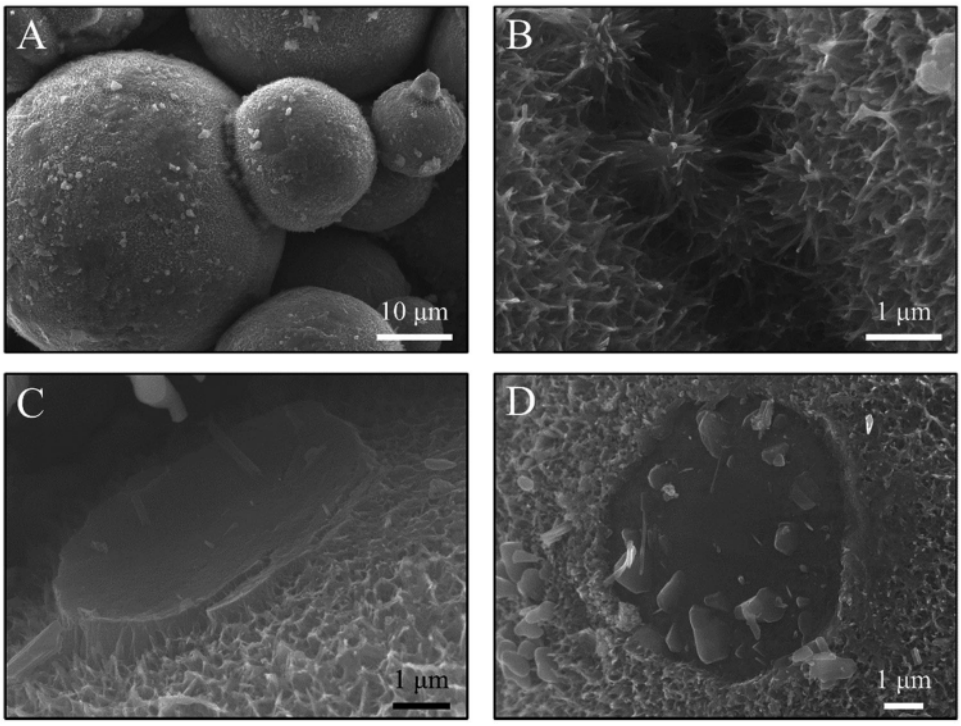

Figure 34. SEM micrographs showing cross growth and fracture features noted on the titanate-converted Ti6Al4V microspheres. (A,B) Cross-linking of two individual microspheres through the growth and bonding of the produced titanate nanostructures at different magnifications. (C,D) Smooth morphology of the microsphere surfaces at the failure of the bonded interface at either end of the failure. Reproduced from Wadge et al. [329], with permission from Elsevier.

applications has yet to be realised. Potential future studies could investigate the production of porous scaffolds, which can be used as an implantable filler for bone defects. Further than this, if the reaction where the titanate struts interlock can occur *in situ*, this would allow injectable pastes which can self-assemble into defects, particularly if the titanate materials can be developed onto degradable materials (either polymeric or Mg).

Remarks and conclusion

The field of nanoporous alkaline titanate structures for medical applications has developed extensively in the past two decades, with highly promising clinical data to suggest their potential for orthopaedic and dental applications. We have highlighted the key processes that have been used to generate such structures, the development of alternative structures (nano-whiskers, titanate glasses, etc.) and materials properties (piezoelectric/ferroelectric), as well as the movement into multifunctional doped titanate coatings to address the significant burden of antibiotic-resistant infections.

Despite the numerous advances, some critical limitations, as well as potential further areas to explore, still exist. It is, therefore, critical that researchers consider these areas, particularly the formalisation of standardised, broad-spectrum antibacterial testing, long-term stability antibacterial titanate coatings, as well as combinatorial surfaces which incorporate titanate structures, in order to bring such advances into clinical practice. This can only be achieved if extensive collaboration, between clinicians, scientists, patients and regulatory bodies is realised. It is critical that translation is considered at all aspects during research, with the long-term goal being clinical deployment.

To conclude, in this review, we have demonstrated that alkaline titanate materials offer a flexible platform to produce a diverse range of multifunctional nanostructures that can be utilised to impart useful properties, such as bioactivity, piezoelectric behaviour, drug delivery and antibacterial protection. The potential to be applied to any surface through suitable interlayer and their unique ability for facile multi-element substitutions make them of significant interest. We have demonstrated that the understanding of the property, processing and performance of the material combinations is still in its infancy in terms of complex *in vivo* interactions. Alkaline titanate multifunctional properties allow for future innovations in addition to those listed above from corrosion and degradable materials, antibacterial surface, controlled release drug delivery, scaffold generation for biomaterials and sensors and are of interest to the biomedical industry and beyond.

Acknowledgements

This work was supported by the Engineering and Physical Sciences Research Council through an EPSRC Doctoral Prize Fellowship [grant number EP/T517902/1].

Funding

This work was supported by Engineering and Physical Sciences Research Council through an EPSRC Doctoral Prize Fellowship [grant number EP/T517902/1].

Disclosure statement

No potential conflict of interest was reported by the author(s).

ORCID

Matthew D. Wadge http://orcid.org/0000-0002-5157-507X
Jamie McGuire http://orcid.org/0000-0002-4162-2987
Reda M. Felfel http://orcid.org/0000-0003-4651-9759
Ifty Ahmed http://orcid.org/0000-0001-7868-3698
David M. Grant http://orcid.org/0000-0002-6786-7720

References

[1] D.o.E. United Nations, P.D. Social Affairs, World Population Prospects. (2019). Highlights.
[2] NJR. NJR 14th Annual Report, National Joint Registry 2017.
[3] Evans JT, Evans JP, Walker RW, et al. How long does a hip replacement last? A systematic review and meta-analysis of case series and national registry reports with more than 15 years of follow-up. Lancet. 2019;393(10172):647–654.
[4] Guo T, Gulati K, Arora H, et al. Race to invade: understanding soft tissue integration at the transmucosal region of titanium dental implants. Dent Mater. 2021;37(5):816–831.
[5] Camargo WA, Takemoto S, Hoekstra JW, et al. Effect of surface alkali-based treatment of titanium implants on ability to promote in vitro mineralization and in vivo bone formation. Acta Biomater. 2017;57:511–523.
[6] Albrektsson T, Brånemark P-I, Hansson H-A, et al. Osseointegrated titanium implants: requirements for ensuring a long-lasting, direct bone-to-implant anchorage in man. Acta Orthop Scand. 1981;52 (2):155–170.
[7] Pilliar RM. Cementless implant fixation – toward improved reliability. Orthoped Clin North Am. 2005;36(1):113–119.
[8] Tsui Y, Doyle C, Clyne T. Plasma sprayed hydroxyapatite coatings on titanium substrates part 2: optimisation of coating properties. Biomaterials. 1998;19 (22):2031–2043.
[9] Zhou H, Li F, He B, et al. Effect of plasma spraying process on microstructure and microhardness of titanium alloy substrate. J Therm Spray Technol. 2008;17(2):284–288.
[10] Liu X, Chu PK, Ding C. Surface modification of titanium, titanium alloys, and related materials for biomedical applications. Mater Sci Eng: R: Reports. 2004;47(3–4):49–121.
[11] Abu-Amer Y, Darwech I, Clohisy JC. Aseptic loosening of total joint replacements: mechanisms underlying osteolysis and potential therapies. Arthritis Res Ther. 2007;9(Suppl 1(1)):S6.
[12] Tufekci E, Brantley WA, Mitchell JC, et al. Crystallographic characteristics of plasma-sprayed calcium phosphate coatings on Ti-6Al-4V. Inter J Oral Maxillofacial Implants. 1999;14:661–672.
[13] Purdue PE, Koulouvaris P, Nestor BJ, et al. The central role of wear debris in periprosthetic osteolysis. HSS J. 2006;2(2):102–113.
[14] Takadama H, Kim HM, Kokubo T, et al. TEM-EDX study of mechanism of bonelike apatite formation on bioactive titanium metal in simulated body fluid. J Biomed Mater Res. 2001;57(3):441–448.
[15] Kokubo T, Kim H-M, Kawashita M. Novel bioactive materials with different mechanical properties. Biomaterials. 2003;24(13):2161–2175.
[16] Kokubo T, Matsushita T, Takadama H. Titania-based bioactive materials. J Eur Ceram Soc. 2007;27(2–3):1553–1553.
[17] Kokubo T. Design of bioactive bone substitutes based on biomineralization process. Mater Sci Eng: C. 2005;25(2):97–104.
[18] Kokubo T, Yamaguchi S. Bioactive titanate layers formed on titanium and its alloys by simple chemical and heat treatments. Open Biomed Eng J. 2015;9 (1):29–41.
[19] Kizuki T, Takadama H, Matsushita T, et al. Preparation of bioactive Ti metal surface enriched with calcium ions by chemical treatment. Acta Biomater. 2010;6(7):2836–2842.
[20] Kizuki T, Matsushita T, Kokubo T. Antibacterial and bioactive calcium titanate layers formed on Ti metal and its alloys. J Mater Sci: Mater Med. 2014;25 (7):1737–1746.
[21] Yamaguchi S, Matsushita T, Kokubo T. A bioactive Ti metal with a Ca-enriched surface layer releases Mg ions. RSC Adv. 2013;3(28):11274–11282.
[22] Yamaguchi S, Nath S, Matsushita T, et al. Controlled release of strontium ions from a bioactive Ti metal with a Ca-enriched surface layer. Acta Biomater. 2014;10(5):2282–2289.
[23] Kim HM, Miyaji F, Kokubo T, et al. Preparation of bioactive Ti and its alloys via simple chemical surface treatment. J Biomed Mater Res. 1996;32 (3):409–417.
[24] Kokubo T, Miyaji F, Kim HM, et al. Spontaneous formation of bonelike apatite layer on chemically treated titanium metals. J Am Ceram Soc. 1996;79 (4):1127–1129.
[25] Kokubo T, Yamaguchi S. Novel bioactive materials developed by simulated body fluid evaluation: surface-modified Ti metal and its alloys. Acta Biomater. 2016;44:16–30.
[26] Kokubo T, Kim H-M, Kawashita M, et al. REVIEW bioactive metals: preparation and properties. J Mater Sci: Mater Med. 2004;15(2):99–107.
[27] Kokubo T, Yamaguchi S. Bioactive Ti metal and its alloys prepared by chemical treatments: state-of-the-art and future trends. Adv Eng Mater. 2010;12 (11):B579–B591.
[28] Kirmanidou Y, Sidira M, Drosou ME, et al. New Ti-alloys and surface modifications to improve the mechanical properties and the biological response to orthopedic and dental implants: a review. Biomed Res Int. 2016: 2908570.
[29] Mbulanga C, Djiokap ST, Urgessa Z, et al. Formation mechanism of the rutile-phase of TiO_2 nanorods on Ti foil substrate by gel-calcination method. J Sol-Gel Sci Technol. 2018;85 (3):610–620.

[30] Sun X, Li Y. Synthesis and characterization of ion-exchangeable titanate nanotubes. Chemistry. 2003;9 (10):2229–2238.
[31] Wang Y, Du G, Liu H, et al. Nanostructured sheets of Ti-O nanobelts for Gas sensing and antibacterial applications. Adv Funct Mater. 2008;18(7):1131–1137.
[32] Sakka S, Kozuka H, Fukumi K, et al. Aluminate and titanate glasses. J Non-Cryst Solids. 1990;123(1–3):176–181.
[33] Genchi GG, Marino A, Rocca A, et al. Barium titanate nanoparticles: promising multitasking vectors in nanomedicine. Nanotechnology. 2016;27(23):232001.
[34] Spriano S, Yamaguchi S, Baino F, et al. A critical review of multifunctional titanium surfaces: new frontiers for improving osseointegration and host response, avoiding bacteria contamination. Acta Biomater. 2018;79:1–22.
[35] Nadimpalli ML, Chan CW, Doron S. Antibiotic resistance: a call to action to prevent the next epidemic of inequality. Nat Med. 2021;27(2):187–188.
[36] Laxminarayan R, Duse A, Wattal C, et al. Antibiotic resistance – the need for global solutions. Lancet Infect Dis. 2013;13(12):1057–1098.
[37] Wadge MD, Turgut B, Murray JW, et al. Developing highly nanoporous titanate structures via wet chemical conversion of DC magnetron sputtered titanium thin films. J Colloid Interface Sci. 2020;566:271–283.
[38] Scerri E. The periodic table: its story and its significance. New York: Oxford University Press; 2019.
[39] Boyer R. An overview on the use of titanium in the aerospace industry. Mater Sci Eng A. 1996;213(1–2):103–114.
[40] Sachdev AK, Kulkarni K, Fang ZZ, et al. Titanium for automotive applications: challenges and opportunities in materials and processing. Jom. 2012;64 (5):553–565.
[41] Geetha M, Singh A, Asokamani R, et al. Ti based biomaterials, the ultimate choice for orthopaedic implants–a review. Prog Mater Sci. 2009;54(3):397–425.
[42] Bergmann CP, Stumpf A. Biomaterials. In: Dental ceramics. Topics in mining, metallurgy and materials engineering. Berlin: Springer; 2013. p. 9–13.
[43] Brunette DM, Tengvall P, Textor M, et al. Titanium in medicine: material science, surface science, engineering, biological responses and medical applications. Springer: Springer Science & Business Media; 2012.
[44] Elias C, Lima J, Valiev R, et al. Biomedical applications of titanium and its alloys. Jom. 2008;60 (3):46–49.
[45] Long M, Rack H. Titanium alloys in total joint replacement – a materials science perspective. Biomaterials. 1998;19(18):1621–1639.
[46] Sabatini AL, Goswami T. Hip implants VII: finite element analysis and optimization of cross-sections. Mater Des. 2008;29(7):1438–1446.
[47] Navarro M, Michiardi A, Castano O, et al. Biomaterials in orthopaedics. J R Soc Interface. 2008;5(27):1137–1158.
[48] Alvarado J, Maldonado R, Marxuach J, et al. Biomechanics of hip and knee prostheses. Applications of Engineering Mechanics in Medicine, GED–University of Puerto Rico Mayaguez; 2003:1–20.
[49] Oldani C, Dominguez A. Titanium as a biomaterial for implants. Recent advances in arthroplasty, InTech 2012.
[50] Hermawan H, Ramdan D, Djuansjah JR. Metals for biomedical applications. Biomedical engineering-from theory to applications, InTech 2011.
[51] Staiger MP, Pietak AM, Huadmai J, et al. Magnesium and its alloys as orthopedic biomaterials: a review. Biomaterials. 2006;27(9):1728–1734.
[52] Nasab MB, Hassan MR, Sahari BB. Metallic biomaterials of knee and hip – a review.
[53] Kuroda D, Niinomi M, Morinaga M, et al. Design and mechanical properties of new β type titanium alloys for implant materials. Mater Sci Eng A. 1998;243(1–2):244–249.
[54] Ozan S, Lin J, Li Y, et al. New Ti-Ta-Zr-Nb alloys with ultrahigh strength for potential orthopedic implant applications. J Mech Behav Biomed Mater. 2017;75:119–127.
[55] Li B-Q, Li C-L, Wang Z-X, et al. Preparation of Ti–Nb–Ta–Zr alloys for load-bearing biomedical applications. Rare Met. 2019;38(6):571–576.
[56] Demirskyi D, Suzuki T, Yoshimi K, et al. Synthesis and high-temperature properties of medium-entropy (Ti, Ta, Zr, Nb) C using the spark plasma consolidation of carbide powders. Open Ceramics. 2020;2:100015.
[57] Li B-Q, Li X-C, Lu X. Microstructure and compressive properties of porous Ti–Nb–Ta–Zr alloy for orthopedic applications. J Mater Res. 2019;34 (24):4045–4055.
[58] Iasnii V, Junga R. Phase transformations and mechanical properties of the nitinol alloy with shape memory. Mater Sci. 2018;54(3):406–411.
[59] Javid F, Angeles J, Pasini D, et al. Shape optimization of a self-deployable anchor designed for percutaneous mitral valve repair. J Med Devices. 2012;6 (1):011003.
[60] Rho J-Y, Kuhn-Spearing L, Zioupos P. Mechanical properties and the hierarchical structure of bone. Med Eng Phys. 1998;20(2):92–102.
[61] Evans FG. Mechanical properties and histology of cortical bone from younger and older men. Anat Rec. 1976;185(1):1–11.
[62] Keaveny TM, Hayes WC. A 20-year perspective on the mechanical properties of trabecular bone. J Biomech Eng. 1993;115(4B):534–542.
[63] Wall A, Board T. The compressive behavior of bone as a two-phase porous structure, classic papers in orthopaedics. London: Springer; 2014. pp. 457–460.
[64] Turner CH. Yield behavior of bovine cancellous bone. J Biomech Eng. 1989;111(3):256–260.
[65] Turner CH, Burr DB. Basic biomechanical measurements of bone: a tutorial. Bone. 1993;14(4):595–608.
[66] Li Y, Yang C, Zhao H, et al. New developments of Ti-based alloys for biomedical applications. Materials (Basel). 2014;7(3):1709–1800.
[67] Mohammed MT, Khan ZA, Siddiquee AN. Beta titanium alloys: the lowest elastic modulus for biomedical applications: a review. Int J Chem Mol Nucl Mater Metall Eng. 2014;8(8):726.
[68] Shabalovskaya S. Physicochemical and biological aspects of nitinol as a biomaterial. Int Mater Rev. 2001;46(5):233–250.
[69] Rocha SSd, Adabo GL, Henriques GEP, et al. Vickers hardness of cast commercially pure titanium and Ti-

6Al-4V alloy submitted to heat treatments. Braz Dent J. 2006;17(2):126–129.
[70] Poondla N, Srivatsan TS, Patnaik A, et al. A study of the microstructure and hardness of two titanium alloys: commercially pure and Ti–6Al–4V. J Alloys Compd. 2009;486(1–2):162–167.
[71] Mantripragada VP, Lecka-Czernik B, Ebraheim NA, et al. An overview of recent advances in designing orthopedic and craniofacial implants. J Biomed Mater Res A. 2013;101(11):3349–3364.
[72] Pantaroto HN, Cordeiro JM, Pereira LT, et al. Sputtered crystalline TiO2 film drives improved surface properties of titanium-based biomedical implants. Mater Sci Eng: C. 2021;119:111638.
[73] Li C, Mason J, Yakimicki D. Thermal characterization of PMMA-based bone cement curing. J Mater Sci Mater Med. 2004;15(1):85–89.
[74] Geetha M, Singh AK, Asokamani R, et al. Ti based biomaterials, the ultimate choice for orthopaedic implants–a review. Prog Mater Sci. 2009;54(3):397–425.
[75] Nakagawa M, Matsuya S, Udoh K. Corrosion behavior of pure titanium and titanium alloys in fluoride-containing solutions. Dent Mater J. 2001;20(4):305–314.
[76] Hanawa T. Reconstruction and regeneration of surface oxide film on metallic materials in biological environments. Corros Rev. 2003;21(2–3):161–182.
[77] Pellizzari M, Jam A, Tschon M, et al. A 3D-printed ultra-low young's modulus β-Ti alloy for biomedical applications. Materials (Basel). 2020;13(12):2792.
[78] Willis J, Li S, Crean SJ, et al. Is titanium alloy Ti-6Al-4V cytotoxic to gingival fibroblasts – a systematic review. Clin Exper Dent Res. 2021;7(6):1037–1044.
[79] Eisenbarth E, Velten D, Müller M, et al. Biocompatibility of β-stabilizing elements of titanium alloys. Biomaterials. 2004;25(26):5705–5713.
[80] Watanabe I, Wataha J, Lockwood P, et al. Cytotoxicity of commercial and novel binary titanium alloys with and without a surface-reaction layer. J Oral Rehabil. 2004;31(2):185–189.
[81] Nag S, Banerjee R, Fraser H. Microstructural evolution and strengthening mechanisms in Ti–Nb–Zr–Ta, Ti–Mo–Zr–Fe and Ti–15Mo biocompatible alloys. Mater Sci Eng: C. 2005;25(3):357–362.
[82] Jäger M, Jennissen HP, Dittrich F, et al. Antimicrobial and osseointegration properties of nanostructured titanium orthopaedic implants. Materials (Basel). 2017;10(11):1302.
[83] Getter L, Bhaskar SN, Cutright DE, et al. Three biodegradable calcium phosphate slurry implants in bone. J Oral Surg. 1972;30(4):263–268.
[84] Coe SC, Wadge MD, Felfel RM, et al. Production of high silicon-doped hydroxyapatite thin film coatings via magnetron sputtering: deposition, characterisation, and In vitro biocompatibility. Coatings. 2020;10(2):190.
[85] Hayashi K, Inadome T, Mashima T, et al. Comparison of bone–implant interface shear strength of solid hydroxyapatite and hydroxyapatite-coated titanium implants. J Biomed Mater Res. 1993;27(5):557–563.
[86] Driskell TD. Early history of calcium phosphate materials and coatings, characterization and performance of calcium phosphate coatings for implants. Philadelphia: ASTM International; 1994.
[87] Junqueira LC, Carneiro J, Kelley RO. Basic histology: text & atlas. New York: McGraw-Hill; 2003.
[88] de Groot K, Geesink R, Klein CP, et al. Plasma sprayed coatings of hydroxylapatite. J Biomed Mater Res. 1987;21(12):1375–1381.
[89] Callahan TJ, Gantenberg J, Sands BE. Calcium phosphate (Ca-P) coating draft guidance for preparation of food and drug administration (FDA) submissions for orthopedic and dental endosseous implants, characterization and performance of calcium phosphate coatings for implants. ASTM Int. 1994: STP25193S, pp. 185-197.
[90] Herman H. Plasma spray deposition processes. MRS Bull. 1988;13(12):60–67.
[91] Mohseni E, Zalnezhad E, Bushroa AR. Comparative investigation on the adhesion of hydroxyapatite coating on Ti–6Al–4V implant: a review paper. Int J Adhes Adhes. 2014;48:238–257.
[92] Ong JL, Carnes DL, Bessho K. Evaluation of titanium plasma-sprayed and plasma-sprayed hydroxyapatite implants in vivo. Biomaterials. 2004;25(19):4601–4606.
[93] Tsui Y, Doyle C, Clyne T. Plasma sprayed hydroxyapatite coatings on titanium substrates part 1: mechanical properties and residual stress levels. Biomaterials. 1998;19(22):2015–2029.
[94] Sun L, Berndt CC, Grey CP. Phase, structural and microstructural investigations of plasma sprayed hydroxyapatite coatings. Mater Sci Eng A. 2003;360(1):70–84.
[95] Takeuchi S, Ito M, Takeda K. Modeling of residual-stress in plasma-sprayed coatings - effect of substrate-temperature. Surf Coat Technol. 1990;43-4(1–3):426–435.
[96] Zheng X, Huang M, Ding C. Bond strength of plasma-sprayed hydroxyapatite/Ti composite coatings. Biomaterials. 2000;21(8):841–849.
[97] Cherian JJ, Jauregui JJ, Banerjee S, et al. What host factors affect aseptic loosening after THA and TKA? Clin Orthopaed Related Research®. 2015;473(8):2700–2709.
[98] Sundfeldt M, Carlsson LV, Johansson CB, et al. Aseptic loosening, not only a question of wear: a review of different theories. Acta Orthop. 2006;77(2):177–197.
[99] Kaddick C, Catelas I, Pennekamp PH, et al. [Implant wear and aseptic loosening. An overview]. Orthopade. 2009;38(8):690–697.
[100] Yang Y, Kim K-H, Ong JL. A review on calcium phosphate coatings produced using a sputtering process – an alternative to plasma spraying. Biomaterials. 2005;26(3):327–337.
[101] Armitage DA, Mihoc R, Tate TJ, et al. The oxidation of calcium implanted titanium in water: a depth profiling study. Appl Surf Sci. 2007;253(8):4085–4093.
[102] Nayab SN, Jones FH, Olsen I. Effects of calcium ion implantation on human bone cell interaction with titanium. Biomaterials. 2005;26(23):4717–4727.
[103] Rautray TR, Narayanan R, Kwon TY, et al. Surface modification of titanium and titanium alloys by ion implantation. J Biomed Mater Res Part B: Appl Biomat. 2010;93(2):581–591.
[104] Tan L, Dodd RA, Crone WC. Corrosion and wear-corrosion behavior of NiTi modified by plasma source ion implantation. Biomaterials. 2003;24(22):3931–3939.

[105] Maitz MF, Pham MT, Matz W, et al. Promoted calcium-phosphate precipitation from solution on titanium for improved biocompatibility by ion implantation. Surf Coat Tech. 2002;158:151–156.
[106] Howlett CR, Zreiqat H, Odell R, et al. The effect of magnesium-Ion implantation into alumina Upon the adhesion of human bone-derived cells. J Mater Sci Mater Med. 1994;5(9–10):715–722.
[107] Davenas J, Thevenard P, Philippe F, et al. Surface implantation treatments to prevent infection complications in short term devices. Biomol Eng. 2002;19 (2–6):263–268.
[108] Parisi G, Cambursano S, Mellano D, et al. Porous titanium plasma-sprayed acetabular cup with hydroxyap-atite-coating in primary total Hip arthroplasty: clinical and radiographic results. JSM Musculoskel Dis. 2019;4(6):1–6.
[109] Castellini I, Andreani L, Parchi PD, et al. Hydroxyapatite in total hip arthroplasty. Our experience with a plasma spray porous titanium alloy/hydroxyapatite double-coated cementless stem. Clin Cases Miner Bone Metab. 2016;13(3):221.
[110] Songur F, Dikici B, Niinomi M, et al. The plasma electrolytic oxidation (PEO) coatings to enhance in-vitro corrosion resistance of Ti–29Nb–13Ta–4.6 Zr alloys: The combined effect of duty cycle and the deposition frequency. Surf Coat Technol. 2019;374:345–354.
[111] Heimann RB. Plasma-sprayed hydroxylapatite-based coatings: chemical, mechanical, microstructural, and biomedical properties. J Therm Spray Technol. 2016;25(5):827–850.
[112] Rahman M, Li Y, Wen C. HA coating on Mg alloys for biomedical applications: A review. J Magnesium and Alloys. 2020;8(3):929–943.
[113] Li P, Ohtsuki C, Kokubo T, et al. The role of hydrated silica, titania, and alumina in inducing apatite on implants. J Biomed Mater Res A. 1994;28 (1):7–15.
[114] ISO. ISO 23317:2014, Implants for surgery – in vitro evaluation for apatite-forming ability of implant materials; 2014, pp. 1–13.
[115] Lu X, Leng Y. Theoretical analysis of calcium phosphate precipitation in simulated body fluid. Biomaterials. 2005;26(10):1097–1108.
[116] Raina SA, Van Eerdenbrugh B, Alonzo DE, et al. Trends in the precipitation and crystallization behavior of supersaturated aqueous solutions of poorly water-soluble drugs assessed using synchrotron radiation. J Pharm Sci. 2015;104(6):1981–1992.
[117] Bohner M, Lemaitre J. Can bioactivity be tested in vitro with SBF solution? Biomaterials. 2009;30 (12):2175–2179.
[118] Kotani S, Fujita Y, Kitsugi T, et al. Bone bonding mechanism of beta-tricalcium phosphate. J Biomed Mater Res. 1991;25(10):1303–1315.
[119] Kokubo T, Takadama H. How useful is SBF in predicting in vivo bone bioactivity? Biomaterials. 2006;27(15):2907–2915.
[120] Kokubo T, Kushitani H, Sakka S, et al. Solutions able to reproduce in vivo surface-structure changes in bioactive glass-ceramic A-W3. J Biomed Mater Res. 1990;24(6):721–734.
[121] Zadpoor AA. Relationship between in vitro apatite-forming ability measured using simulated body fluid and in vivo bioactivity of biomaterials. Mater Sci Eng C Mater Biol Appl. 2014;35:134–143.
[122] He K, Sawczyk M, Liu C, et al. Revealing nanoscale mineralization pathways of hydroxyapatite using in situ liquid cell transmission electron microscopy. Sci Adv. 2020;6(47):eaaz7524.
[123] Revie RR, Uhlig HH. Corrosion and corrosion control: an introduction to corrosion science and engineering. Hoboken, NJ: John Wiley & Sons; 2008.
[124] Hurlen T, Wilhelmsen W. Passive behaviour of titanium. Electrochim Acta. 1986;31(9):1139–1146.
[125] Arsov LD, Kormann C, Plieth W. In situ Raman spectra of anodically formed titanium dioxide layers in solutions of H_2SO_4, KOH, and HNO_3. J Electrochem Soc. 1991;138(10):2964–2970.
[126] Prusi AR, Arsov LD. The growth-kinetics and optical-properties of films formed under open circuit conditions on a titanium surface in potassium hydroxide solutions. Corros Sci. 1992;33(1):153–164.
[127] Kim HM, Miyaji F, Kokubo T, et al. Effect of heat treatment on apatite-forming ability of Ti metal induced by alkali treatment. J Mater Sci: Mater Med. 1997;8(6):341–347.
[128] Miyaji F, Zhang X, Yao T, et al. Chemical treatment of Ti metal to induce its bioactivity. Bioceramics: Proceedings of the 7th International Symposium on Ceramics in Medicine, Elsevier, 1994, pp. 119–124.
[129] Tengvall P, Lundström I. Physico-chemical considerations of titanium as a biomaterial. Clin Mater. 1992;9(2):115–134.
[130] Healy KE, Ducheyne P. The mechanisms of passive dissolution of titanium in a model physiological environment. J Biomed Mater Res. 1992;26 (3):319–338.
[131] Healy K, Ducheyne P. Passive dissolution kinetics of titanium in vitro. J Mater Sci: Mater Med. 1993;4 (2):117–126.
[132] Kim HM, Miyaji F, Kokubo T, et al. Graded surface structure of bioactive titanium prepared by chemical treatment. Japan Soc Biomat Austr Soc Biomater. 1999;45(2):100–107.
[133] Ueno T, Tsukimura N, Yamada M, et al. Enhanced bone-integration capability of alkali- and heat-treated nanopolymorphic titanium in micro-to-nanoscale hierarchy. Biomaterials. 2011;32(30):7297–7308.
[134] Tsukimura N, Ueno T, Iwasa F, et al. Bone integration capability of alkali-and heat-treated nanobimorphic Ti–15Mo–5Zr–3Al. Acta Biomater. 2011;7 (12):4267–4277.
[135] Rahimipour S, Salahinejad E, Sharifi E, et al. Structure, wettability, corrosion and biocompatibility of nitinol treated by alkaline hydrothermal and hydrophobic functionalization for cardiovascular applications. Appl Surf Sci. 2020;506:144657.
[136] Norouzi N, Nouri Z. The effect of two-stage acid treatment on surface behavior and improvement of bioactivity of nitinol alloy. Biointerface Res. Appl. Chem. 2020;11:10690–10702.
[137] Rao X, Chu C, Chung CY, et al. Hydrothermal growth mechanism of controllable hydrophilic titanate nanostructures on medical NiTi shape memory alloy. J Mater Eng Perform. 2012;21(12):2600–2606.
[138] Rahimipour S, Rafiei B, Salahinejad E. Organosilane-functionalized hydrothermal-derived coatings on titanium alloys for hydrophobization and corrosion protection. Prog Org Coat. 2020;142:105594.

[139] Chu C-L, Tao H, Jun Z, et al. Effects of H_2O_2 pretreatment on surface characteristics and bioactivity of NaOH-treated NiTi shape memory alloy. Trans Nonferrous Metals Soc China. 2006;16(6):1295–1300.
[140] Fathyunes L, Sheykholeslami SOR. The surface modification of nitinol superelastic alloy with alkaline-heat treatment and hydroxyapatite/chitosan composite coating for biomedical applications. J Ultrafine Grained Nanostruct Mater. 2020;53(2):166–176.
[141] Conforto E, Caillard D, Muller L, et al. The structure of titanate nanobelts used as seeds for the nucleation of hydroxyapatite at the surface of titanium implants. Acta Biomater. 2008;4(6):1934–1943.
[142] Muniz FT, Miranda MA, Morilla Dos Santos C, et al. The Scherrer equation and the dynamical theory of X-ray diffraction. Acta Crystallogr A Found Adv. 2016;72(Pt 3):385–390.
[143] Bamberger CE, Begun GM. Sodium titanates: stoichiometry and Raman spectra. J Am Ceram Soc. 1987;70(3):C-48–C-51.
[144] Andersson S, Wadsley AD. The structures of $Na_2Ti_6O_{13}$ and $Rb_2Ti_6O_{13}$ and the alkali metal titanates. Acta Crystallogr. 1962;15(3):194–201.
[145] Gold J. XPS study of amino acid adsorption to titanium surfaces. Helv Phys Acta. 1989;62:246–249.
[146] Takadama H, Kim HM, Kokubo T, et al. An X-ray photoelectron spectroscopy study of the process of apatite formation on bioactive titanium metal. J Biomed Mater Res A. 2001;55(2):185–193.
[147] Kim HM, Himeno T, Kawashita M, et al. Surface potential change in bioactive titanium metal during the process of apatite formation in simulated body fluid. J Biomed Mater Res A. 2003;67(4):1305–1309.
[148] Yamaguchi S, Takadama H, Matsushita T, et al. Cross-sectional analysis of the surface ceramic layer developed on Ti metal by NaOH-heat treatment and soaking in SBF. J Ceram Soc Jpn. 2009;117(1370):1126–1130.
[149] Li N-b, Xiao G-y, Tsai I-H, et al. Transformation of surface compositions of titanium during alkali and heat treatment with different vacuum degrees. New J Chem. 2018;42(14):11991–12000.
[150] Hunter RJ. Zeta potential in colloid science: principles and applications. London: Academic Press; 2013.
[151] Somasundaran P, Markovic B. Interfacial properties of calcium phosphates, calcium phosphates in biological and industrial systems. Boston, MA: Springer; 1998, pp. 85–101.
[152] Takadama H, Kim H-M, Kokubo T, et al. XPS study of the process of apatite formation on bioactive Ti–6Al–4V alloy in simulated body fluid. Sci Technol Adv Mater. 2001;2(2):389.
[153] Neuman WF, Neuman MW. The chemical dynamics of bone mineral. The chemical dynamics of bone mineral (1958).
[154] Pattanayak DK, Yamaguchi S, Matsushita T, et al. Apatite-forming ability of titanium in terms of pH of the exposed solution. J R Soc Interface. 2012;9(74):2134–2155.
[155] Mozafari M, Salahinejad E, Shabafrooz V, et al. Multilayer bioactive glass/zirconium titanate thin films in bone tissue engineering and regenerative dentistry. Int J Nanomed. 2013;8:1665.
[156] Triviño-Bolaños DF, Camargo-Amado RJ. Synthesis and characterization of porous structures of rutile TiO_2/Na08Ti_4O_8/$Na_2Ti_6O_{13}$ for biomedical applications. MethodsX. 2019;6:1114–1123.
[157] Rao X, Yang J, Feng X, et al. Replication and bioactivation of Ti-based alloy scaffold macroscopically identical to cancellous bone from polymeric template with TiNbZr powders. J Mech Behav Biomed Mater. 2018;88:296–304.
[158] Lee T, Abdullah H, Koshy P, et al. Deposition of novel bioactive nanoflower-like sodium titanate on TiO2 coating via anodic oxidation for biomedical applications. Mater Lett. 2018;216:256–260.
[159] Arsecularatne JA, Colusso E, Della Gaspera E, et al. Nanomechanical and tribological characterization of silk and silk-titanate composite coatings. Tribol Int. 2020;146:106195.
[160] Colusso E, Perotto G, Wang Y, et al. Bioinspired stimuli-responsive multilayer film made of silk–titanate nanocomposites. J Mater Chem C. 2017;5(16):3924–3931.
[161] Zhang M, Gong Z, Zhang J, et al. Engineered zinc titanate coatings on the titanium surface with enhanced antitumor properties and biocompatibility. ACS Biomater Sci Eng. 2019;5(11):5935–5946.
[162] Hossain KMZ, Patel U, Ahmed I. Development of microspheres for biomedical applications: a review. Prog Biomater. 2015;4(1):1–19.
[163] Hsu H-C, Wu S-C, Hsu S-K, et al. Fabrication and characterization of novel porous titanium microspheres for biomedical applications. Mater Charact. 2015;106:317–323.
[164] Milošević MM, Milanović M, Stijepović I, et al. Evaluation of mesoporous silica and Nb-doped titanate as molecule carriers through adsorption/desorption study. Part Sci Technol. 2019;38(5):1–10.
[165] Li W, Deng Y, Wu Z, et al. Hydrothermal etching assisted crystallization: a facile route to functional yolk-shell titanate microspheres with ultrathin nanosheets-assembled double shells. J Am Chem Soc. 2011;133(40):15830–15833.
[166] Kasuga T, Hiramatsu M, Hoson A, et al. Formation of titanium oxide nanotube. Langmuir. 1998;14(12):3160–3163.
[167] Eslami H, Moztarzadeh F, Kashi TSJ, et al. Hydrothermal synthesis and characterization of TiO_2-derived nanotubes for biomedical applications. Synth React Inorg Met-Org Nano-Met Chem. 2016;46(8):1149–1156.
[168] Kim G-S, Seo H-K, Godble V, et al. Electrophoretic deposition of titanate nanotubes from commercial titania nanoparticles: application to dye-sensitized solar cells. Electrochem Commun. 2006;8(6):961–966.
[169] Torrente-Murciano L, Lapkin AA, Chadwick D. Synthesis of high aspect ratio titanate nanotubes. J Mater Chem. 2010;20(31):6484–6489.
[170] Papa A-L, Dumont L, Vandroux D, et al. Titanate nanotubes: towards a novel and safer nanovector for cardiomyocytes. Nanotoxicology. 2012;7(6):1131–1142.
[171] Papa A-L, Boudon J, Bellat V, et al. Dispersion of titanate nanotubes for nanomedicine: comparison of PEI and PEG nanohybrids. Dalton Trans. 2015;44(2):739–746.

[172] Rodrigues GL, de Oliveira TG, Gusmão SB, et al. Titanate nanotubes: effect of rare earth insertion, thermal treatment and their optical properties. Opt Mater. 2022;127:112302.
[173] Wang X, Liu SJ, Qi YM, et al. Behavior of potassium titanate whisker in simulated body fluid. Mater Lett. 2014;135:139–142.
[174] Zhao H, Dong W, Zheng Y, et al. The structural and biological properties of hydroxyapatite-modified titanate nanowire scaffolds. Biomaterials. 2011;32 (25):5837–5846.
[175] Islam MT, Felfel RM, Abou Neel EA, et al. Bioactive calcium phosphate–based glasses and ceramics and their biomedical applications: a review. J Tissue Eng. 2017;8:2041731417719170.
[176] Mabwa D, Kubiena T, Parnell H, et al. Evaluating the cytotoxicity of Ge–Sb–Se chalcogenide glass optical fibres on 3T3 mouse fibroblasts. RSC Adv. 2021;11 (15):8682–8693.
[177] Hum J, Boccaccini AR. Bioactive glasses as carriers for bioactive molecules and therapeutic drugs: a review. J Mater Sci: Mater Med. 2012;23(10):2317–2333.
[178] Sanzana ES, Navarro M, Ginebra MP, et al. Role of porosity and pore architecture in the in vivo bone regeneration capacity of biodegradable glass scaffolds. J Biomed Mater Res A. 2014;102(6):1767–1773.
[179] Kasunic KJ. Optomechanical systems engineering. Hoboken, NJ: John Wiley & Sons; 2015.
[180] Jijian C, Wei C. Formation and structure of titanate glasses. J Non-Cryst Solids. 1986;80(1–3):135–140.
[181] Darafsheh A, Guardiola C, Nihalani D, et al. Biological super-resolution imaging by using novel microsphere-embedded coverslips. Nanoscale Imaging, Sensing, and Actuation for Biomedical Applications XII, SPIE, 2015, pp. 16–22.
[182] Hofmann DC, Suh J-Y, Wiest A, et al. Development of tough, low-density titanium-based bulk metallic glass matrix composites with tensile ductility. Proc Natl Acad Sci USA. 2008;105(51):20136–20140.
[183] Wu F-F, Chan KC, Jiang S-S, et al. Bulk metallic glass composite with good tensile ductility, high strength and large elastic strain limit. Sci Rep. 2014;4(1):1–6.
[184] Qin F, Yoshimura M, Wang X, et al. Corrosion behavior of a Ti-based bulk metallic glass and its crystalline alloys. Mater Trans. 2007;48(7):1855–1858.
[185] Jiang J, Saida J, Kato H, et al. Is Cu 60 Ti 10 Zr 30 a bulk glass-forming alloy? Appl Phys Lett. 2003;82 (23):4041–4043.
[186] Kasuga T, Kimata T, Obata A. Preparation of a calcium titanium phosphate glass–ceramic with improved chemical durability. J Am Ceram Soc. 2009;92(8):1709–1712.
[187] Das S, Manpoong C, Gautam S, et al. Tribological study of strontium bismuth titanate borosilicate glass ceramics. Mater Today Proc. 2018;5(9):20306–20313.
[188] Phromyoo S, Lertcumfu N, Jaita P, et al. Effects of barium zirconium titanate on the properties of β-tricalcium phosphate bioceramics. Ceram Int. 2018;44 (3):2661–2667.
[189] Ehterami A, Kazemi M, Nazari B, et al. Fabrication and characterization of highly porous barium titanate based scaffold coated by Gel/HA nanocomposite with high piezoelectric coefficient for bone tissue engineering applications. J Mech Behav Biomed Mater. 2018;79:195–202.
[190] Vouilloz F, Castro MS, Vargas GE, et al. Reactivity of BaTiO3-Ca10 (PO4) 6 (OH) 2 phases in composite materials for biomedical applications. Ceram Int. 2017;43(5):4212–4221.
[191] Ciofani G, Danti S, Moscato S, et al. Preparation of stable dispersion of barium titanate nanoparticles: potential applications in biomedicine. Colloids Surf B. 2010;76(2):535–543.
[192] Ciofani G, Danti S, D'Alessandro D, et al. Enhancement of neurite outgrowth in neuronal-like cells following boron nitride nanotube-mediated stimulation. ACS Nano. 2010;4(10):6267–6277.
[193] Darafsheh A, Guardiola C, Palovcak A, et al. Optical super-resolution imaging by high-index microspheres embedded in elastomers. Opt Lett. 2015;40(1):5–8.
[194] Baxter FR, Turner IG, Bowen CR, et al. An in vitro study of electrically active hydroxyapatite-barium titanate ceramics using saos-2 cells. J Mater Sci: Mater Med. 2009;20(8):1697–1708.
[195] Bowen CR, Gittings J, Turner IG, et al. Dielectric and piezoelectric properties of hydroxyapatite-BaTiO3 composites. Appl Phys Lett. 2006;89(132906):1–3. DOI:10.1063/1.2355458.
[196] Tariverdian T, Behnamghader A, Milan PB, et al. 3D-printed barium strontium titanate-based piezoelectric scaffolds for bone tissue engineering. Ceram Int. 2019;45(11):14029–14038.
[197] Rahmati S, Basiriani MB, Rafienia M, et al. Synthesis and in vitro evaluation of electrodeposited barium titanate coating on Ti6Al4V. J Med Signals Sens. 2016;6(2):106.
[198] Tang Y, Chen L, Duan Z, et al. Graphene/barium titanate/polymethyl methacrylate bio-piezoelectric composites for biomedical application. Ceram Int. 2020;46(5):6567–6574.
[199] Anderson J, Eriksson C. Piezoelectric properties of dry and wet bone. Nature. 1970;227(5257):491–492.
[200] Xu Q, Li Z. Dielectric and ferroelectric behaviour of Zr-doped $BaTiO_3$ perovskites. Process Appl Ceram. 2020;14(3):188–194.
[201] Yu Z, Ang C, Guo R, et al. Piezoelectric and strain properties of Ba (Ti 1− xZrx) O_3 ceramics. J Appl Phys. 2002;92(3):1489–1493.
[202] Nanakorn N, Jalupoom P, Vaneesorn N, et al. Dielectric and ferroelectric properties of Ba (ZrxTi1 − x) O_3 ceramics. Ceram Int. 2008;34(4):779–782.
[203] Polley C, Distler T, Detsch R, et al. 3D printing of piezoelectric barium titanate-hydroxyapatite scaffolds with interconnected porosity for bone tissue engineering. Materials (Basel). 2020;13(7):1773.
[204] Zhang Y, Chen L, Zeng J, et al. Aligned porous barium titanate/hydroxyapatite composites with high piezoelectric coefficients for bone tissue engineering. Mater Sci Eng: C. 2014;39:143–149.
[205] Liu B, Chen L, Shao C, et al. Improved osteoblasts growth on osteomimetic hydroxyapatite/$BaTiO_3$ composites with aligned lamellar porous structure. Mater Sci Eng: C. 2016;61:8–14.
[206] Tang Y, Wu C, Wu Z, et al. Fabrication and in vitro biological properties of piezoelectric bioceramics for bone regeneration. Sci Rep. 2017;7(1):1–12.
[207] Liu J, Gu H, Liu Q, et al. An intelligent material for tissue reconstruction: the piezoelectric property of polycaprolactone/barium titanate composites. Mater Lett. 2019;236:686–689.

[208] Janson O, Gururaj S, Pujari-Palmer S, et al. Titanium surface modification to enhance antibacterial and bioactive properties while retaining biocompatibility. Mater Sci Eng: C. 2018;96:272–279.
[209] Tengvall P, Hornsten EG, Elwing H, et al. Bactericidal properties of a titanium-peroxy gel obtained from metallic titanium and hydrogen peroxide. J Biomed Mater Res A. 1990;24(3):319–330.
[210] Kizuki T, Takadama H, Matsushita T, et al. Effect of Ca contamination on apatite formation in a Ti metal subjected to NaOH and heat treatments. J Mater Sci: Mater Med. 2013;24(3):635–644.
[211] Kawai T, Kizuki T, Takadama H, et al. Apatite formation on surface titanate layer with different Na content on Ti metal. J Ceram Soc Jpn. 2010;118 (1373):19–24.
[212] Ammann C, Brunner A, Spirig C, et al. Water vapour concentration and flux measurements with PTR-MS. Atmos Chem Phys. 2006;6(12):4643–4651.
[213] Yamaguchi S, Takadama H, Matsushita T, et al. Preparation of bioactive Ti-15Zr-4Nb-4Ta alloy from HCl and heat treatments after an NaOH treatment. J Biomed Mater Res A. 2011;97(2):135–144.
[214] Okazaki Y, Rao S, Ito Y, et al. Corrosion resistance, mechanical properties, corrosion fatigue strength and cytocompatibility of new Ti alloys without Al and V. Biomaterials. 1998;19(13):1197–1215.
[215] Cho K, Niinomi M, Nakai M, et al. Effects of alloying elements on the HAp formability on Ti alloys after alkali treatment. Mater Trans. 2013;54(8):1295–1301.
[216] Niinomi M. Design and development of metallic biomaterials with biological and mechanical biocompatibility. J Biomed Mater Res A. 2019;107 (5):944–954.
[217] Del Valle HB, Yaktine AL, Taylor CL, et al. Dietary reference intakes for calcium and vitamin D. Washington, DC: National Academies Press; 2011.
[218] Moudgil S, Ying JY. Calcium-doped organosilicate nanoparticles as gene delivery vehicles for bone cells. Adv Mater. 2007;19(20):3130–3135.
[219] Li B, Hao J, Min Y, et al. Biological properties of nanostructured Ti incorporated with Ca, P and Ag by electrochemical method. Mater Sci Eng C Mater Biol Appl. 2015;51:80–86.
[220] Webster TJ, Ergun C, Doremus RH, et al. Increased osteoblast adhesion on titanium-coated hydroxylapatite that forms $CaTiO_3$. J Biomed Mater Res A. 2003;67(3):975–980.
[221] Coreno J, Coreno O. Evaluation of calcium titanate as apatite growth promoter. J Biomed Mater Res A. 2005;75(2):478–484.
[222] Suh JY, Jeung OC, Choi BJ, et al. Effects of a novel calcium titanate coating on the osseointegration of blasted endosseous implants in rabbit tibiae. Clin Oral Implants Res. 2007;18(3):362–369.
[223] Rakngarm A, Miyashita Y, Mutoh Y. Formation of hydroxyapatite layer on bioactive Ti and Ti–6Al–4V by simple chemical technique. J Mater Sci: Mater Med. 2008;19(5):1953–1961.
[224] Kizuki T, Matsushita T, Kokubo T. Antibacterial and bioactive calcium titanate layers formed on Ti metal and its alloys. J Mater Sci: Mater Med. 2014;25 (7):1737–1746.
[225] Yamaguchi S, Takadama H, Matsushita T, et al. Apatite-forming ability of Ti–15Zr–4Nb–4Ta alloy induced by calcium solution treatment. J Mater Sci: Mater Med. 2010;21(2):439–444.
[226] Yamaguchi S, Kizuki T, Takadama H, et al. Formation of a bioactive calcium titanate layer on gum metal by chemical treatment. J Mater Sci: Mater Med. 2012;23(4):873–883.
[227] Fukuda A, Takemoto M, Saito T, et al. Bone bonding bioactivity of Ti metal and Ti–Zr–Nb–Ta alloys with Ca ions incorporated on their surfaces by simple chemical and heat treatments. Acta Biomater. 2011;7(3):1379–1386.
[228] Tanaka M, Takemoto M, Fujibayashi S, et al. Bone bonding ability of a chemically and thermally treated low elastic modulus Ti alloy: gum metal. J Mater Sci Mater Med. 2014;25(3):635–643.
[229] Gathen M, Ploeger MM, Jaenisch M, et al. Outcome evaluation of new calcium titanate Schanz-screws for external fixators. first clinical results and cadaver studies. J Mater Sci Mater Med. 2019;30(11):124.
[230] Yuan X, Cao H, Wang J, et al. Immunomodulatory effects of calcium and strontium Co-doped titanium oxides on osteogenesis. Front Immunol. 2017;8:1196.
[231] Vormann J. Magnesium: nutrition and metabolism. Mol Asp Med. 2003;24(1–3):27–37.
[232] Shi X, Nakagawa M, Kawachi G, et al. Surface modification of titanium by hydrothermal treatment in Mg-containing solution and early osteoblast responses. J Mater Sci Mater Med. 2012;23(5):1281–1290.
[233] Okuzu Y, Fujibayashi S, Yamaguchi S, et al. Strontium and magnesium ions released from bioactive titanium metal promote early bone bonding in a rabbit implant model. Acta Biomater. 2017;63:383–392.
[234] Lingli X, Xingling S, Chun O, et al. In vitro apatite formation, protein adsorption and initial osteoblast responses on titanium surface enriched with magnesium. Rare Met Mater Eng. 2017;46(6):1512–1517.
[235] Pors Nielsen S. The biological role of strontium. Bone. 2004;35(3):583–588.
[236] Yamaguchi S, Nath S, Matsushita T, et al. Controlled release of strontium ions from a bioactive Ti metal with a Ca-enriched surface layer. Acta Biomater. 2014;10(5):2282–2289.
[237] Shimizu Y, Fujibayashi S, Yamaguchi S, et al. Bioactive effects of strontium loading on micro/nano surface Ti6Al4V components fabricated by selective laser melting. Mater Sci Eng: C. 2020;109:110519.
[238] Sahoo S, Sinha A, Das M. Synthesis, characterization and in vitro biocompatibility study of strontium titanate ceramic: A potential biomaterial. J Mech Behav Biomed Mater. 2020;102:103494.
[239] Zhou J, Jian L, Xie J, et al. Strontium-Containing barium titanate-modified titanium for enhancement of osteointegration. ACS Biomater Sci Eng. 2022;8 (3):1271–1278.
[240] Ahrens LH. The use of ionization potentials part 1. Ionic radii of the elements. Geochim Cosmochim Acta. 1952;2(3):155–169.
[241] Park YJ, Hwang KS, Song JE, et al. Growth of calcium phosphate on poling treated ferroelectric BaTiO3 ceramics. Biomaterials. 2002;23(18):3859–3864.
[242] Baxter FR, Bowen CR, Turner IG, et al. Electrically active bioceramics: a review of interfacial responses. Ann Biomed Eng. 2010;38(6):2079–2092.
[243] Ciofani G, Ricotti L, Canale C, et al. Effects of barium titanate nanoparticles on proliferation and differentiation of rat mesenchymal stem cells. Colloids Surf B Biointerfaces. 2013;102:312–320.

[244] Yao M, Li L, Wang Y, et al. Mechanical energy harvesting and specific potential distribution of a flexible piezoelectric nanogenerator based on 2-D BaTiO3-oriented polycrystals. ACS Sustain Chem Eng. 2022;10(10):3276–3287.
[245] Fernandez J, Bindhu B, Prabu M, et al. Effects of hafnium on the structural, optical and ferroelectric properties of sol–gel synthesized barium titanate ceramics. J Korean Ceram Soc. 2022;59:240–251.
[246] Hossain S, Hossain S. Magnetic and optical characterization of cobalt ferrite-barium titanate core-shell for biomedical applications. IEEE Trans Magn. 2021;58(3):1–8.
[247] Osredkar J, Sustar N. Copper and zinc, biological role and significance of copper/zinc imbalance. J Clinic Toxicol S. 2011;3(2161):0495.
[248] Yamaguchi S, Matsushita T, Nakamura T, et al. Bioactive Ti metal with Ca-enriched surface layer able to release Zn ion, Key engineering materials. Trans Tech Publ. 2013;529:547–552.
[249] Yamaguchi S, Nath S, Sugawara Y, et al. Two-in-one biointerfaces – antimicrobial and bioactive nanoporous gallium titanate layers for titanium implants. Nanomaterials. 2017;7(8):229.
[250] Brett DW. A discussion of silver as an antimicrobial agent: alleviating the confusion. Ostomy Wound Management. 2006;52(1):34–41.
[251] Stickler DJ. Biomaterials to prevent nosocomial infections: is silver the gold standard? Curr Opin Infect Dis. 2000;13(4):389–393.
[252] Inoue Y, Uota M, Torikai T, et al. Antibacterial properties of nanostructured silver titanate thin films formed on a titanium plate. J Biomed Mater Res A. 2010;92(3):1171–1180.
[253] Lee SB, Otgonbayar U, Lee JH, et al. Silver ion-exchanged sodium titanate and resulting effect on antibacterial efficacy. Surf Coat Tech. 2010;205: S172–S176.
[254] Inoue Y, Uota M, Torikai T, et al. Antibacterial properties of nanostructured silver titanate thin films formed on a titanium plate. Japan Soc Biomater and Austr Soc Biomater Kor Soc Biomat. 2010;92(3):1171–1180.
[255] Yamaguchi S, Thi Minh Le P, Ito M, et al. Tri-functional calcium-deficient calcium titanate coating on titanium metal by chemical and heat treatment. Coatings. 2019;9(9):561.
[256] Okuzu Y, Fujibayashi S, Yamaguchi S, et al. In vitro study of antibacterial and osteogenic activity of titanium metal releasing strontium and silver ions. J Biomater Appl. 2021;35(6):670–680.
[257] Masamoto K, Fujibayashi S, Yamaguchi S, et al. Bioactivity and antibacterial activity of strontium and silver ion releasing titanium. J Biomed Mater Res Part B: Appl Biomater. 2021;109(2):238–245.
[258] Shuai C, Liu G, Yang Y, et al. A strawberry-like Ag-decorated barium titanate enhances piezoelectric and antibacterial activities of polymer scaffold. Nano Energy. 2020;74:104825.
[259] Minandri F, Bonchi C, Frangipani E, et al. Promises and failures of gallium as an antibacterial agent. Future Microbiol. 2014;9(3):379–397.
[260] Cochis A, Azzimonti B, Della Valle C, et al. The effect of silver or gallium doped titanium against the multidrug resistant *Acinetobacter baumannii*. Biomaterials. 2016;80:80–95.
[261] Kubista B, Schoefl T, Mayr L, et al. Distinct activity of the bone-targeted gallium compound KP46 against osteosarcoma cells-synergism with autophagy inhibition. J Exp Clin Cancer Res. 2017;36(1):52.
[262] Kaneko Y, Thoendel M, Olakanmi O, et al. The transition metal gallium disrupts *Pseudomonas aeruginosa* iron metabolism and has antimicrobial and antibiofilm activity. J Clin Invest. 2007;117(4):877.
[263] Hall TJ, Chambers TJ. Gallium inhibits bone resorption by a direct effect on osteoclasts. Bone Miner. 1990;8(3):211–216.
[264] Villers D, Espaze E, Coste-Burel M, et al. Nosocomial *Acinetobacter baumannii* infections: microbiological and clinical epidemiology. Ann Intern Med. 1998;129(3):182–189.
[265] Baldoni D, Steinhuber A, Zimmerli W, et al. In vitro activity of gallium maltolate against staphylococci in logarithmic, stationary, and biofilm growth phases: comparison of conventional and calorimetric susceptibility testing methods. Antimicrob Agents Chemother. 2010;54(1):157–163.
[266] Wadge MD, Stuart BW, Thomas KG, et al. Generation and characterisation of gallium titanate surfaces through hydrothermal ion-exchange processes. Mater Des. 2018;155:264–277.
[267] Rodríguez-Contreras A, Torres D, Guillem-Marti J, et al. Development of novel dual-action coatings with osteoinductive and antibacterial properties for 3D-printed titanium implants. Surf Coat Technol. 2020;403:126381.
[268] Krasner RI, Shors T. The microbial challenge: a public health perspective. Burlington, MA: Jones & Bartlett Publishers; 2014.
[269] Bauman R. Microbiology with diseases by taxonomy. 2nd ed., Pearson San Francisco, CA, USA: 2007.
[270] Cai Z, Song J, Li J, et al. Synthesis and characterization of zinc titanate fibers by sol-electrospinning method. J Sol-Gel Sci Technol. 2012;61(1):49–55.
[271] Li M, Zhu L, Lin D. Toxicity of ZnO nanoparticles to *Escherichia coli*: mechanism and the influence of medium components. Environ Sci Technol. 2011;45 (5):1977–1983.
[272] Pasquet J, Chevalier Y, Pelletier J, et al. The contribution of zinc ions to the antimicrobial activity of zinc oxide. Colloids Surf, A. 2014;457:263–274.
[273] Stoyanova A, Dimitriev Y, Shalaby A, et al. Antibacterial properties of $ZnTiO_3$ prepared by sol–gel method. J Optoelectron Biomed Mater. 2011;3:24–29.
[274] Cortes AA, Zuñiga JM. The use of copper to help prevent transmission of SARS-coronavirus and influenza viruses. A general review. Diagn Microbiol Infect Dis. 2020;98(4):115176.
[275] Rónavári A, Kovács D, Vágvölgyi C, et al. Ion exchange defines the biological activity of titanate nanotubes. J Basic Microbiol. 2016;56(5):557–565.
[276] Zamora JL. Chemical and microbiologic characteristics and toxicity of povidone-iodine solutions. Am J Surg. 1986;151(3):400–406.
[277] Yamaguchi S, Le PTM, Shintani SA, et al. Iodine-Loaded calcium titanate for bone repair with sustainable antibacterial activity prepared by solution and heat treatment. Nanomaterials. 2021;11(9):2199.
[278] Ikeda N, Fujibayashi S, Yamaguchi S, et al. Bioactivity and antibacterial activity of iodine-containing calcium titanate against implant-associated infection. Biomater Advan. 2022;138:212952.
[279] Seyhan AA. Lost in translation: the valley of death across preclinical and clinical divide–identification

of problems and overcoming obstacles. Translat Med Commun. 2019;4(1):1–19.
[280] Yılmaz E, Türk S. Loading antibiotics on the surface of nano-networked sodium hydroxide treated titanium. Chem Pap. 2022;76(4):2459–2467.
[281] Yan WQ, Nakamura T, Kobayashi M, et al. Bonding of chemically treated titanium implants to bone. J Biomed Mater Res A. 1997;37(2):267–275.
[282] Fujibayashi S, Nakamura T, Nishiguchi S, et al. Bioactive titanium: effect of sodium removal on the bone-bonding ability of bioactive titanium prepared by alkali and heat treatment. J Biomed Mater Res A. 2001;56(4):562–570.
[283] Nishiguchi S, Fujibayashi S, Kim HM, et al. Biology of alkali-and heat-treated titanium implants. J Biomed Mater Res A. 2003;67(1):26–35.
[284] Nishiguchi S, Nakamura T, Kobayashi M, et al. The effect of heat treatment on bone-bonding ability of alkali-treated titanium. Biomaterials. 1999;20 (5):491–500.
[285] Nishiguchi S, Kato H, Fujita H, et al. Titanium metals form direct bonding to bone after alkali and heat treatments. Biomaterials. 2001;22(18):2525–2533.
[286] Nishiguchi S, Kato H, Neo M, et al. Alkali-and heat-treated porous titanium for orthopedic implants. J Biomed Mater Res A. 2001;54(2):198–208.
[287] Nishiguchi S, Kato H, Fujita H, et al. Enhancement of bone-bonding strengths of titanium alloy implants by alkali and heat treatments. J Biomed Mater Res A. 1999;48(5):689–696.
[288] Kawanabe K, Ise K, Goto K, et al. A new cementless total hip arthroplasty with bioactive titanium porous-coating by alkaline and heat treatment: average 4.8-year results. J. Biomed Mater Res Part B: Appl Biomater. 2009;90(1):476–481.
[289] Mibe J, Imakiire A, Watanabe T, et al. Results of total hip arthroplasty with bone graft and support ring for protrusio acetabuli in rheumatoid arthritis. J Orthop Sci. 2005;10(1):8–14.
[290] So K, Kaneuji A, Matsumoto T, et al. Is the bone-bonding ability of a cementless total hip prosthesis enhanced by alkaline and heat treatments? Clin Orthopaed Related Res. 2013;471(12):3847–3855.
[291] Garcia-Cimbrelo E, Cruz-Pardos A, Madero R, et al. Total hip arthroplasty with use of the cementless zweymüller alloclassic system: a ten to thirteen-year follow-up study. J Bone Joint Surg. 2003;85(2):296–303.
[292] Shetty AA, Slack R, Tindall A, et al. Results of a hydroxyapatite-coated (furlong) total hip replacement: A 13- to 15-year follow-up. J Bone Joint Surg. 2005;87(8):1050–1054.
[293] de Witte PB, Brand R, Vermeer HG, et al. Mid-term results of total hip arthroplasty with the CementLess spotorno (CLS) system. J Bone Joint Surg. 2011;93 (13):1249–1255.
[294] Sariali E, Mouttet A, Mordasini P, et al. High 10-year survival rate with an anatomic cementless stem (SPS). Clin Orthopaed Related Res. 2012;470 (7):1941–1949.
[295] Nourissat C, Essig J, Asencio G. The cementless anatomic benoist girard (ABG) II total hip arthroplasty: a minimum 8-year follow-up study. J Arthropl. 2013;28(4):707–711.
[296] Wittenberg RH, Steffen R, Windhagen H, et al. Five-year results of a cementless short-hip-stem prosthesis. Orthopaedic Reviews. 2013;5(1):4.
[297] Jameson SS, Baker PN, Mason J, et al. Independent predictors of failure up to 7.5 years after 35,386 single-brand cementless total hip replacements: a retrospective cohort study using national joint registry data. Bone Joint J. 2013;95B(6):747–757.
[298] Makela KT, Matilainen M, Pulkkinen P, et al. Failure rate of cemented and uncemented total hip replacements: register study of combined nordic database of four nations. Br Med J. 2014;348:f7592.
[299] Noiseux NO, Long WJ, Mabry TM, et al. Uncemented porous tantalum acetabular components: early follow-up and failures in 613 primary total hip arthroplasties. J Arthropl. 2014;29(3):617–620.
[300] Hoskins WT, Bingham RJ, Lorimer M, et al. The effect of size for a hydroxyapatite-coated cementless implant on component revision in total hip arthroplasty: an analysis of 41,265 stems. J Arthropl. 2020;35(4):1074–1078.
[301] Uchida M, Kim HM, Kokubo T, et al. Effect of water treatment on the apatite-forming ability of NaOH-treated titanium metal. J Biomed Mater Res A. 2002;63(5):522–530.
[302] Uchida M, Kim H-M, Kokubo T, et al. Apatite-forming ability of titania gels with different structures, Bioceramics: Volume 12, World Scientific 1999, pp. 149–152.
[303] Uchida M, Kim HM, Kokubo T, et al. Apatite-forming ability of sodium-containing titania gels in a simulated body fluid. J Am Ceram Soc. 2001;84 (12):2969–2974.
[304] Wei M, Uchida M, Kim HM, et al. Apatite-forming ability of CaO-containing titania. Biomaterials. 2002;23(1):167–172.
[305] Fujibayashi S, Neo M, Kim HM, et al. Osteoinduction of porous bioactive titanium metal. Biomaterials. 2004;25(3):443–450.
[306] Takemoto M, Fujibayashi S, Neo M, et al. Osteoinductive porous titanium implants: effect of sodium removal by dilute HCl treatment. Biomaterials. 2006;27(13):2682–2691.
[307] Fukuda A, Takemoto M, Saito T, et al. Osteoinduction of porous Ti implants with a channel structure fabricated by selective laser melting. Acta Biomater. 2011;7(5):2327–2336.
[308] Takemoto M, Fujibayashi S, Neo M, et al. Mechanical properties and osteoconductivity of porous bioactive titanium. Biomaterials. 2005;26(30):6014–6023.
[309] Pattanayak DK, Kawai T, Matsushita T, et al. Effect of HCl concentrations on apatite-forming ability of NaOH–HCl-and heat-treated titanium metal. J Mater Sci: Mater Med. 2009;20(12):2401–2411.
[310] Pattanayak DK, Yamaguchi S, Matsushita T, et al. Effect of heat treatments on apatite-forming ability of NaOH- and HCl-treated titanium metal. J Mater Sci: Mater Med. 2011;22(2):273–278.
[311] Pattanayak DK, Yamaguchi S, Matsushita T, et al. Nanostructured positively charged bioactive TiO_2 layer formed on Ti metal by NaOH, acid and heat treatments. J Mater Sci: Mater Med. 2011;22 (8):1803–1812.
[312] Kokubo T, Pattanayak DK, Yamaguchi S, et al. Positively charged bioactive Ti metal prepared by simple chemical and heat treatments. J R Soc Interface. 2010;7(Suppl 5):503–513.
[313] Wadge MD. Developing unique nanoporous titanate structures for biomedical applications: mechanisms,

conversion and substitution. Nottingham: University of Nottingham.
[314] Kawai T, Takemoto M, Fujibayashi S, et al. Osteoconduction of porous Ti metal enhanced by acid and heat treatments. J Mater Sci: Mater Med. 2013;24(7):1707–1715.
[315] Kokubo T, Pattanayak DK, Yamaguchi S, et al. Positively charged bioactive Ti metal prepared by simple chemical and heat treatments. J R Soc Interface. 2010;7(suppl_5):S503–S513.
[316] Takemoto M, Fujibayashi S, Neo M, et al. A porous bioactive titanium implant for spinal interbody fusion: an experimental study using a canine model. J Neurosurg-Spine. 2007;7(4):435–443.
[317] Fujibayashi S, Takemoto M, Neo M, et al. A novel synthetic material for spinal fusion: A prospective clinical trial of porous bioactive titanium metal for lumbar interbody fusion. Eur Spine J. 2011;20 (9):1486–1495.
[318] Ma J, Wong HF, Kong LB, et al. Biomimetic processing of nanocrystallite bioactive apatite coating on titanium. Nanotechnology. 2003;14(6):619–623.
[319] Hughes A, Jordan B. The mechanical properties of surgical bone screws and some aspects of insertion practice. Injury. 1972;4(1):25–38.
[320] Zhu Y, Wang X, Zhou Y, et al. In situ formation of bioactive calcium titanate coatings on titanium screws for medical implants. RSC Adv. 2016;6 (58):53182–53187.
[321] Wang Z-l, He R-z, Tu B, et al. Enhanced biocompatibility and osseointegration of calcium titanate coating on titanium screws in rabbit femur. J Huazhong Univ Sci Technol [Med Sci]. 2017;37(3):362–370.
[322] Gathen M, Ploeger MM, Jaenisch M, et al. Outcome evaluation of new calcium titanate Schanz-Screws for external fixators. first clinical results and cadaver studies. J Mater Sci: Mater Med. 2019;30(11):1–8.
[323] Wadge MD, McGuire J, Hanby BVT, et al. Tailoring the degradation rate of magnesium through biomedical nano-porous titanate coatings. J Magnes Alloy. 2020;9(1):336–350.
[324] Devi KB, Singh K, Rajendran N. Synthesis and characterization of nanoporous sodium-substituted hydrophilic titania ceramics coated on 316L SS for biomedical applications. J Coat Technol Res. 2011;8(5):595.
[325] Mohanta M, Thirugnanam A. Development of multifunctional commercial pure titanium-polyethylene glycol drug-eluting substrates with enhanced optical and antithrombotic properties. Cardiovasc Eng Technol. 2022: 1–15. DOI:10.1007/s13239-022-00637-z.
[326] Yamaguchi S, Akeda K, Shintani SA, et al. Drug-Releasing gelatin coating reinforced with calcium titanate formed on Ti–6Al–4V alloy designed for osteoporosis bone repair. Coatings. 2022;12(2):139.
[327] Cloutier M, Mantovani D, Rosei F. Antibacterial coatings: challenges, perspectives, and opportunities. Trends Biotechnol. 2015;33(11):637–652.
[328] Hall TJ, Villapún VM, Addison O, et al. A call for action to the biomaterial community to tackle antimicrobial resistance. Biomater Sci. 2020;8(18):4951–4974.
[329] Wadge MD, Carrington MJ, Constantin H, et al. Characterization of potential nanoporous sodium titanate film formation on Ti_6Al4_V and TiO_2 microspherical substrates via wet-chemical alkaline conversion. Mater Charact. 2022;185:111760.